

DISSERTATION

FUNCTIONAL ORGANIZATION OF A CORTICAL-MEDULLARY NEURAL CIRCUIT
MEDIATING ORGANISMAL ADAPTATION TO STRESS

Submitted by

Sebastian A Pace

Department of Biomedical Sciences

In partial fulfillment of the requirements

For the Degree of Doctor of Philosophy

Colorado State University

Fort Collins, Colorado

Fall 2023

Doctoral Committee:

Advisor: Brent Myers

Co-Advisor: Shane Hentges

Stuart Tobet

Michelle Foster

Copyright by Sebastian A Pace 2023
All Rights Reserved

ABSTRACT

FUNCTIONAL ORGANIZATION OF A CORTICAL-MEDULLARY NEURAL CIRCUIT MEDIATING ORGANISMAL ADAPTATION TO STRESS

Hindbrain regions responsible for epinephrine and norepinephrine production are critical for orchestrating stress responses, maintaining physiological equilibrium and integrating afferent information. The nuclei central to hindbrain epinephrine and norepinephrine production, create a neural network that interfaces with forebrain and spinal cord regions, facilitating the integration of neuroendocrine and autonomic functions. Despite significant strides in our comprehension of stress response systems, questions concerning the roles of sex, stress history, and circuit mechanisms endure. In this study, we unveil and characterize a prefrontal-medullary circuit crucial for the suppression of stress responses. First, anterograde and retrograde tract-tracing studies demonstrated a stress-reactive vmPFC-RVLM circuit. Activation of this vmPFC-RVLM circuit mitigates glucocorticoid stress reactivity in both males and females, by targeting non-catecholaminergic neurons. Therefore, vmPFC-RVLM circuit activation may utilize local inhibitory neurons to limit catecholaminergic activation. To better understand how chronic stress affects the medulla, we explored the impact of chronic stress on signaling machinery and revealed elevated tyrosine hydroxylase (TH) levels in both male and female rats following chronic variable stress (CVS). To understand how CVS interacts with the vmPFC-RVLM circuit, we used an intersectional TeLC (Tetanus toxin - light chain) approach to disrupt the circuit and evaluate multiple stress response systems. In males, circuit disruption and CVS largely left behavioral and cardiovascular stress reactivity unaltered, however, some neuroendocrine

endpoints were affected. Conversely, females exposed to circuit disruption and chronic stress exhibited heightened stress reactivity in glycemic, corticosterone, and arterial pressure responses, coupled with avoidant-like behaviors. These findings underscore the sex-specific necessity of the vmPFC-RVLM circuit in countering chronic stress-related outcomes, emphasizing a greater protective role in females relative to males. To gain deeper insights into the role of vmPFC inputs to the RVLM in females, we once again utilized a circuit-based TeLC approach, employing in situ hybridization (ISH) coupled with immunohistochemistry (IHC) to assess TH and phenylethanolamine N-methyltransferase (PNMT) transcript density across various VLM subregions. Notably, the TeLC-induced elevation of PNMT expression in females suggests that disrupting this circuit could potentially enhance epinephrine production by RVLM neurons, potentially intensifying stress reactivity post-CVS. This comprehensive study demonstrated the critical role of the vmPFC-RVLM circuit in modulating stress responses and revealing female-specific effects in mitigating physiological, behavioral, and transcriptional outcomes after chronic stress. These findings emphasize the significance of the vmPFC-RVLM circuit in managing stress reactivity in the context of chronic stress and identify the circuit as a potential candidate for reducing stress responding.

ACKNOWLEDGEMENTS

I received help and support from many people throughout the past 5+ years. To start, Brent has my heartfelt thanks for being a fantastic teacher and mentor. Working for you has been both enjoyable and educational. Your approach and enthusiasm for science helped fuel my own and have led me on the path I'm on today. It has been a tremendous opportunity, and I'm incredibly grateful you gave it to me.

Next, I want to thank my lab mates who have collaborated with me and been a part of my work family. Ema - your hilarious memes are second only to your work ethic and productivity. You are elite. For this, I award 50 points to Gryffindor. Tyler – your macros have saved my butt at work almost as often as you've saved my butt outside of work. Thank you for your dependability and humor. Derek – I admire your consistency in and out of the lab. Thank you for helping with my telemetry project and letting me make fun of your love of Star Wars: Episode 1. Courtney – I am honestly upset we didn't get to work together more. I know we will be running into each other in the future, and I very much look forward to our continuing friendship. Paige – Thank you for making me laugh whenever you're in lab. It has been enjoyable working with you, and I look forward to you moving to California and not Vermont. I also want to thank Jake, Carlie, Carley, and Payton for their contributions to my projects – I appreciate the time, effort, and help you have given to help me succeed. Additionally, I want to thank my dissertation committee: Drs. Hentges, Tobet, and Foster, for their support and constructive advice.

I also want to thank the network of researchers who have supported me since I arrived at CSU. From the Handa Lab to the Tobet Lab, the PIs and students from these groups have served as a network of support that helped me feel like I belong. I thank Nik for being my work wife

and partner in shenanigans. Your support in all-things lab, family, and self has been immense and I am incredibly grateful. I also want to thank all the graduate students/colleagues who have served as emotional and moral support: Zephyr, Erica, Jordan, Amir, Emily, Hayley, Jules, Jasmin (and of course Quinn and Joey) – you all are awesome, and I appreciate your friendships. I am so happy we got to spend this time together.

Lastly, I thank my wonderful family for their unwavering support. From my sisters to my Buella and my Parents – you all have always been there to cheer me on and support me long before this Ph.D. started. The love you’ve showered me with has been a lifeline at times and I truly appreciate it. Mom and Dad – thank you so much for your warmth and support. Most importantly, I thank my family here in Colorado. Kayla – you’ve been the definition of support throughout this process. Your care of Landon and me has made completing this Ph.D. possible. Thank you for your love, thank you for your patience, and thank you for being my partner through all the crazy. Landon – You’ve been the best part of Colorado, and something tells me you will be the best part of California. Thank you for being the best of babies, going to daycare at 8-weeks old, to the best of big boys as we move to our new home. I know you can’t appreciate it now but thank you for your patience. You’ve been a beacon of happiness and a respite from all the stress of the world. Thank you for being you.

TABLE OF CONTENTS

ABSTRACT.....	ii
ACKNOWLEDGEMENTS.....	iv
Chapter 1 – Introduction.....	1
1.1 Endocrine and autonomic stress responses.....	1
1.2 Brainstem adrenergic/noradrenergic nuclei.....	2
1.2.1 Anatomy.....	2
1.2.2 Neurochemistry.....	4
1.3 Adrenergic/noradrenergic stress regulation.....	5
1.3.1 Acute stress.....	5
1.3.2 Chronic stress.....	6
1.4 Ascending adrenergic and noradrenergic circuits.....	7
1.4.1 Projections to the PVN.....	7
1.4.2 Forebrain projections.....	8
1.5 Descending adrenergic and noradrenergic projections.....	9
1.5.1 Bulbospinal neurons.....	9
1.5.2 The baroreflex.....	10
1.6 Endocrine-autonomic integration by adrenergic/noradrenergic nuclei.....	11
1.6.1 Endocrine feedback and autonomic function.....	11
1.6.2 Brainstem circuit integration.....	12
1.7 Sex differences in adrenergic/noradrenergic nuclei.....	13
1.7.1 Female-specific regulation.....	13
1.7.2 Estrogen receptor expression.....	14
1.8 Conclusion.....	15
Chapter 2 – Cortical-brainstem circuitry attenuates physiological stress reactivity.....	17
2.1 Introduction.....	17
2.2 Methods.....	19
2.2.1 Animals.....	19
2.2.2 Experimental Design.....	19
2.2.3 Stereotaxic Surgery.....	20

2.2.4 Fiber Optic Cannulations	21
2.2.5 Photostimulation Parameters	22
2.2.6 Estrous Cycle Cytology	22
2.2.7 Restraint Stress	23
2.2.8 Real-Time Place Preference	24
2.2.9 Tissue Collection	24
2.2.10 Immunohistochemistry	25
2.2.11 Microscopy	27
2.2.12 Image Analysis	28
2.2.13 Neuroanatomy	28
2.2.14 Data Analysis.....	29
2.3 Results	30
2.2.1 vmPFC Glutamate Projections to Catecholaminergic VLM Neurons.....	30
2.3.2 Organization and Stress Responsiveness of RVLM- and CVLM-Projecting vmPFC Neurons.....	33
2.3.3 Optogenetic vmPFC-RVLM Circuit Stimulation.....	35
2.3.4 Motivational Valence of vmPFC-RVLM Circuit Stimulation	36
2.3.5 vmPFC-RVLM Circuit Regulation of Stress Reactivity	37
2.3.6 The vmPFC-RVLM Circuit Preferentially Activates Non-Catecholaminergic Cells ..	39
2.3.7 vmPFC Inputs Target Medullary Inhibitory Neurons	40
2.4 Discussion	42
2.4.1 vmPFC Regulation of Stress Responding	43
2.4.2 Importance of Biological Sex	44
2.4.3 Regulation of RVLM Catecholaminergic Neurons	45
2.4.4 The vmPFC-RVLM in Brain-Body Function.....	47
2.5 Conclusions	47
Chapter 3 – The Necessity of vmPFC-RVLM Circuit Function to Limit Stress Reactivity After Chronic Variable Stress Differs Between Sexes.....	49
3.1 Overview	49
3.2 Methods.....	51
3.2.1 Animals.....	51
3.2.2 Experimental design	52
3.2.3 Stereotaxic surgery	53

3.2.4 Telemetry implantations	54
3.2.5 Estrous cycle cytology	54
3.2.6 Restraint stress	55
3.2.7 Chronic Variable Stress	56
3.2.8 VLM microdissection	56
3.2.9 Nanostring nCounter	56
3.2.10 in situ hybridization and immunohistochemistry	57
3.2.11 Open Field Assay	58
3.2.12 Tissue collection	59
3.2.13 Immunohistochemistry	59
3.2.14 Microscopy	60
3.2.15 Image analysis	60
3.2.16 Neuroanatomy	61
3.4.14 Data analysis	62
3.3 Results	63
3.3.1 VLM gene expression changes after CVS	63
3.3.2 vmPFC-RVLM Circuit Disruption Approach While Measuring Physiological Endpoints	65
3.3.3 vmPFC-RVLM Circuit is Crucial for Regulating Neuroendocrine Stress Responses in Females and Males following CVS	66
3.3.4 vmPFC-RVLM Circuit is Necessary to Limit CVS Effects on Behavior in Females, But Not Males	70
3.3.5 vmPFC-RVLM Circuit is Needed to Appropriate Cardiovascular Function in Males and Females After CVS	72
3.3.6 RVLM-projecting vmPFC Neurons Have Collaterals Throughout the Brain	81
3.3.7 vmPFC-RVLM Circuit is Necessary to Reduce PNMT Expression in Females	82
3.4 Discussion	84
3.5 Conclusion	89
Chapter 4: Discussion	91
4.1 Circuit manipulation approaches	92
4.2 Role of PFC in stress responding	94
4.3 Role of RVLM in stress	96
4.5 Female vmPFC-RVLM function	100

4.6 Conclusion.....	101
References.....	104
Appendix.....	140

Chapter 1 – Introduction¹

1.1 Endocrine and autonomic stress responses

Organismal survival in threatening situations is dependent on energy-mobilizing biological response systems. In the context of real or perceived threats, cognitive appraisal of external sensory modalities and internal states elicits widespread biological responses to promote adaptation (Daskalakis et al., 2022). Stress-responsive systems engage neural circuits to generate behavioral as well as neurosecretory and autonomic processes. Peripheral physiological systems are characterized by distinct temporal profiles and signaling molecules. However, neurosecretory and autonomic systems interact to coordinate the responses necessary to maintain or restore homeostasis. Importantly, the effector cells of endocrine and autonomic systems are modulated by epinephrine- and norepinephrine-synthesizing cell groups in the brainstem (Wood & Valentino, 2017).

The neuroendocrine stress response engages the hypothalamic-pituitary-adrenal (HPA) axis, culminating in the synthesis and release of glucocorticoids (Herman et al., 2016; Myers, McKlveen, et al., 2014). Neurosecretory cells in the paraventricular nucleus of the hypothalamus (PVN) secrete corticotropin-releasing hormone (CRH) into the hypophyseal portal. CRH stimulates the anterior pituitary to release adrenocorticotrophic hormone (ACTH) into the bloodstream. Subsequently, ACTH reaches the adrenal cortex where glucocorticoids (cortisol in humans, corticosterone in rats and mice) are released. Glucocorticoids then bind

¹ Pace SA & Myers B. Hindbrain adrenergic/noradrenergic control of integrated endocrine and autonomic stress responses. *Accepted at Endocrinology*

mineralocorticoid (MR) and glucocorticoid receptors (GR) to mediate cellular signaling and transcriptional regulation throughout the brain and body (Reul & De Kloet, 1985). Here, negative feedback mediated by GR and MR promotes HPA axis recovery (Dallman, 2005). In contrast, the autonomic stress response primarily relies on the sympathetic nervous system to mediate fight-or-flight responses. Neural signals from the hypothalamus and brainstem synapse onto preganglionic sympathetic neurons in intermediolateral cell column of the thoracolumbar spinal cord (Ulrich-Lai & Herman, 2009). Preganglionic sympathetic neurons target both postganglionic sympathetic neurons that innervate target organs, as well as the adrenal medulla, which comprises the sympathoadrenomedullary (SAM) axis. Sympathetic stress responses generated by peripheral synaptic norepinephrine and adrenal epinephrine release increase heart rate, blood pressure, and glucose mobilization (Guyenet et al., 2013). The sympathetic stress response is countered by the parasympathetic nervous system to restore autonomic balance.

1.2 Brainstem adrenergic/noradrenergic nuclei

1.2.1 Anatomy

In rodents, stressors including restraint, noise, forced swim, immune challenge, hemorrhage, and glucoprivation activate epinephrine- and norepinephrine-synthesizing cells (Dayas et al., 2001; Ritter et al., 2019b). In turn, epinephrine- and norepinephrine-synthesizing neurons project to the effectors of the HPA and SAM axes (Plotsky et al., 1989; Ulrich-Lai & Herman, 2009). Consequently, adrenergic/noradrenergic circuits are essential for counterregulatory responses and the restoration of homeostasis. Brainstem adrenergic/noradrenergic neurons are the primary source of epinephrine and norepinephrine in the central nervous system (Fuxe, 1965; Fuxe et al., 2010). Both epinephrine- and

norepinephrine-producing cells express dopamine beta-hydroxylase (DBH), the enzyme that converts dopamine to norepinephrine. However, only epinephrine-synthesizing cells express phenylethanolamine-N-methyl transferase (PNMT), which synthesizes epinephrine from norepinephrine. The distinction between epinephrine and norepinephrine neurons is explicit, with epinephrine-synthesizing neurons labeled as “C” populations and norepinephrine-synthesizing populations labeled as “A” nuclei. These adrenergic/noradrenergic nuclei are further identified by their anatomical location (e.g. C1 neurons in the ventral medulla and C2 in the dorsal medulla) (Fuxe, 1965; Hokfelt, 1984). The locus coeruleus (LC/A6), nucleus of the solitary tract (NTS/C2/A2), and ventrolateral medulla (VLM/C1/A1) account for the majority of epinephrine and norepinephrine produced by the brain (Fuxe, 1965; Hokfelt, 1984) (Figure 1.1). These regions constitute a core of evolutionarily-conserved circuits that are critical for the regulation of neuroendocrine function, glucose metabolism, blood pressure, breathing, sleep-wake cycles, and behavior (Patrice G. Guyenet et al., 2013; Rinaman, 2011; S. K. Wood & Valentino, 2017).

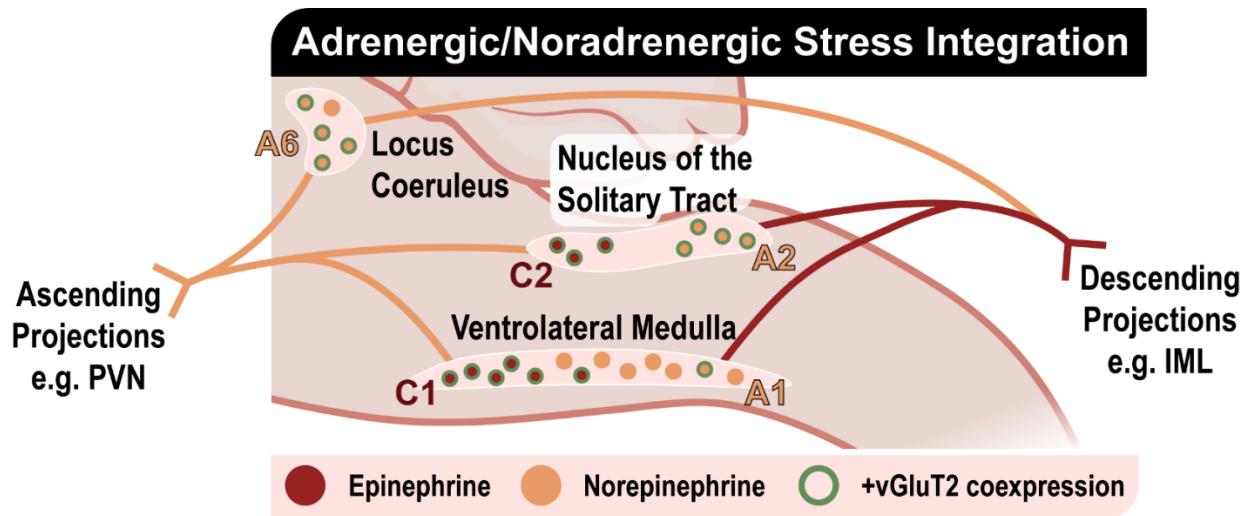


Figure 1.1 Organization of brainstem adrenergic/noradrenergic nuclei. Hindbrain adrenergic/noradrenergic cell groups regulate both endocrine and autonomic responses to physical and psychological stressors. These nuclei synthesize epinephrine (C1, C2) and/or norepinephrine (A1, A2, A6) with a subset coexpressing vGluT2. Ascending outputs target the hypothalamus to regulate neuroendocrine processes, while spinal projections govern sympathetic

functions. PVN: paraventricular nucleus of the hypothalamus, IML: intermediolateral cell column, vGluT2: vesicular glutamate transporter-2.

1.2.2 Neurochemistry

Although brainstem adrenergic/noradrenergic cells are defined by the presence of epinephrine and norepinephrine synthesis enzymes, these nuclei co-express other neurotransmitter and neuropeptide transcripts. In rats, mRNA for the glutamatergic marker vesicular glutamate transporter 2 (vGluT2) colocalizes with approximately 75% of C2 nuclei and 80% of A2 cells in the NTS (Stornetta et al., 2002). Similarly, vGluT2 colocalizes with approximately 75% of C1 cells in the rostral VLM (Stornetta et al., 2002). These observations suggest that glutamate is co-released with epinephrine or norepinephrine, although the functional consequences remain to be defined (Guyenet et al., 2013; Rinaman, 2011; Ruth L. Stornetta, 2009). Other norepinephrine nuclei appear to colocalize with vGluT2 to a lesser degree. vGluT2 only colocalizes with approximately 16% of A1 cells in the VLM, while the same study found no colocalization with A6 cells in the LC (Stornetta et al., 2002). However, recent studies genetically identified LC norepinephrine and glutamate co-expression and confirmed functional synaptic glutamate release from LC catecholaminergic neurons (Yang et al., 2021). In addition to glutamate, NTS and VLM adrenergic/noradrenergic cells also express neuropeptides including neuropeptide Y (NPY), substance P, calcitonin, enkephalin, pituitary adenylate cyclase-activating peptide, cocaine- and amphetamine-related transcript (Stornetta, 2009). Neuropeptide expression in the LC is less diverse and includes NPY and galanin (Xu et al., 1998). Although adrenergic/noradrenergic neurons commonly express neuropeptides, little is known about release dynamics or the functional consequences for stress integration.

1.3 Adrenergic/noradrenergic stress regulation

1.3.1 Acute stress

Stimulating epinephrine- and norepinephrine-synthesizing neurons in the LC, VLM, or NTS emulates neuroendocrine, autonomic, and behavioral responses to stress. For example, stimulation of VLM C1 neurons in stress-naïve animals increases sympathetic nerve activity, blood glucose mobilization, heart rate, arterial pressure, and respiration (Burke et al., 2014; Kanbar et al., 2010; Souza et al., 2022; Zhao et al., 2017). Loss of function approaches targeting VLM adrenergic/noradrenergic neurons also provide evidence for adrenergic/noradrenergic augmentation of blood pressure and circulating epinephrine and glucose (Madden et al., 2006; Madden & Sved, 2003; Marina et al., 2011; Wenker et al., 2017; Zhao et al., 2017). Numerous studies investigating the immediate-early gene c-Fos indicate that brainstem adrenergic/noradrenergic neurons are responsive to both homeostatic disturbances and psychosocial stressors (Cullinan et al., 1995; Dayas et al., 2001; Pezzone et al., 1993). Recent *in vivo* studies further implicate the necessity and sufficiency of adrenergic/noradrenergic neural activity for sensing and responding to stressors. For instance, calcium imaging in rostral VLM C1 neurons during hemorrhage demonstrates increased activity during hemorrhagic compensation that declines at the onset of decompensation (Souza et al., 2022). Moreover, C1 activation increases sympathetic nerve activity and blood pressure stability to prevent hemorrhage-induced cardiovascular collapse (Souza et al., 2022). Other studies report that CRH-dependent increases in tonic, but not phasic, LC neural activity promote stress-induced behaviors (McCall et al., 2015). Additionally, administration of a catecholaminergic toxin to NTS A2 cells reduces corticosterone and heart rate responses to restraint (Bundzikova-Osacka et al., 2015), indicating this population is a primary integrator of endocrine and autonomic physiology.

Overall, epinephrine and norepinephrine circuits both encode stressors and coordinate stress responses, suggesting that chronic stress effects on adrenergic and noradrenergic nuclei may contribute to stress-related disorders.

1.3.2 Chronic stress

Brainstem adrenergic/noradrenergic activity is engaged by multiple chronic stress paradigms. The expression of tyrosine hydroxylase (TH), the rate-limiting enzyme for catecholamine synthesis, is commonly used as a measure of catecholaminergic activity after chronic stress. Repeated homotypic stress paradigms (repeated restraint or cold room) increase TH mRNA in caudal VLM A1 neurons in male and female rats, as well as TH immunoreactivity in male LC A6 cells (Melia et al., 1992; Tóth et al., 2008). While no changes in TH are observed after homotypic stress in NTS A2 cells of either sex (Tóth et al., 2008), NTS adrenergic and noradrenergic neurons are sensitive to chronic heterotypic stressor paradigms. After chronic variable stress (CVS) in male rats, the NTS has increased TH mRNA (Zhang et al., 2010), as well as expression of the long-term activity marker FosB/DFosB in DBH-positive cells (Flak et al., 2012). Moreover, loss of NTS A2 neurons prevents CVS-induced cardiac autonomic imbalance (Bundzikova-Osacka et al., 2015). In terms of social stress, hierarchically subordinate male rats have increased TH mRNA and protein in the LC compared to controls (Watanabe et al., 1995). This effect is also found in human psychosocial distress, as donors diagnosed with major depressive disorders have increased TH mRNA expression in the LC as well as the noradrenergic developmental transcription factors Phox2a and Phox2b (Fan et al., 2018; Zhu et al., 1999). Furthermore, LC TH immunoreactivity is elevated in suicidal depressive patients (Gos et al., 2008). Taken together, prolonged stress upregulates brainstem epinephrine and

norepinephrine synthesis enzymes across species and chronic stress paradigms, suggesting increased epinephrine and norepinephrine production may contribute to stress-related health consequences. However, it remains to be determined how upregulation of epinephrine and norepinephrine in NTS, LC, and VLM neurons modulates signaling within projection circuitry.

1.4 Ascending adrenergic and noradrenergic circuits

1.4.1 Projections to the PVN

The NTS, LC, and VLM give rise to parallel and divergent projections to stress-regulatory nuclei, pathways that provide a circuit basis for adrenergic/noradrenergic stress integration (Guyenet et al., 2013; Myers et al., 2017; Rinaman, 2011; Valentino & Van Bockstaele, 2008). Notably, DBH- and PNMT-immunoreactive processes target CRH-, vasopressin-, and oxytocin-producing PVN neurons that also express adrenergic receptors (Cummings & Seybold, 1988; Cunningham & Sawchenko, 1988; Füzesi et al., 2007; Raby & Renaud, 1989; Russell et al., 2003). Functional studies lesioning adrenergic/noradrenergic cells or tracts reveal that ascending pathways excite CRH neurons and facilitate HPA axis responses to a variety of stressors (Bienkowski & Rinaman, 2008; Flak et al., 2014; Khan et al., 2011; H. Y. Li et al., 1996; Ritter et al., 2001, 2003; Sawchenko, 1988). Specifically, norepinephrine activates a subset of PVN CRH neurons through $\alpha 1$ adrenergic receptors (Boudaba et al., 2003; Gouws et al., 2022). CRH neuronal activation by $\alpha 1$ receptors also increases dendritic volume transmission to promote retrograde glial signaling that activates presynaptic inputs to CRH neurons (Chen et al., 2019), demonstrating multiple pathways through which adrenergic inputs may regulate HPA axis activity. Although, PVN adrenergic modulation is dependent on stressor modality as glucocorticoid-induced $\alpha 1$ receptor internalization desensitizes CRH neurons in

response to immune challenge but not restraint (Jiang et al., 2022). In addition to adrenergic receptor signaling, ascending norepinephrine synapses also activate CRH neurons through corelease of glutamate (Bains et al., 2015). Ultimately, further investigation is needed to determine the context-dependent aspects of adrenergic/noradrenergic and glutamatergic cotransmission in the hypothalamus.

Adrenergic/noradrenergic innervation of the PVN exhibits considerable plasticity after chronic stress. Overall, chronic stress shifts the excitatory/inhibitory balance of CRH neurons through decreases in GABA receptor expression, inhibitory postsynaptic current frequency, and glucocorticoid negative feedback (Franco et al., 2016; Herman & Tasker, 2016; Verkuyl et al., 2004). Chronic stress also increases vGluT2- and DBH-positive synaptic density, excitatory postsynaptic current frequency, and NMDA receptor subunit expression in CRH neurons (Flak et al., 2009; Franco et al., 2016). Reducing adrenergic/noradrenergic innervation of the PVN in male rats prevents CVS-induced increases in synaptophysin and vGluT2 expression on presynaptic afferents (Flak et al., 2014), suggesting that sensitization of PVN glutamatergic transmission is dependent on adrenergic/noradrenergic circuits. Further, loss of PVN-projecting epinephrine and norepinephrine cells reduces HPA axis responses to acute restraint and diminishes ACTH release after CVS (Flak et al., 2014). Altogether, chronic stress may facilitate neuroendocrine stress responses by enhancing adrenergic and glutamatergic transmission in ascending brainstem-PVN projections.

1.4.2 Forebrain projections

The NTS, LC, and VLM also generate distinct patterns of ascending projections that target the forebrain. For instance, LC projections that signal through hippocampal beta-

adrenergic receptors mediate the discrimination of aversive contextual stimuli (Seo et al., 2021), while LC inputs to beta-adrenergic receptors in the basolateral amygdala promote anxiety-like avoidance behaviors (Mccall et al., 2017). Additionally, VLM catecholaminergic projections to the midline thalamus are necessary for glucoprivation-induced food seeking (Beas et al., 2020). While much of the work on forebrain adrenergic/noradrenergic signaling has focused on behavior, multiple studies have utilized retrograde catecholaminergic toxins to examine the ascending circuitry of neuroendocrine control. Reduction of adrenergic/noradrenergic inputs to the bed nucleus of the stria terminalis from the NTS and VLM inhibits glucocorticoid responses to a systemic α 2-adrenergic receptor antagonist (Banihashemi & Rinaman, 2006). Similarly, removal of adrenergic/noradrenergic innervation of frontal cortex by the LC attenuates HPA axis responses to restraint (Radley et al., 2008). Chronic stress impacts ascending adrenergic/noradrenergic circuits as social defeat in male rats increases DBH protein levels in the LC, hippocampus, frontal cortex, and amygdala (Fan et al., 2013). Human and non-human primate studies suggest that either high or low norepinephrine release in the frontal cortices during stress exposure leads to cognitive impairment (Arnsten, 2009, 2015), signifying that cortical norepinephrine functions with an inverted-U dose response (Arnsten, 2011). However, less is known about how prolonged stress may alter adrenergic/noradrenergic interactions with the forebrain to regulate endocrine-autonomic integration.

1.5 Descending adrenergic and noradrenergic projections

1.5.1 Bulbospinal neurons

Descending epinephrine- and norepinephrine-producing circuits provide neurogenic regulation of the sympathetic stress response (Saper & Stornetta, 2014). Specifically,

adrenergic/noradrenergic axonal processes are present in the intermediolateral cell column, superficial dorsal horn, ventral horn motor neuron pools, and lamina X of the spinal cord (Fritschy & Grzanna, 1990; Westlund et al., 1983). Despite some variations in bulbospinal tracing studies, adrenergic/noradrenergic projections largely arise from the NTS C2 and A2, VLM C1, and LC (Bruinstroop et al., 2012; Loewy & Burton, 1978; Morrison et al., 1988; Strack et al., 1989). Descending adrenergic/noradrenergic circuits are sympathoexcitatory with VLM C1 neurons particularly important for sympathetic control of the cardiovascular system (Dampney, 2015; Guyenet et al., 2013) and SAM axis activation after stress (Ruth L. Stornetta & Guyenet, 2018; Zhao et al., 2017). Reflexive circuitry connecting NTS and VLM also underlies long-term blood pressure control (Dampney et al., 2002; Guyenet et al., 2020).

1.5.2 The baroreflex

Interoceptive inputs to the NTS regulate VLM activity and gate sympathetic outflow from C1 neurons via the baroreflex (Andresen et al., 2001). Here, carotid sinus and aortic arch baroreceptors transmit mechanical stretch sensation via the glossopharyngeal and vagal nerves (Benarroch, 2008). These afferents synapse in the NTS where second-order glutamatergic neurons stimulate GABAergic neurons in the caudal VLM that then inhibit rostral VLM C1 activity. This reflexive circuit allows arterial pressure to influence sympathetic output and maintain cardiovascular homeostasis (Dampney et al., 2002; Madden & Sved, 2003). Notably, chronic stress reduces baroreflex sensitivity leading to increased blood pressure and decreased heart rate variability (Firmino et al., 2019; Grippo et al., 2002), exacerbating risk for cardiovascular disease development (Kivimäki & Steptoe, 2017; Steptoe & Kivimäki, 2012). Accordingly, multiple studies employing rodent models of elevated blood pressure (e.g.

spontaneously hypertensive, obese, or salt-sensitive) point to elevated tonic activity of C1 neurons as a substrate for sympathetic-mediated hypertension (Huber & Schreihofner, 2011; Ito et al., 2000, 2001; Minson et al., 1996; Stocker et al., 2007). In all, imbalanced activity of NTS afferents and C1 efferents is likely to disrupt homeostatic adaptation and broadly impact health (Guyenet et al., 2020).

1.6 Endocrine-autonomic integration by adrenergic/noradrenergic nuclei

1.6.1 Endocrine feedback and autonomic function

Glucocorticoid feedback in adrenergic/noradrenergic nuclei coordinates long-term physiological regulation (Scheuer, 2010). Chronic corticosterone administration in the dorsal hindbrain increases resting heart rate and arterial pressure, as well as stress-induced pressor responses (Scheuer et al., 2004, 2007). Additionally, chronic dorsal medulla GR antagonism in borderline hypertensive rats attenuates arterial pressure responses to acute and repeated restraint (Bechtold et al., 2009), suggesting the NTS mediates glucocorticoid effects on blood pressure. However, blockade of GR in the A2 region of the NTS sensitizes HPA axis responses to acute and chronic stress and promotes anxiety-like avoidance behaviors. Taken together, these data suggest that GR signaling may inhibit the NTS to both enhance negative feedback of the HPA axis and impair the afferent limb of the baroreflex. In fact, a recent study reports that GR signaling in the NTS inhibits presynaptic glutamate afferents through retrograde cannabinoid signaling (Ragozzino et al., 2020). Similar mechanisms may act in the LC, where GR signaling prevents TH mRNA upregulation after acute stress (Makino et al., 2002). While corticosteroid receptors are expressed throughout the VLM (Reul & De Kloet, 1985; Sosa et al., 2023), much less is known regarding the impacts on endocrine-autonomic integration.

The interplay between neuroendocrine and autonomic function also relies on PVN inputs to adrenergic/noradrenergic nuclei. PVN projections to the NTS, VLM, and LC arise predominately from CRH- and vasopressin-expressing neurons (Swanson & Sawchenko, 1980; Zhao et al., 2017). These projections largely drive postsynaptic excitation and coexpress glutamatergic markers (Hernández-Pérez et al., 2019). Vasopressin and CRH projections from the PVN to the NTS stimulate barosensitive NTS neurons to elevate blood pressure and heart rate (Hegarty & Felder, 1997; Wang et al., 2019). Activation of the LC by hypotensive stress is also CRH-dependent (Curtis et al., 1994; Valentino et al., 1991). Conversely, optogenetic stimulation of PVN CRH terminals in the VLM does not modulate counterregulatory glycemic responses (Zhao et al., 2017). While early life maternal separation increases the density of vasopressin inputs to the LC (Hernández-Pérez et al., 2019), the broader role of PVN projections to adrenergic/noradrenergic neurons in long-term stress regulation is not well understood. However, chronic stress reduces GR expression in the PVN and increases CRH and vasopressin (Chappell et al., 1986; Herman et al., 1995; Ma et al., 1999; Makino et al., 1995), suggesting impaired HPA axis negative feedback and increased outflow from the PVN may enhance the activity of projections to the hindbrain.

1.6.2 Brainstem circuit integration

Brainstem catecholaminergic neurons are densely interconnected through direct synaptic communication (Owens & Verberne, 2001). Specifically, vagal-dependent reflex arcs stimulate NTS norepinephrine and glutamate outputs to inhibitory VLM neurons to attenuate C1 activity (Schreihofer & Guyenet, 2002; Verberne, 1996; Verberne et al., 1999). There is also regional differentiation of cell group function. Chemogenetic activation of distinct cell populations across

the rostral-caudal axis of the VLM demonstrates that corticosterone release is stimulated by the rostral A1 cells that transition to C1, whereas glucose mobilization is controlled by the cells in mid and rostral C1 (Li et al., 2018; Ritter et al., 2019). Thus, hindbrain adrenergic/noradrenergic cells form an interwoven network to promote physiological adaptation. However, other aspects of adrenergic/noradrenergic circuit integration remain to be determined. For example, adrenergic/noradrenergic nuclei interact with preganglionic parasympathetic neurons, likely shifting autonomic balance. Although VLM C1 epinephrine neurons can activate pre-ganglionic neurons of the dorsal motor nucleus of the vagus, how these circuits regulate processes such as cardiac output and gastric function under differing environmental contexts requires more investigation (Card et al., 2006; Cheng et al., 1999; DePuy et al., 2013; Machhada et al., 2015; Travagli et al., 2006). Moreover, this review has focused on the adrenergic/noradrenergic cell groups that have been most thoroughly investigated; however, additional noradrenergic regions such as A5 and A7 are also likely integrators of stress physiology (Kvetnansky et al., 2006; Souza et al., 2022). Additional investigation of adrenergic/noradrenergic brainstem networks would provide more mechanistic information about the fine-tuning of physiological response patterns and the pathogenesis of negative health states.

1.7 Sex differences in adrenergic/noradrenergic nuclei

1.7.1 Female-specific regulation

Most studies of VLM and NTS adrenergic/noradrenergic cells have focused exclusively on males. Conversely, the pioneering work of Valentino and colleagues has uncovered significant sex differences in stress-related LC function (Bangasser et al., 2016; Bangasser & Valentino, 2012; Valentino et al., 1993; Wood & Valentino, 2017). The female LC is structurally

larger with more norepinephrine neurons and greater dendritic arborization than males (Bangasser et al., 2011; Guillamón et al., 1988). Further, female LC neurons have increased postsynaptic sensitivity to CRH via enhanced g-protein-dependent cAMP signaling (Curtis et al., 2005). Interestingly, sex differences in LC CRH signaling are stress-dependent as the male LC amplifies CRH sensitivity after stress exposure, while female LC CRH signaling is stable regardless of stress history (Bangasser et al., 2010; Curtis et al., 2005). Additionally, CRH overexpression in mice disproportionately increases female LC tonic firing relative to males (Bangasser et al., 2013). There are also sex differences in CRH receptor internalization with elevated CRH reducing male dendritic receptor expression while female receptor expression is maintained (Bangasser et al., 2010, 2013; Reyes et al., 2006, 2008). These studies collectively demonstrate sexual dimorphism of LC stress-responsiveness and suggest that sex-specific signaling may be present in other catecholaminergic cell groups.

1.7.2 Estrogen receptor expression

Sex differences in LC noradrenergic activity and function may relate to hormonal and/or chromosomal differentiation. The concentration of hypothalamic norepinephrine varies with reproductive status and is highest during proestrus (Selmanoff et al., 1976). Likewise, estradiol increases norepinephrine in the hippocampus, cortex, and hypothalamus of ovariectomized rats (Alfinito et al., 2009; Lubbers et al., 2010). Together, these data suggest that increased norepinephrine release may be a result of estrogenic signaling. Importantly, the NTS, VLM, and LC express estrogen receptor alpha (ERa) and beta (ERb) (Hay, 2016; Mitra et al., 2003; Saleh & Connell, 2000; Shughrue et al., 1997; Simerly et al., 1990; Spary et al., 2009; G. Wang et al., 2006). Estradiol treatment upregulates expression of TH and DBH in the LC and NTS (Serova et

al., 2002; Serova et al., 2004). However, ERb in the rostral VLM reduces the excitability of adrenergic/noradrenergic neurons and elicits vasodepressor effects in male and female rodents that also protect female mice from aldosterone/salt-induced hypertension (Shih, 2009; G. Wang et al., 2006; Xue et al., 2013). Therefore, the relative distribution of ERa and ERb may increase LC and NTS adrenergic/noradrenergic signaling while restricting VLM output. Ultimately, adrenergic/noradrenergic neurons acts as central regulators of endocrine-autonomic integration and may contribute to sex differences in stress-related outcomes (Handa et al., 2022; Littlejohn et al., 2020).

1.8 Conclusion

The hindbrain regions that synthesize epinephrine and norepinephrine play a pivotal role in coordinating endocrine and autonomic responses to stress. These cells interpret interoceptive and exteroceptive cues and coordinate physiology and behavior to maintain homeostasis. The NTS, VLM, and LC are the primary sources of epinephrine and norepinephrine in the brain. During acute stress, increased adrenergic and noradrenergic activity leads to widespread physiological adaptation that increases HPA axis activity, heart rate, blood pressure, and glucose mobilization (Stornetta & Guyenet, 2018). Chronic stress can alter catecholamine biosynthesis which may impact signaling and, subsequently, stress-related health outcomes. Ascending adrenergic/noradrenergic projections to forebrain nuclei, including the hypothalamus, and descending spinal projections are critical for integrating neuroendocrine and autonomic functions. Although significant progress has been made in understanding the functional organization of this circuitry, many questions related to the importance of sex and stress history remain. Investigating the neural and endocrine regulation of brainstem adrenergic and

noradrenergic nuclei holds considerable promise for advancing our knowledge of stress-related physiology and the consequences for health and well-being.

Chapter 2 – Cortical-brainstem circuitry attenuates physiological stress reactivity²

2.1 Introduction

Organismal adaptation to stress is essential for survival. These adaptations are dependent on forebrain structures such as the ventromedial prefrontal cortex (vmPFC) that appraise stressful stimuli and orchestrate appropriate responses (Duncan, 2001; McKlveen et al., 2015; Ulrich-Lai & Herman, 2009). Additionally, stress-related disorders such as depression and post-traumatic stress disorder are associated with altered structure and function of the vmPFC (Drevets et al., 1997; Drevets et al., 2008; Hamani et al., 2011; Liotti et al., 2000). In rodents, male vmPFC glutamate neurons promote socio-motivational behaviors and reduce physiological stress responses, including hyperglycemia, tachycardia, and corticosterone release (Myers et al., 2017; Schaeuble et al., 2019; Wallace et al., 2021). Notably, vmPFC neurons do not directly project to neurosecretory cells or preganglionic sympathetic neurons, requiring intervening effector(s) to modulate physiological responses (Ulrich-Lai & Herman, 2009). Tract-tracing experiments examined long-range vmPFC projections to the brainstem with some reporting projections to the rostral ventrolateral medulla (RVLM) (Gabbott et al., 2005; Hurley et al., 1991), a key pre-sympathetic nucleus. Moreover, vmPFC neurons innervate catecholaminergic and non-catecholaminergic neurons in the RVLM (Gabbott et al., 2007). However, little is known about the stress responsiveness or function of vmPFC projections to the medulla, nor whether cortical inputs activate the epinephrine/norepinephrine-producing neurons that initiate physiological stress responses.

²Pace SA, Lukinic E, Wallace T, McCartney C & Myers B. Cortical-brainstem circuitry attenuates physiological stress reactivity. *Accepted at Journal of Physiology*

Brainstem catecholaminergic neurons are evolutionarily-conserved nuclei facilitating metabolic, neuroendocrine, and autonomic responses to physical and psychological stimuli (Ritter et al., 2019; Stornetta & Guyenet, 2018). Specifically, catecholaminergic neurons in the RVLM activate spinal preganglionic sympathetic neurons to elicit widespread physiological adaptations, including vasoconstriction and hyperglycemia (Guyenet et al., 2013). Additionally, ascending RVLM projections target paraventricular hypothalamic neuroendocrine cells that initiate hypothalamic-pituitary-adrenal (HPA) axis glucocorticoid release (Card et al., 2006; Stornetta et al., 2016). Collectively, these physiological effects support a vital homeostatic role for RVLM catecholaminergic neurons (Ritter, 2017). However, the mechanisms regulating RVLM activity during stress have received limited attention. Further, little is known regarding the functional effects of forebrain circuits targeting the RVLM. Here, we examined cortical afferents targeting the RVLM and the neurogenic regulation of stress reactivity by the prefrontal-medullary neural circuit.

To determine if glutamatergic vmPFC projections target RVLM catecholaminergic neurons, an anterograde genetically-encoded vmPFC tract-tracing approach was used to quantify cortical appositions onto epinephrine/norepinephrine-synthesizing neurons throughout the ventrolateral medulla. Further, dual retrograde-transported viruses were used to determine cortical-medullary projections' circuit organization and stress responsiveness. Next, optogenetic stimulation of vmPFC synapses in the RVLM was used to examine motivational behavior as well as glycemic and glucocorticoid responses to stress as end products of the sympathetic and HPA axes, respectively (Bialik et al., 1988; Myers et al., 2014). Additionally, vmPFC-RVLM stimulation tissue was assessed to examine catecholaminergic and non-catecholaminergic

cellular activation and vmPFC projections onto RVLM inhibitory GABAergic and glycinergic neurons.

2.2 Methods

2.2.1 Animals

Adult male and female Sprague-Dawley rats (Envigo, Denver, CO) weighing 250-300g and 150-200g, respectively were housed in temperature- and humidity-controlled vivarium with a 12-hour light-dark cycle (lights on at 0600, and off at 1800). Holding rooms were restricted to same-sex conspecific rats. Incoming rats were acclimated to the vivarium for 1-week before the start of the experiment. Water and chow were available ad libitum throughout the experiment. All procedures and protocols were approved by the Institutional Animal Care and Use Committee of Colorado State University (protocol: 1392) and complied with the National Institutes of Health Guidelines for the Care and Use of Laboratory Animals. The experimental procedures used in the current experiments received veterinary consultation and all animals had daily welfare assessments by veterinary and/or animal medical service staff.

2.2.2 Experimental Design

Experiment 1 was an anterograde tract-tracing experiment comprised of 5 male and 4 female rats for identification of inputs to catecholamine-producing cells. 3 male and female rats from this experiment were also used to for immunolabeling RVLM inhibitory neurons to examine vmPFC terminals appositions. Experiment 2 was a retrograde tract-tracing experiment comprised of 5 male and female rats. Experiment 3 was a vmPFC-RVLM circuit stimulation study that used 2 cohorts of male rats to generate 16 ChR2 and 12 YFP rats. 1 cohort of female

rats was used to produce 17 ChR2 and 11 YFP rats. All cohorts were run separately, and all rats underwent real-time place preference (RTPP) and restraint stress. Tissue from Experiment 3 was used for Experiment 4, which examined the neurochemical identity of cells activated by vmPFC-RVLM stimulation.

2.2.3 Stereotaxic Surgery

Male and female rats were anesthetized with aerosolized isoflurane (1-5%) and administered an analgesic (0.6 mg/kg buprenorphine-SR, subcutaneous) as previously described (Wallace et al., 2021). For anterograde tract-tracing experiments (Experiment 1), rats received bilateral microinjections (males 1.5 μ L, females 1 μ L) of adeno-associated virus (AAV) constructs (UNC Vector Core, Chapel Hill, NC) in the vmPFC (males: 0.6 mm lateral to midline, 2.7 mm anterior to bregma, and 4.2 mm ventral from dura; females: 0.5 mm lateral to midline, 2.3 mm anterior to bregma, and 4 mm ventral from dura). This experiment used an AAV5-packaged construct to induce expression of yellow fluorescent protein (YFP) under a calcium/calmodulin-dependent protein kinase II alpha (CaMKII α) promoter. CaMKII α promoters predominantly induce expression in excitatory glutamatergic neurons (Wood et al., 2019). For retrograde tract-tracing experiments (Experiment 2), rats received 2 separate unilateral microinjections (males 0.2 μ L, females 0.15 μ L) of retrograde-transported AAV (AAVretro) constructs (Addgene) in the RVLM and CVLM (RVLM-males: +1.9 mm lateral to midline, -12.25 mm posterior to bregma, and -10.4 mm ventral from skull; CVLM-males: +1.85 mm lateral to midline, -12.45 mm posterior to bregma, -12.00 mm ventral from skull, and angled at -8° directed-posteriorly; RVLM-females: +1.8 mm lateral to midline, -12 mm posterior to bregma, and -10.1 mm ventral from skull; CVLM-females: +1.65 mm lateral to midline, -12.40

mm posterior to bregma, -11.3 mm ventral from skull, and angled at -8° directed-posteriorly). An AAVretro construct encoding a mCherry fluorophore targeted the RVLM while an AAVretro encoding a GFP fluorophore targeted the CVLM. Injection laterality was counter-balanced throughout the experiment. AAVretro constructs expressed under a human synapsin promoter (hSyn1). For optogenetic terminal stimulation experiments (Experiment 3), rats received bilateral microinjections (males 1.5 μL , females 1 μL) of AAV constructs (UNC Vector Core) in the vmPFC (males: 0.6 mm lateral to midline, 2.7 mm anterior to bregma, and 4.2 mm ventral from dura; females: 0.5 mm lateral to midline, 2.3 mm anterior to bregma, and 4 mm ventral from dura). AAV5-packaged constructs induced expression of YFP in control rats or channelrhodopsin-2 (ChR2) conjugated to YFP. These viral constructs were under the control of the hSyn promoter as long-range vmPFC projection neurons are overwhelming glutamatergic (Myers et al., 2014). All microinjections used a 25-gauge, 2- μL microsyringe (Hamilton, Reno, NV) and a microinjector (Kopf, Tujunga, CA) at a rate of 5 minutes/ μL for vmPFC injections and a rate of 10 minutes/ μL for RVLM and CVLM injections. For RVLM injections, the needle was lowered ventrally to -6 mm from the skull and then lowered in -0.5 mm increments every 4 minutes to reduce damage to the respiratory column. The needle was left in place for 10 minutes before and after injections to facilitate viral diffusion. The skin was closed with wound clips that were removed after 2 weeks of recovery. 6 weeks of incubation was given to ensure appropriate viral construct expression (Wallace et al., 2021; Wood et al., 2019).

2.2.4 Fiber Optic Cannulations

For Experiment 3, male and female rats were anesthetized with aerosolized isoflurane (1-5%) and administered an analgesic (0.6 mg/kg buprenorphine-SR, subcutaneous) and antibiotic

(5 mg/kg gentamicin, intramuscular) 4 weeks after microinjections. Unilateral fiber optic cannulas (flat tip, 200 μ m diameter, 9.7 mm long for males, 9.4 mm long for females) (Doric Lenses, Québec, Canada) targeted the RVLM (males: +1.82 mm lateral to midline, -12.25 mm posterior to bregma, and -10.2 mm ventral from bregma; females: +1.79 mm lateral to midline, -11.9 mm anterior to bregma, and -9.95 mm ventral from bregma). Fiber optic laterality was counterbalanced, and cannulas were secured via a dental cement headcap (Stoelting, Wood Dale, IL) using dispersed metal screws (Plastics One, Roanoke, VA) as support points. Skin was sutured closed then sutures were removed 10-14 days later. After 2 weeks of recovery, rats underwent 3 days of handling for habituation to tethering.

2.2.5 Photostimulation Parameters

Light pulses (5.9-6.4 mW, 5 ms pulses, 10 Hz) were delivered through a fiber-optic patch cord (400 μ m core diameter, NA = 0.57; Doric Lenses, Québec, Canada) connected to a 473 nm LED driver (Doric Lenses) (Wallace et al., 2021). Optic power was measured using a photodiode sensor (PM160; Thorlabs Inc, Newton, NJ) at the cannula fiber tip in a dark room.

2.2.6 Estrous Cycle Cytology

Female rats for each experiment were run simultaneously, housed in the same room, and swabbed for estrous cycle cytology. Following experimental assays, vaginal cytology was examined to approximate the estrous cycle stage. A cotton swab dipped in deionized water was used to collect cells from the vaginal canal and roll them onto a glass slide. When dried, slides were viewed under a 10x objective light microscope by a minimum of two blind observers and were categorized as proestrus, estrus, metestrus, or diestrus (Cora et al., 2015; Solomon et al.,

2007; Wallace et al., 2021). Any cases with differing estrous stages were resolved by a third blind observer. The distribution of rats in each estrous phase are in Table S1 for each in vivo assay.

2.2.7 Restraint Stress

Restraint stress was used for identifying stress-activated cells (Experiment 2) and to examine neuroendocrine responses to acute stress (Experiment 3). Rats were placed in plastic decapicones (Braintree Scientific, Braintree, MA) and a small window was cut in the plastic to expose the cannula as previously described (Wallace & Myers, 2023). Next, fiber-optic patch cords were attached for optic stimulation throughout the 30-minute restraint. Blood samples were collected via tail clip at the start of restraint with sequential samples taken at 15- and 30-minute timepoints (Myers et al., 2017). At 30 minutes, patch cords were detached and rats returned to the homecage for recovery. Additional blood samples were collected at 60- and 90-minute timepoints. Blood glucose was measured as an indicator of sympathetic outflow to the periphery as acute glucose mobilization is epinephrine-dependent and enhanced by RVLM catecholaminergic stimulation (Zhao et al., 2017). Blood glucose was measured with Contour Next EZ glucometers (Bayer, Parsippany, NJ) and an average of 2 readings were used at each time point. Blood samples were centrifuged at $3000 \times g$ for 15 minutes at $4^{\circ} C$ and plasma was stored at $-20^{\circ} C$ until ELISA analysis. Plasma corticosterone was measured using an ENZO Corticosterone ELISA (ENZO Life Sciences, Farmingdale, NY) with an intra-assay coefficient of variation of 8.4% and an inter-assay coefficient of variation of 8.2% (Bekhbat et al., 2018; Dearing et al., 2021).

2.2.8 Real-Time Place Preference

The RTPP assay was used to assess valence, or the hedonic quality of vmPFC-RVLM stimulation (Stamatakis & Stuber, 2012). Cannulated rats were attached to fiber-optic patch cord for light delivery and rats were placed in a matte black fiberglass arena (Alpha Plastics and Design, Fort Collins, CO) with two chambers connected by a corridor (chambers: 15" x 15"; corridor: 8" x 6"; entire arena 15" deep). Rats explored the arena for 15 minutes for habituation. During another 15-minute session the next day, rats received 473 nm light pulses when occupying an assigned stimulation chamber. Assigned stimulation chambers were counter-balanced and animal testing was randomized throughout the experiment. Each trial was recorded by a camera mounted above the arena and rat movement was tracked using Ethovision software (Noldus Information Technologies, Leesburg, VA). Tracking software was linked to the LED drivers to automate optics during the assay by a mini USB-IO box (Noldus Information Technologies). The time rats spent on the stimulation side was divided by the total time and multiplied by 100 to calculate the percentage of time spent on the stimulation side.

2.2.9 Tissue Collection

After experiments, all rodents were anesthetized using sodium pentobarbital (≥ 100 mg/kg, intraperitoneal) and then transcardially perfused with 0.9% saline followed by 4% phosphate-buffered paraformaldehyde. Brains were post-fixed in paraformaldehyde overnight and then stored in 30% sucrose at 4 °C. Brains were subsequently sectioned (30 μ m thick 1:12 serial coronal sections) and stored in cryoprotectant solution at -20 °C until immunohistochemistry. Rats in experiment 2 were exposed to a 30 min restraint stressor 90 min prior to euthanasia. Rats involved in experiment 3 received optical stimulation before tissue

collection. Rats were tethered to a fiber optic patch cord and received 5 min of optic stimulation (5.9-6.4 mW, 5 ms pulses, 10 Hz) followed by 90 min of recovery for immediate-early gene (c-Fos) expression before euthanasia, as described above.

2.2.10 Immunohistochemistry

For fluorescent labeling of dopamine beta-hydroxylase (DBH), coronal sections were removed from the cryoprotectant and rinsed in phosphate buffered saline (PBS) (5 x 5 min) at room temperature. Sections were then moved to blocking solution (PBS, 0.1% bovine serum albumin, 0.2% Triton X-100) for 1 hr. Sections were then incubated overnight in mouse anti-DBH primary antibody (1:2500 in blocking solution, MAB394, RRID: AB_94983; MilliporeSigma, Burlington, MA). Next, sections were rinsed in PBS (5 x 5 min) and then incubated in donkey anti-mouse Cy3 secondary antibody (1:200 in PBS, 715-165-020, RRID: AB_2340811; Jackson ImmunoResearch, West Grove, PA) for 1 hr. The tissue was then washed in PBS (5 x 5 min) and placed into a DAPI stain solution (300 nM in PBS, D3571, RRID: AB_2307445; ThermoFisher Scientific, Portsmouth, NH) for 10 minutes. After another PBS wash (5 x 5 min), the tissue was mounted in polyvinyl medium and cover-slipped for imaging.

For fluorescent labeling of c-Fos (Experiment 3), coronal sections were rinsed in PBS (5 x 5 min) and moved to blocking solution (PBS, 0.1% bovine serum albumin, 0.2% Triton X-100) for 1 hr. Sections were incubated for 48 hours in rabbit anti-c-Fos primary antibody (1:1000 in blocking solution, 226_003, waiting on RRID approval; Synaptic Systems, Goettingen, Germany). Next, sections were rinsed in PBS (5 x 5 min) and incubated in donkey anti-rabbit Cy5 secondary antibody (1:1000 in PBS, 711-175-152, RRID: AB_2340607; Jackson ImmunoResearch) for 1 hr. After, the tissue was washed in PBS (5 x 5 min), mounted in

polyvinyl medium, and cover-slipped for imaging. For retrograde tract-tracing experiments (Experiment 2), a different version of the c-Fos antibody (226_008, Synaptic Solutions, Goettingen, Germany) was used due to the original version being discontinued.

When double labeling DBH and c-Fos (Experiment 4), sections were rinsed in PBS (5 x 5 min) then moved to blocking solution (PBS, 0.1% bovine serum albumin, 0.2% Triton X-100) for 1 hr. Subsequently, sections were incubated overnight in mouse anti-DBH primary antibody. Next, sections were rinsed in PBS (5 x 5 min) then incubated in donkey anti-mouse Cy3 secondary antibody for 1 hr. The tissue was then washed in PBS (5 x 5 min) and blocking solution (PBS, 0.1% bovine serum albumin, 0.2% Triton X-100) for 1 hr. Sections were incubated for 48 hours in rabbit anti-c-Fos primary antibody. Next, sections were rinsed in PBS (5 x 5 min) and incubated in donkey anti-rabbit Cy5 secondary antibody for 1 hr. Lastly, the tissue was washed in PBS (5 x 5 min), mounted in polyvinyl medium, and cover-slipped for imaging.

To visualize GABA, sections were retrieved, rinsed, and incubated for 4 hr in blocking solution (7.5% normal goat serum, 6% BSA, 1.5% normal donkey serum in 50 mM KPBS). Sections were then incubated in rabbit anti-GABA primary antibody (1:250 in blocking solution, AB141, RRID: AB_11214017; MilliporeSigma) for 60 h. Primary antibody labeling was amplified with biotinylated goat anti-rabbit IgG for 2 hr (1:500 in PBS, BA-1000, RRID: AB_2313606; Vector Laboratories; Burlingame, CA) followed by Vectastain ABC Solution for 1 hr (1:500 in PBS, PK-7100, RRID: AB_2336827; Vector Laboratories) then Cy3-conjugated streptavidin for 1 hr (1:500 in PBS, 016-160-084, RRID: AB_2337244; Jackson ImmunoResearch). Finally, the tissue was washed in PBS (5 x 5 min), mounted in polyvinyl medium, and cover-slipped for imaging.

For immunolabeling glycine transporter 2 (GlyT2), sections were rinsed and blocked for 1 hr (PBS, 0.1% bovine serum albumin, 0.2% Triton X-100). Sections were incubated for 48 hours in rabbit anti-GlyT2 primary antibody (1:1000 in blocking solution, Af1290, RRID: AB_2571606; Frontier Institute, Japan, Shinkonishi). Sections were then rinsed in PBS (5 x 5 min) and incubated in donkey anti-rabbit Cy5 secondary antibody (1:1000 in PBS, 711-175-152, RRID: AB_2340607; Jackson ImmunoResearch) for 1 hr. After, the tissue was washed in PBS (5 x 5 min), mounted in polyvinyl medium, and cover-slipped for imaging.

2.2.11 Microscopy

All fluorescent microscopy used a Zeiss Axio Imager Z2 microscope (Carl Zeiss Microscopy, Jena, Germany) and the corresponding ZEN 2.6 blue edition software (Carl Zeiss Microscopy). To determine injection placement, YFP was imaged using the 10x objective, while YFP and DBH dual fluorescence imaging used a 63x objective and 0.5- μ m thick optical sectioning to produce Z-stacks. For mapping AAVretro-mCherry and -GFP injections and labeled cells, 20x tiled images were taken. Co-localization was defined as purple or yellow fluorescence from the overlap between labeled mCherry or GFP terminals and c-Fos Cy5. RVLM cannula placements were mapped using a 10x tiled slide scan. For c-Fos and c-Fos/DBH quantification after stimulation, 10x tiled images were acquired to determine if nuclear c-Fos labeling was surrounded by the cytosolic DBH labeling. Lastly, GABA and GlyT2 were imaged with a 63x objective and 0.5- μ m thick optical sectioning. In all imaging cases, an off-channel filter was used to exclude auto-fluorescent cells that may affect results.

2.2.12 Image Analysis

For anterograde tract-tracing experiments (Experiment 1), Carl Zeiss Images (CZIs) were imported to a computer equipped with Imaris 8.1.2 (Oxford Instruments, Oxford, UK) to identify and quantify DBH-labeled neurons and YFP-expressing vmPFC terminals. Further, high-magnification 3-D imaging enabled identification of putative terminal appositions on medullary cell bodies, or YFP-expressing fibers overlapping with DBH-labeled neurons. For retrograde tract-tracing experiments (Experiment 2), tiled CZI images were analyzed using ImageJ Fiji (ver. 1.51N) to quantify RVLM- and CVLM-projecting vmPFC neurons. For c-Fos quantification of vmPFC-RVLM terminal stimulation cases (Experiment 3), ImageJ Fiji was utilized to quantify c-Fos-labeled cells in the RVLM. For c-Fos/DBH colocalization experiments (Experiment 4), ImageJ Fiji was used to quantify the number of cells expressing c-Fos and DBH separately or together. Colocalization was defined by nuclear c-Fos-Cy5 signal surrounded by DBH-Cy3 signal.

2.2.13 Neuroanatomy

To anatomically delineate mPFC, the bregma location and area delineations of each tissue section were defined according to the Brain Maps III: Structure of the Rat Brain (Swanson, 2004). The atlas was used to identify the anterior forceps of the corpus callosum as the lateral boundary and the coronal midline as the medial boundary. The rostral-caudal emergence of the corpus callosum was used to divide the subregions from dorsal to ventral and the subependymal zone guided the identification of the ventral vmPFC boundary. To delineate the RVLM, The Rat Brain atlas (Paxinos & Watson, 2006) was used for area delineations and landmark identification throughout the brainstem. The RVLM lacks distinct cytoarchitecture, therefore, DBH-labeling

was repeatedly used to identify the RVLM while landmarks such as the facial nucleus served as the rostral boundary, spinal trigeminal nucleus served as the lateral boundary, and lateral portions of the inferior olive guided distinguishing the medial boundary. Regarding VLM subregions, The Rat Brain atlas (Paxinos and Watson, 2006) defines the whole VLM as -12.00 to -15.00 mm from bregma, with catecholaminergic populations transitioning from C1, C1/A1, and A1 in a rostro-caudal orientation. We used these catecholaminergic populations to define what we considered RVLM (-12.00 to -13.56 mm posterior to bregma), intermediate VLM (-13.68 to -14.16 mm posterior to bregma), and CVLM (Bregma -14.28 to -15.00 mm posterior to bregma) (Li et al., 2018). Notably, our classification regards the RVLM as containing catecholaminergic neurons that have bulbospinal as well as ascending projections. Further, templates of rat brain coronal sections from Brain Maps III (Swanson, 2004) were used to illustrate virus and cannula placement.

2.2.14 Data Analysis

Data are expressed as mean \pm standard error of the mean. Data were analyzed using Prism 9 (GraphPad, San Diego, CA), with statistical significance set at $p < 0.05$ for all tests. A one-way ANOVA was used to analyze the number of cells with appositions and the number of appositions per cell across VLM subregions. For retrograde tract-tracing experiments, a one-way ANOVA was used to analyze density of medullary-projecting vmPFC neurons. Stimulation induced c-Fos counts were analyzed with Welch's unpaired t-test comparing treatment groups. RTPP stimulation preference was assessed via Welch's unpaired t-test comparing treatment groups. Corticosterone and glucose measured during restraint stress were analyzed using a repeated mixed-effects analysis with treatment and time as factors. If significant main or

interaction effects are present, then a Fisher's post-hoc test was used. DBH/c-Fos colocalization analyses used a Welch's unpaired t-test. Throughout all experiments, comparisons were limited to within-sex as differences in construct expression across sexes confound comparisons.

2.3 Results

2.2.1 vmPFC Glutamate Projections to Catecholaminergic VLM Neurons

Microinjections of the viral construct expressing YFP under the CaMKII α promoter targeted the vmPFC of adult male and female rats (Figure 2.1A), and placement was mapped using a rat brain atlas (Figure 2.1C,G). Anterograde injections typically infected fewer vmPFC starter neurons in females than males (average surface area of YFP injection site: males 2.149 mm²; females 1.397 mm²). YFP-expressing vmPFC fibers were observed following viral transduction in the ventrolateral medulla (VLM) (Figure 2.1B). In the VLM, neurons were immunolabeled for the epinephrine- and norepinephrine-synthesis enzyme, DBH. Further, given the lack of cytoarchitectonic parcellations or laminations in the VLM, the presence of DBH+ neurons and the use of regional landmarks (facial, trigeminal, and olivary nuclei) helped to define VLM spatial boundaries. Next, putative appositions of YFP-expressing vmPFC fibers on catecholaminergic VLM cell bodies were quantified throughout the VLM in male (Figure 2.1D) and female (Figure 2.1H) rats. In males, vmPFC fibers apposed most DBH+ VLM neurons in the rostral, intermediate, and caudal portions of the VLM (Figure 2.1E). The quantity and density of vmPFC appositions on catecholaminergic neurons did not vary by VLM subregion, (Figure 2.1E,F) [quantity of appositions, $n = 6$, one-way ANOVA ($F(2,12) = 0.43$, $p = 0.66$); number of appositions, $n = 5$, one-way ANOVA ($F(2,12) = 0.57$, $p = 0.58$). Similarly, in females, YFP-expressing vmPFC fibers apposing DBH+ neurons were seen across the VLM (Fig. 1H, I)

[F(2,6) = 0.22, p = 0.98]. Again, appositions on DBH+ neurons were not significantly different by VLM subregion (Fig. 1J) [F(2,6) = 0.052, p = 0.95]. These anterograde tract-tracing studies revealed glutamatergic vmPFC neurons target catecholaminergic neurons throughout the VLM in male and female rats.

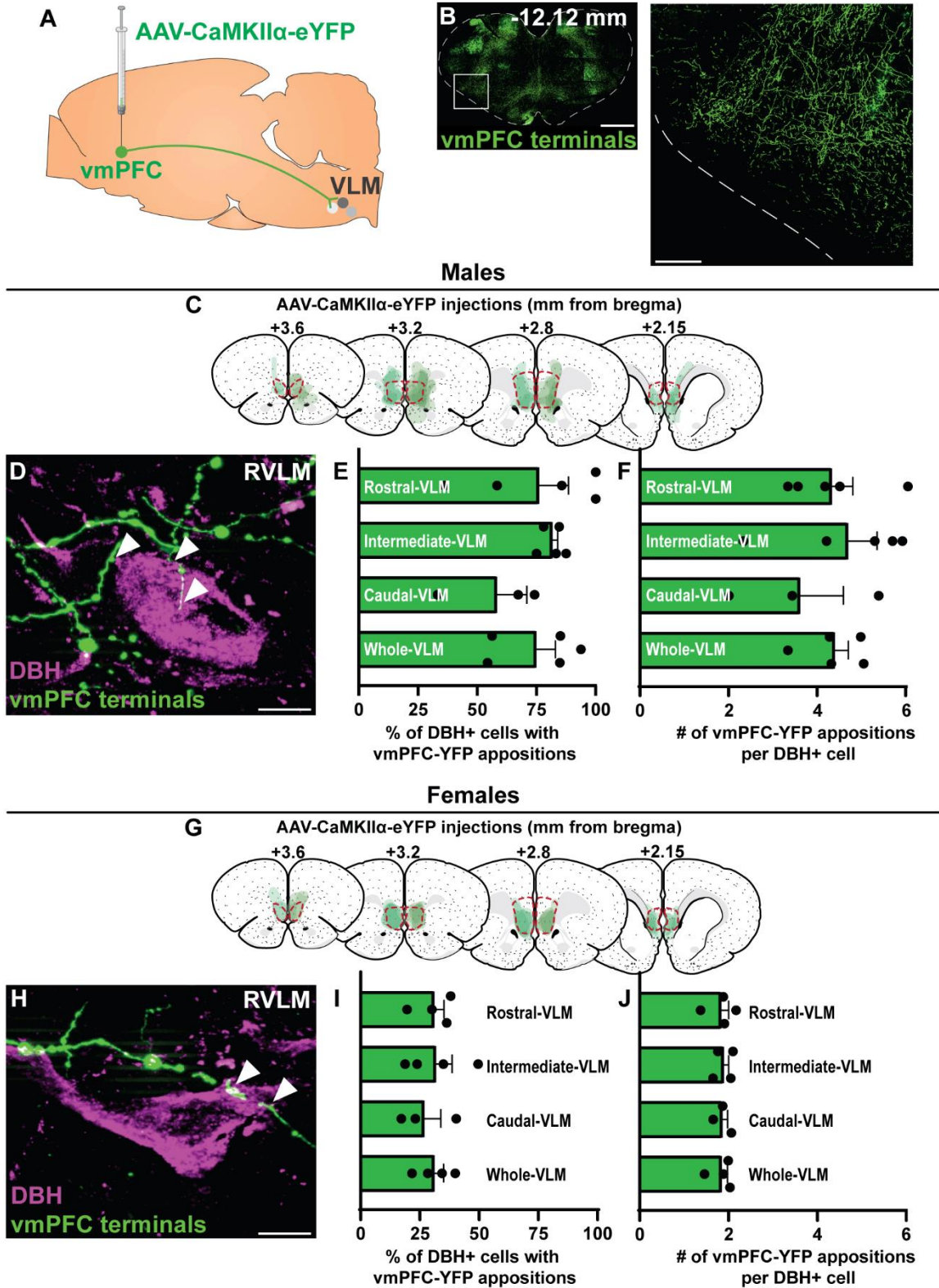


Figure 2.1 vmPFC neurons project to catecholaminergic neurons throughout the VLM. AAV-YFP was injected into the vmPFC and terminal expression of YFP was identified in the VLM, scale bar: 1 mm, inset scale bar: 250 μ m (A, B). Male rat microinjections were mapped onto

Swanson Rat Brain Atlas (3rd edition) coronal sections with the vmPFC outlined and rostral-caudal distance to bregma noted above sections (C). YFP-expressing terminals apposed catecholaminergic neurons, labeled with DBH, arrowheads denote appositions, scale bar: 5 μm (D). vmPFC terminals apposed the majority of male DBH+ neurons throughout the VLM subregions (E). The number of vmPFC terminal appositions per each DBH+ VLM neuron was similar throughout the VLM (F). Female rat microinjections were mapped onto coronal sections with the vmPFC (red outline) and rostral-caudal distance to bregma noted above sections (G). Putative appositions of YFP-expressing on DBH+ neurons were observed, arrowheads denote appositions, scale bar: 5 μm (H). vmPFC terminal appositions similarly targeted DBH+ neurons throughout the female VLM and individual subregions (I). The number of vmPFC terminal appositions per each DBH+ VLM neuron was similar throughout the VLM (J). AAV-CaMKII α -eYFP: adeno-associated virus to express YFP under a calcium/calmodulin-dependent protein kinase II alpha promoter, DBH: dopamine beta-hydroxylase, RVLM: rostral ventrolateral medulla, vmPFC: ventromedial prefrontal cortex, YFP: yellow fluorescent protein.

2.3.2 Organization and Stress Responsiveness of RVLM- and CVLM-Projecting vmPFC Neurons

The parallel, divergent, or mixed circuit organization of stress-activated vmPFC ensembles that target the RVLM and CVLM was investigated. Dual injections of retrograde-transported viruses separately targeted the RVLM and CVLM in the same subjects (Figure 2.2A). AAVretro-mCherry was injected into the RVLM and AAVretro-GFP was injected into the CVLM (Figure 2.2B). Viral injection spread and placement were mapped using a rat brain atlas (Figure 2.2D,G). Here, the male and female vmPFC was surveyed for RVLM- and CVLM-projecting neurons, as well as co-labeling of c-Fos in response to stress (Figure 2.2C). In males, no differences were seen in the density of vmPFC cells projecting to the RVLM and CVLM individually, as well as both the RVLM and CVLM [$n = 3/\text{group}$, one-way ANOVA: $F(2,6) = 0.33$, $p = 0.73$] (Figure 2.2E). Further, the percentage of stress-reactive vmPFC neurons did not change across neuroanatomical targets [$n = 3/\text{group}$, one-way ANOVA: $F(2,6) = 0.14$, $p = 0.87$] (Figure 2.2F). Similar trends were seen in females. No differences were evident between the density of vmPFC cells projecting to differing medullary areas [$n = 3/\text{group}$, one-way ANOVA:

$F(2,9) = 1.07, p = 0.38]$ (Figure 2.2H). Additionally there were no differences between the percentage of stress-reactive vmPFC neurons across neuroanatomical targets [$n = 3/\text{group}$, one-way ANOVA: $F(2,9) = 0.33, p = 0.73]$ (Figure 2.2I). In all, stress-reactive vmPFC cells targeted the RVLM and CVLM through both parallel and divergent pathways.

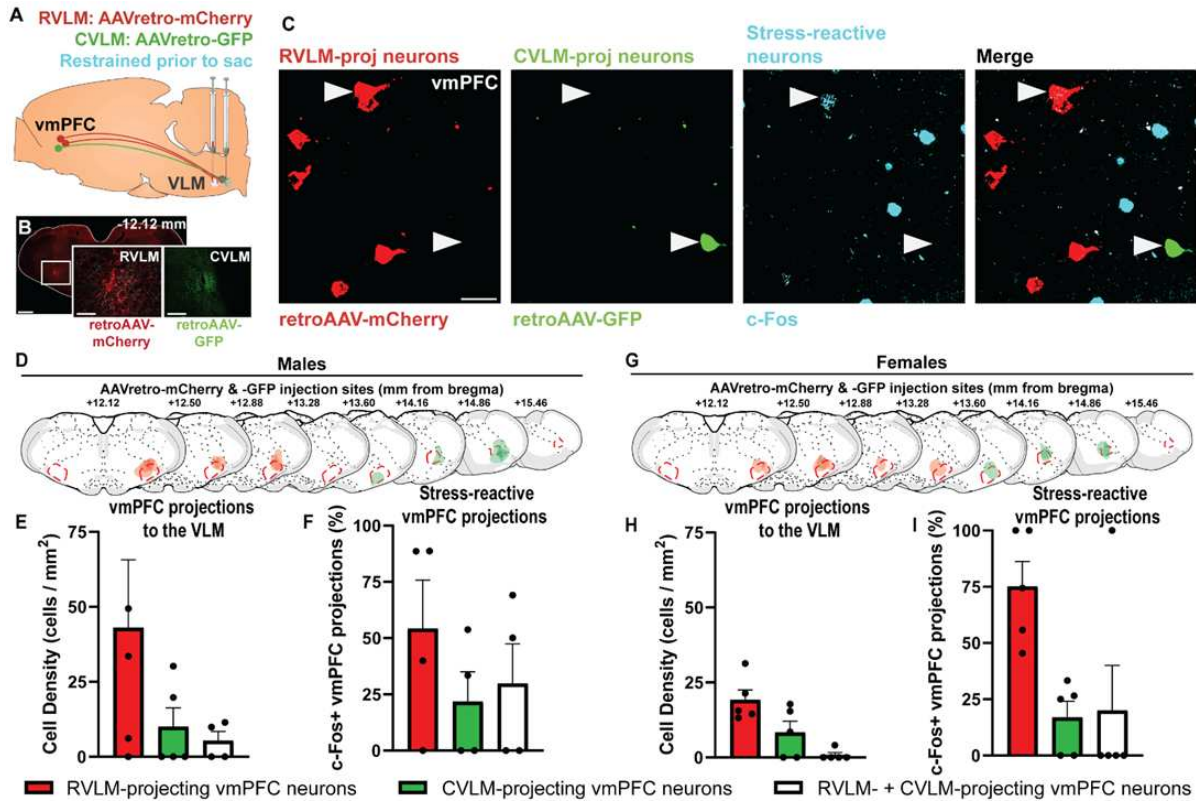


Figure 2.2 Stress-activated vmPFC neurons target the RVLM and CVLM. AAVretro constructs expressing mCherry or GFP were injected into the RVLM and the CVLM, respectively, scale bar: 1 mm, inset scale bar: 250 μm (A, B). mCherry- and GFP-labeled neurons were present in the vmPFC, as well as c-Fos+ cells following restraint stress, scale bar: 10 μm (C). Male and female rodent microinjections were mapped onto Swanson Rat Brain Atlas (3rd edition) coronal sections with the RVLM and CVLM outlined (D, G). In male rats, the density of vmPFC neurons projecting to the RVLM, CVLM, and both regions simultaneously were not statistically different (E). VLM-projecting neurons were stress-reactive across the vmPFC (F). In female rats, the density of vmPFC neurons projecting to the RVLM, CVLM, and both regions simultaneously were not significantly different (H). Female VLM-projecting neurons throughout the vmPFC were stress-reactive (I). AAVretro: retrograde-traveling adeno-associated virus, CVLM: caudal ventrolateral medulla, GFP: green fluorescent protein, RVLM: rostral ventrolateral medulla, vmPFC: ventromedial prefrontal cortex.

2.3.3 Optogenetic vmPFC-RVLM Circuit Stimulation

To determine the functional effects of the vmPFC-RVLM circuit, we used an optogenetic terminal stimulation strategy (Figure 2.3A-D). Stimulation increased RVLM c-Fos+ cell density (# of c-Fos+ cells /mm²) of ChR2 compared to YFP controls, in both male and female rats [males (n = 4-5/group, unpaired t-test: ChR2 vs YFP $t(7) = 3.70$, $p = 0.0076$); females (n = 4-6/group, unpaired t-test: ChR2 vs YFP $t(7) = 4.02$, $p = 0.0051$)] (Figure 2.3E-J).

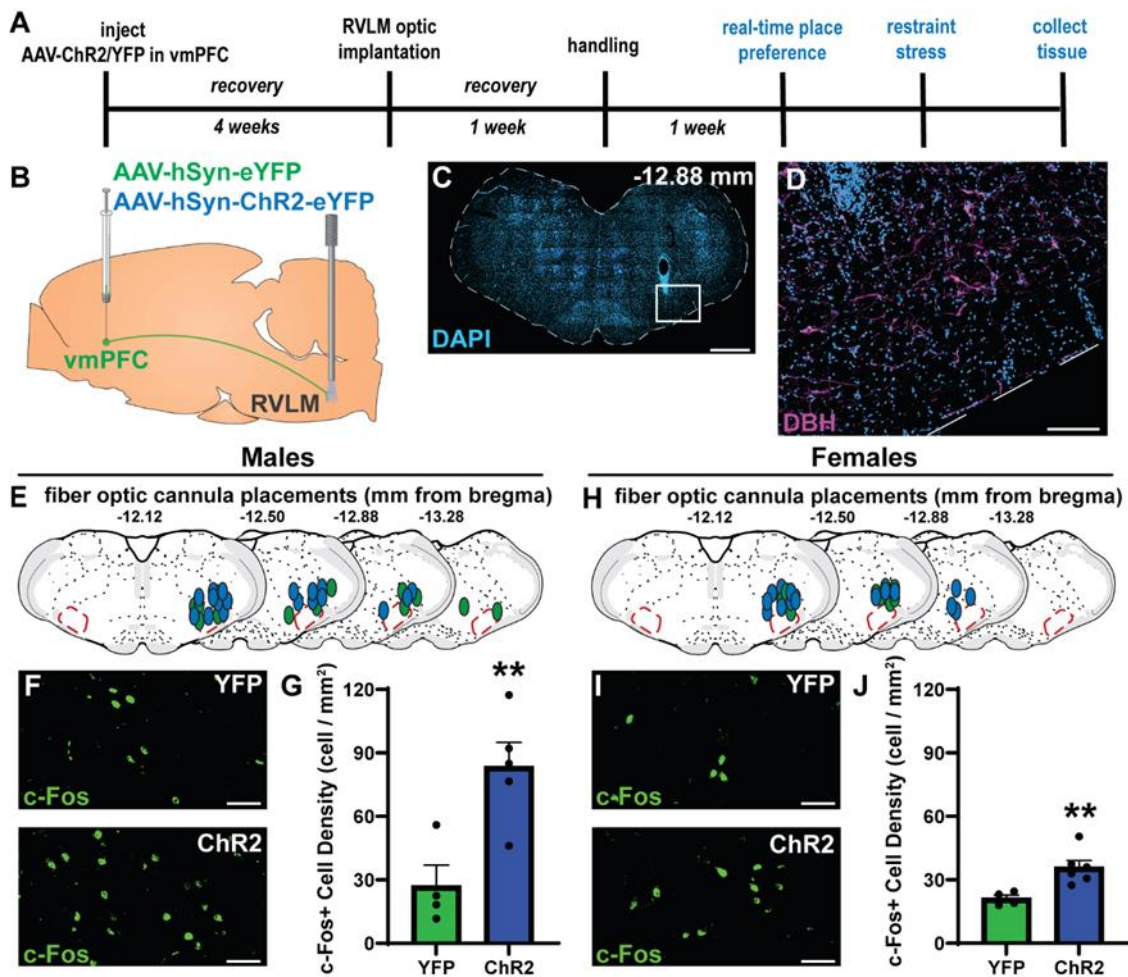


Figure 2.3 vmPFC terminals stimulated in RVLM increase c-Fos+ neurons. vmPFC-RVLM terminal stimulation experiment timeline (A). AAV-YFP or -ChR2 was injected into the vmPFC and a light-emitting optic fiber was implanted dorsal to the RVLM to stimulate vmPFC synapses at the vmPFC, scale bar: 1 mm, inset scale bar: 200 μ m (B-D). Male and female counterbalanced unilateral cannulations were mapped onto Swanson Rat Brain Atlas (3rd edition) coronal

sections with the RVLM outlined (E, H). vmPFC-RVLM stimulation increased immunoreactive c-Fos cells in the RVLM of male and female rats, scale bars: 50 μm (F, G, I, J). AAV-hSyn-eYFP: adeno-associated virus to express YFP under a synapsin promoter, AAV-hSyn-ChR2: adeno-associated viral package to express ChR2 under the under a synapsin promoter, ChR2: channelrhodopsin-2, DBH: dopamine beta-hydroxylase, RVLM: rostral ventrolateral medulla, vmPFC: ventromedial prefrontal cortex, YFP: yellow fluorescent protein. * $p < 0.05$, ** $p < 0.01$.

2.3.4 Motivational Valence of vmPFC-RVLM Circuit Stimulation

We examined whether vmPFC-RVLM circuit stimulation induces preference or avoidance behavior using the RTPP assay (Figure 2.4A). Here, the ChR2 and YFP groups spent the similar amounts of time in both chambers of the RTPP arena [males ($n = 11-17/\text{group}$, unpaired t-test: ChR2 vs YFP $t(30) = 0.26$, $p = 0.79$); females ($n = 12-16/\text{group}$, unpaired t-test: ChR2 vs YFP $t(26) = 0.78$, $p = 0.44$)] (Figure 2.4B,C). Further, no locomotive phenotype was observed in male or female rats [males distance ($n = 11-17/\text{group}$, unpaired t-test: ChR2 vs YFP $t(26) = 0.48$, $p = 0.63$); females distance ($n = 12-16/\text{group}$, unpaired t-test: ChR2 vs YFP $t(26) = 0.25$, $p = 0.80$)] (Figure 4D,E). Thus, although vmPFC mediates affective and reward behaviors (Fuchikami et al., 2015; Pace et al., 2020; Wallace et al., 2021), the vmPFC-RVLM circuit has neutral valence.

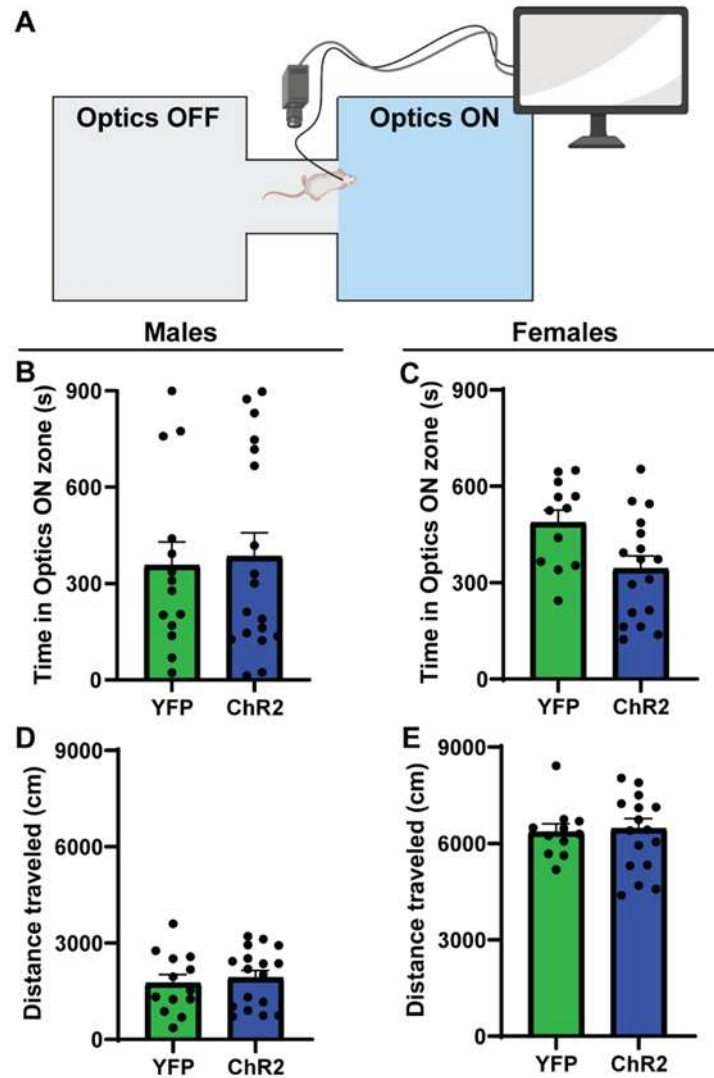


Figure 2.4 Stimulating the vmPFC-RVLM circuit does not change preference behavior. Cannulated rats underwent a real-time place preference assay in a 2-chamber arena with a connecting space (A). Male and female rats did not show preference or aversion for vmPFC-RVLM stimulation (B, C). Male and female ChR2 groups had no differences in total locomotion relative to YFP controls (D, E).

2.3.5 vmPFC-RVLM Circuit Regulation of Stress Reactivity

Next, we sought to examine physiological regulation by the vmPFC-RVLM pathway by activating the circuit during stress. We assessed sympathetic and neuroendocrine stress responses by measuring blood glucose and plasma corticosterone, respectively. In males, glucose levels were decreased in ChR2 rats compared to controls at the 30 minute time point of restraint stress

[n = 11–17/group, mixed-effects: time F(4,125) = 17.51, p < 0.0001; time x ChR2 F(4,125) = 2.79, p = 0.029; 30 min ChR2, p = 0.0088] (Figure 2.5A). Additionally, corticosterone levels were decreased in the ChR2 group following stress (Figure 2.5B) at the 60-minute time point [n = 11–17/group, mixed-effects: time F(4,80) = 10.26, p < 0.0001; 60 min ChR2, p = 0.035]. In contrast, glucose levels were not different at any timepoint (Figure 2.5C) in female rats [n = 12–16/group, mixed-effects: time F(4,121) = 19.71, p > 0.05]. However, corticosterone was significantly decreased (Figure 2.5D) at the 30-minute time point in female ChR2 rats compared to YFP controls [n = 12–16/group, mixed-effects: time F(4,116) = 19.71, p < 0.0001; 30 min ChR2, p = 0.025]. These results indicate that activation of the vmPFC-RVLM pathway reduced stress-induced glucocorticoid release in both sexes and stress-induced hyperglycemia in males.

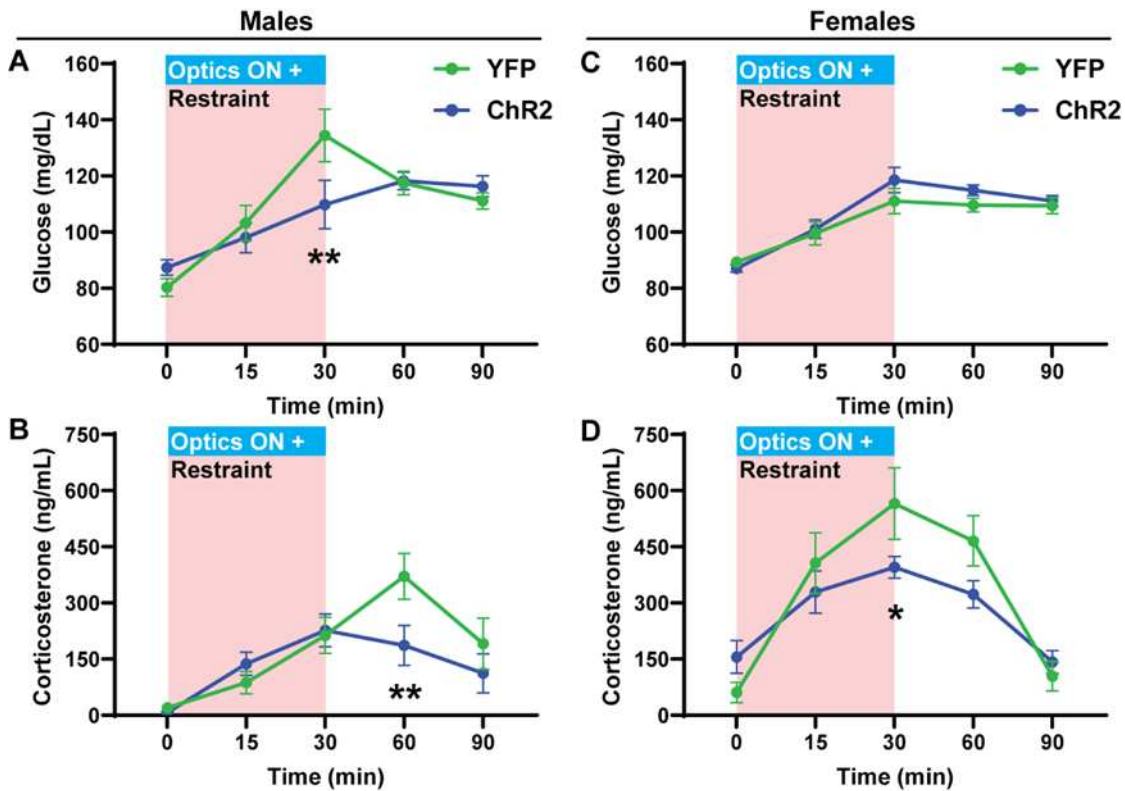


Figure 2.5 Stimulating the vmPFC-RVLM circuit during restraint stress blunts corticosterone release in both sexes and glucose mobilization in males. Male ChR2 rats had blunted stress-induced glucose mobilization (A). Similarly, male ChR2 rats had reduced corticosterone stress

responses (B). Female Chr2 and YFP groups had similar glycemic responses to stress (C). Female Chr2 rats had reduced stress-induced corticosterone secretion (D). * $p < 0.05$, ** $p < 0.01$.

2.3.6 The vmPFC-RVLM Circuit Preferentially Activates Non-Catecholaminergic Cells

Tissue was collected after vmPFC-RVLM stimulation and immunolabeled for DBH and c-Fos to determine if circuit stimulation activated catecholaminergic RVLM neurons (Figure 2.5A,B). In males, c-Fos+ cell density (# of c-Fos+ cells / mm^2) in DBH+ neurons was comparable in YFP and Chr2 groups [whole VLM ($n = 4\text{-}5/\text{group}$, unpaired t-test: Chr2 vs YFP $t(7) = 2.69$, $p = 0.07$)] (Figure 2.5C). Further, VLM DBH+ cells had no differences in c-Fos expression within VLM subregions [rostral VLM (unpaired t-test: Chr2 vs YFP $t(6) = 0.28$, $p > 0.99$); intermediate VLM (unpaired t-test: Chr2 vs YFP $t(3) = 2.48$, $p = 0.17$); caudal VLM (unpaired t-test: Chr2 vs YFP $t(4) = 3.25$, $p = 0.053$)] (Figure 2.5D-F). In contrast, c-Fos+ cell density was significantly increased in DBH- cells in Chr2 rats compared to YFP [whole VLM ($n = 4\text{-}5/\text{group}$, unpaired t-test: Chr2 vs YFP $t(7) = 3.67$, $p = 0.016$)] (Figure 2.5C). This effect was present in the rostral, intermediate, and caudal subregions of the VLM [rostral VLM (unpaired t-test: Chr2 vs YFP $t(5) = 5.49$, $p = 0.0055$); intermediate VLM (unpaired t-test: Chr2 vs YFP $t(6) = 3.04$, $p = 0.048$); caudal VLM (unpaired t-test: Chr2 vs YFP $t(5) = 4.016$, $p = 0.023$)] (Figure 2.5D-F).

Similar trends were observed in females. Chr2 stimulation increased the density of c-Fos+ DBH- cells in the VLM as a whole, as well as within the rostral and intermediate subregions [whole VLM ($n = 4\text{-}6/\text{group}$, unpaired t-test: Chr2 vs YFP $t(8) = 3.34$, $p = 0.022$); rostral VLM (unpaired t-test: Chr2 vs YFP $t(8) = 4.49$, $p = 0.0049$); intermediate VLM (unpaired t-test: Chr2 vs YFP $t(6) = 3.23$, $p = 0.036$)] (Figure 2.5G-I). Although, there was no change in cFos+ DBH- cell density in the caudal VLM (unpaired t-test: Chr2 vs YFP $t(3) =$

2.50, $p = 0.17$)] (Figure 2.5J). Similar to males, there were no effects on c-Fos+ cell density of DBH+ neurons in any female VLM region [whole VLM ($n = 4-6$ /group, unpaired t-test: ChR2 vs YFP $t(7) = 1.58$, $p = 0.32$); rostral VLM (unpaired t-test: ChR2 vs YFP $t(4) = 1.63$, $p = 0.16$); intermediate VLM (unpaired t-test: ChR2 vs YFP $t(3) = 1.79$, $p = 0.16$); caudal VLM (unpaired t-test: ChR2 vs YFP $t(6) = 0.21$, $p > 0.99$)] (Figure 2.5G-J). Collectively, these data demonstrate that vmPFC terminal stimulation preferentially activates non-catecholaminergic neurons throughout the VLM in both sexes.

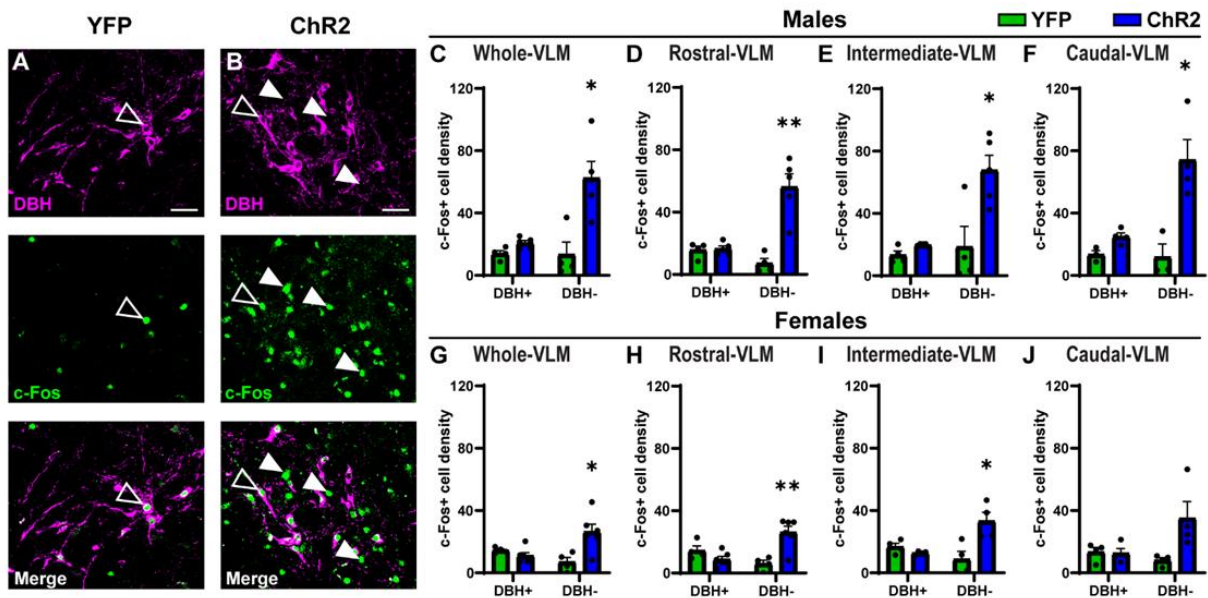


Figure 2.6 Stimulating the vmPFC-RVLM circuit preferentially activates non-catecholaminergic neurons in the ventrolateral medulla. YFP and ChR2 groups were immunolabeled for DBH and c-Fos, DBH+ and c-Fos+ cells are marked by unfilled arrowheads, DBH- and c-Fos+ cells marked by filled arrowheads, scale bars: 50 μ m (A, B). Male ChR2 rats expressed increased c-Fos in DBH- neurons throughout the VLM (C-F). Female ChR2 rats expressed increased c-Fos in DBH- neurons throughout the VLM (G-J). * $p < 0.05$, ** $p < 0.01$.

2.3.7 vmPFC Inputs Target Medullary Inhibitory Neurons

Next, we sought to identify the non-catecholaminergic VLM neurons targeted by the vmPFC. Prior work has demonstrated that a local network of inhibitory neurons acts on VLM catecholaminergic neurons to regulate sympathoexcitation (Gao et al., 2019; Guyenet et al.,

1990; Heesch et al., 2006). In fact, GABAergic and glycinergic neurons are recruited by barosensitive-neurons in the nucleus of the solitary tract to regulate RVLM outflow and control blood pressure (Guyenet, 2006; Schreihofner & Guyenet, 2002). Here, GABA and GlyT2, a marker for glycinergic neurons, were immunolabeled and YFP-expressing vmPFC fibers were found to appose GABAergic and glycinergic neurons in the RVLM (Figure 2.7A). Additionally, optogenetic stimulation led to c-Fos expression in GABAergic RVLM neurons (Figure 2.7B). The current data in aggregate support a model where vmPFC projections to inhibitory RVLM neurons provide a mechanism for limiting catecholaminergic output and subsequent physiological stress responses (Figure 2.7C).

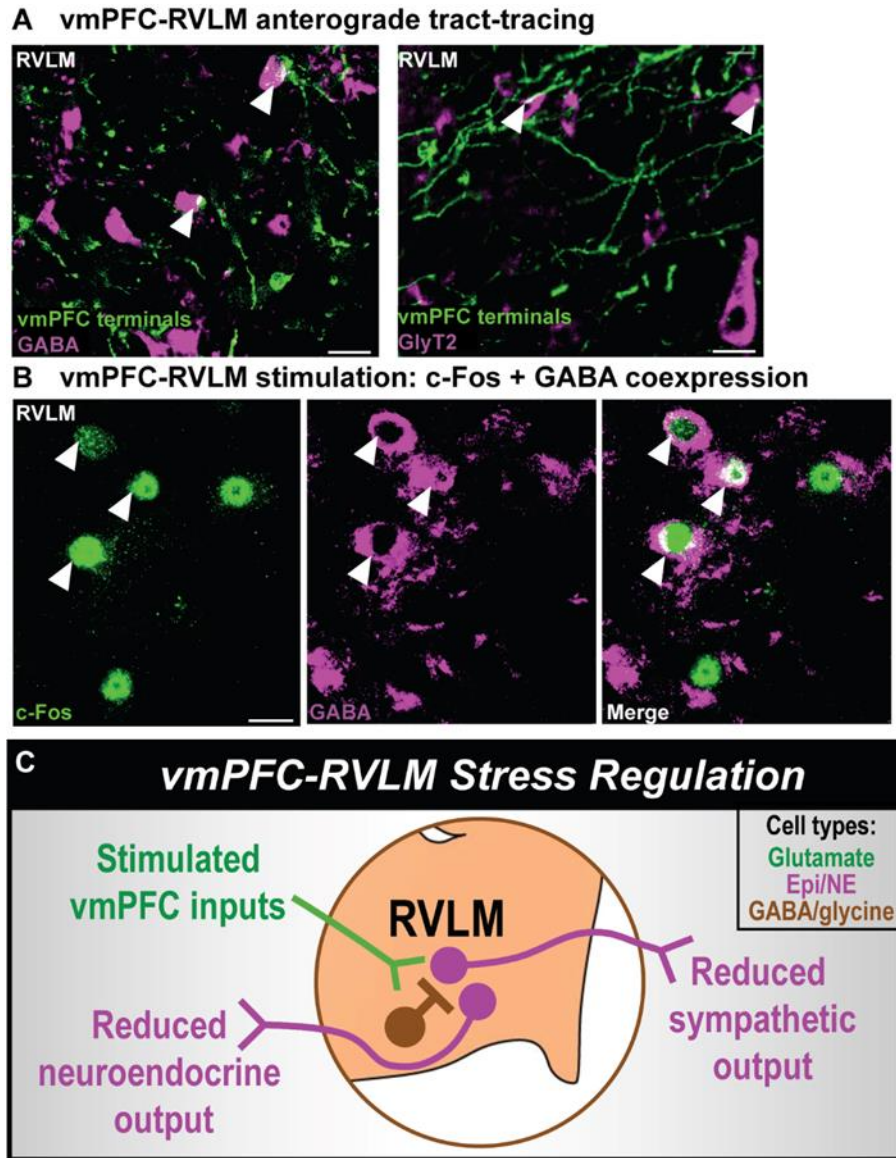


Figure 2.7 vmPFC-RVLM circuit mechanism. vmPFC terminals expressing YFP apposed GABA- and GlyT2- expressing RVLM cells, arrowheads denote appositions, scale bars: 20 μm (A). Chr2 rats were immunolabeled for c-Fos and GABA following vmPFC-RVLM stimulation, GABA+ and c-Fos+ cells are marked by arrowheads, scale bars: 20 μm (B). A schema illustrating a proposed mechanism for the vmPFC-RVLM circuit (C). Epi/NE: Epinephrine/Norepinephrine-synthesizing neurons.

2.4 Discussion

The current studies mapped a prefrontal-medullary circuit's structural and functional connectivity and identified a role in stress response inhibition. Here, vmPFC terminals apposed

catecholaminergic neurons throughout the VLM. Additionally, stress-reactive vmPFC neurons project to the RVLM and CVLM through parallel and divergent pathways. vmPFC-RVLM circuit activation also reduced glucocorticoid stress reactivity in both male and female rats, while stress-induced hyperglycemia was blunted only in males. However, the vmPFC-RVLM circuit did not mediate preference or aversion behavior in either sex. The vmPFC-RVLM circuit preferentially activated non-catecholaminergic neurons and targeted GABAergic and glycinergic neurons in the RVLM. These studies reveal a vmPFC-RVLM circuit that inhibits endocrine stress responses in male and female rats, potentially via RVLM inhibitory neurons.

2.4.1 vmPFC Regulation of Stress Responding

Human neuroimaging studies have identified the vmPFC as an integral hub for emotion, cognition, goal-directed behavior, and physiological regulation (Jennings et al., 2016; Kraynak et al., 2018; Nestler et al., 2002; Saper & Stornetta, 2014). Additionally, vmPFC gray matter and functional activity are frequently altered in depression and other stress-related disorders that disproportionately burden females (Drevets et al., 2008; Riecher-Rössler, 2017). Accordingly, rodent studies have examined the vmPFC to identify neural substrates contributing to sex-specific vulnerability (Hurley & Carelli, 2020; van der Zee et al., 2022; Woodward et al., 2023). In vivo monitoring of vmPFC projection neurons also revealed that sex and stress history shape neural activity in response to positive and aversive stimuli (Wallace & Myers, 2023). Further, stimulation of vmPFC glutamate neurons produces opposing outcomes in male and female rats. Male vmPFC neuronal stimulation reduces the HPA axis and autonomic responses to stress while enhancing sociability and motivation (Wallace et al., 2021). Female vmPFC stimulation facilitates stress responses, including hyperglycemia and tachycardia, but does not affect social

motivation (Wallace et al., 2021). Mechanisms for cortical regulation of stress responding may lie in downstream circuitry. The current report found that the vmPFC-RVLM pathway inhibits physiological stress responding in both sexes without effects on preference behavior. Therefore, this projection to the brainstem may account, in part, for the stress-inhibitory effects of male vmPFC (Wallace et al., 2021). However, the current results do not align with prior reports of female cortical stress excitation (Wallace et al., 2021). The vmPFC-RVLM circuit inhibits stress responding in both sexes, a largely sex-similar function.

2.4.2 Importance of Biological Sex

Although our findings demonstrate that vmPFC-RVLM activation reduces stress reactivity in both sexes, differences may still exist between the sexes. Male and female data were not statistically compared due to experiments occurring at different times. However, there appear to be magnitude differences in circuit structure and function as anterograde/retrograde mapping and c-Fos expression point toward more robust connectivity in males. The sex-specific glycemic regulation reported may relate to differences in circuit strength. However, it is challenging to disentangle the potential effects of biological sex from necessary differences in experimental parameters. There were subtle differences in the volume of viral constructs administered to generate similar anatomical coverage in the targeted nuclei of the male and female brains. Hence, although the general properties of circuit organization and function were similar in males and females, multiple factors prevent direct comparison of male and female results and limit the interpretation of sex-specific outcomes such as glucose mobilization. Nonetheless, there are reports of sex differences in sympathoexcitation, and endogenous glucose production is higher in males than females (Amiel et al., 1993). Sex differences in sympathetic activity likely involve

the RVLM as estrogen receptors alpha ($ER\alpha$) and beta ($ER\beta$) are present in catecholaminergic and non-catecholaminergic RVLM neurons of female rats (Hay, 2016; Saleh & Connell, 2000; Wang et al., 2006). Interestingly, ultrastructural imaging found immunoreactive- $ER\beta$ predominately in extra-nuclear sites, while $ER\alpha$ localizes to the nucleus (Wang et al., 2006). Additionally, 17β -estradiol acting through $ER\beta$ inhibits voltage-gated calcium currents in bulbospinal RVLM neurons, and RVLM $ER\beta$ knockdown in female mice exacerbates aldosterone/salt-induced hypertension (Xue et al., 2013). $ER\beta$ signaling also elicits transient vasodepressor effects in male rats (Shih, 2009). Together, these studies demonstrate that $ER\beta$ limits neurogenic sympathetic outflow, possibly through a nongenomic mechanism in RVLM neurons. Other hormone receptors, including androgen receptors, are present in RVLM catecholaminergic neurons and glia of male and female rodents (Milner et al., 2007; Sheng et al., 2021), but little is known about the impact on stress physiology.

2.4.3 Regulation of RVLM Catecholaminergic Neurons

Catecholaminergic neurons in the RVLM are often defined as C1 neurons and characterized by phenylethanolamine N-methyl transferase (PNMT), the synthesis enzyme for epinephrine. These epinephrine-synthesizing neurons target preganglionic sympathetic neurons in the spinal cord to trigger the sympathomedullary (SAM) axis and induce physiological responses such as elevated arterial pressure and blood glucose (Guyenet, 2006; Guyenet et al., 2013). Additionally, caudal RVLM and CVLM catecholaminergic neurons are often labeled as A1 neurons and characterized by the presence of DBH and the absence of PNMT (Stornetta, 2009). These norepinephrine-synthesizing neurons target the paraventricular hypothalamus to influence HPA axis output (Guyenet et al., 2013; Ritter, 2017). When stimulated, medullary

catecholaminergic neurons increase SAM and HPA axes activity, prompting corticosterone and glucose synthesis and release (Li et al., 2018; Zhao et al., 2017). This study measured glucose and corticosterone to evaluate SAM and HPA axes function during stress. To restrain physiological stress responses, outputs from medullary catecholaminergic neurons are tonically inhibited by GABAergic and glycinergic VLM neurons (Gao et al., 2019; Guyenet et al., 1990; Heesch et al., 2006). The baroreflex engages this microcircuitry to regulate sympathetic output and maintain blood pressure homeostasis (Guyenet, 2006), providing an intrinsic network for cortical modulation.

Prior ultrastructural studies identified vmPFC synapses in the RVLM (Gabbott et al., 2007), yet the functional organization of this circuitry has not been reported. In this study, stimulating the vmPFC-RVLM circuit increased c-Fos expression preferentially in non-catecholaminergic neurons. Although we cannot rule out activation of non-catecholaminergic glutamatergic neurons, this is a relatively small cell population with the majority of RVLM catecholaminergic neurons expressing vGluT2 (Stornetta et al., 2002; Stornetta, 2009). Thus, the identified vmPFC inputs to VLM inhibitory populations represent a potential mechanism for cortical inhibition of stress responding. Nevertheless, the widespread vmPFC innervation of multiple VLM cell-types suggests the circuit is dynamically regulated and that different physiological or environmental states may lead to divergent circuit signaling and homeostatic regulation. Ultimately, the potential for differential vmPFC inputs to catecholaminergic and non-catecholaminergic VLM cells may provide a cellular basis for stimulus-specific physiological reactivity.

2.4.4 The vmPFC-RVLM in Brain-Body Function

Responding to challenges requires the coordination of autonomic and neuroendocrine systems for optimal physiological adaptation. Considering the current results, the vmPFC-RVLM appears to be an effective means for modulating physiological function. Conventionally, physiological response patterns have been proposed to involve networks of top-down neural pathways that integrate cortical and limbic information to provide inputs to midbrain nuclei that ultimately modulate descending brainstem outflow. Yet, a monosynaptic cortical-medullary pathway offers a rapid and direct path for controlling homeostatic functions. As the vmPFC is essential for contextual appraisal and emotional processing while also processing visceral information (Kraynak et al., 2018; Saper, 2002; Verberne & Owens, 1998), this circuit may provide a direct link for psychosomatic coordination that relates emotion and physical health.

2.5 Conclusions

The current studies advance our understanding of how neural areas mediating cognitive appraisal of stressors may impact physiological function. Here, male and female rats have a direct stress-reactive vmPFC projection to the RVLM that reduces endocrine stress responses, likely by recruiting local RVLM inhibitory neurons. These data represent the only downstream vmPFC circuitry to attenuate stress reactivity in both male and female rats. Somatic stimulation of vmPFC neurons and preliminary cortical-hypothalamic studies have only reduced male stress response (Wallace et al., 2021). Previous vmPFC circuit studies have largely excluded females, although downstream circuit function may be sexually dimorphic (Shansky et al., 2010). Downstream terminal-specific activation can elicit opposite behavioral patterns during acute stress (Warden et al., 2012). Therefore, circuit-dependent vmPFC function to stress-critical areas

like the RVLM need to be better studied to best understand how vmPFC outputs regulate whole body physiology. These studies point to vmPFC neurons being modulated contextually based on sex, stress, and downstream target. Notably, these results show a sex-similar circuit attenuating glucocorticoid stress reactivity. Additional investigation of cortical glutamate signaling within the microcircuitry of the medulla is likely to identify novel aspects of endocrine-autonomic integration that could represent therapeutic interventions to improve cardiometabolic health. Ultimately, the excitatory/inhibitory balance of vmPFC synapses in the RVLM may regulate stress reactivity and stress-related health outcomes.

Chapter 3 – The Necessity of vmPFC-RVLM Circuit Function to Limit Stress Reactivity After Chronic Variable Stress Differs Between Sexes

3.1 Overview

Stress is an inevitable part of life in modern society. Adapting to that stress over time is critical for survival and well-being. However, chronic exposure to stress can cause deleterious physiological changes, leading to the risk of cardiovascular and metabolic diseases (Kivimäki & Steptoe, 2017; Steptoe & Kivimäki, 2012). While cardiovascular disease is the leading cause of death worldwide, our understanding of how chronic stress alters neurogenic physiological stress responses is not understood. Therefore, these collective studies aim to identify a specific neural process that may be integral to the consequences of chronic stress on cardiovascular health.

In the ventromedial prefrontal cortex (vmPFC), chronic stress causes functional and structural deficits in humans and rodents (Anderson et al., 2019; Drevets et al., 2008; Drevets et al., 2008; Radley et al., 2004). Notably, the vmPFC assesses environmental stimuli while regulating endocrine and autonomic stress responses (McKlveen et al., 2015). Clinical interventions targeting the vmPFC have had success in improving depression-related symptomologies while also demonstrating an ability to reduce systolic blood pressure (Holtzheimer et al., 2012; Kennedy et al., 2011; Lacuey et al., 2018; Lozano et al., 2008; Mayberg, 2005). However, vmPFC downstream neural circuit effectors that limit the cardiovascular consequences of chronic stress are yet to be identified. The medulla is a likely vmPFC effector based on previous work that identified a vmPFC-rostral ventrolateral medulla (RVLM) circuit capable of reducing glucocorticoid stress reactivity in both sexes (Chapter 2).

The ventrolateral medulla (VLM) is a pre-sympathetic brainstem region characterized by epinephrine/norepinephrine-synthesizing (Epi/NE) neurons. When experiencing physical, immune, or psychological stress, Epi/NE neurons in the VLM act as emergency mediators to drive the fight-or-flight response (Guyenet et al., 2013). Interestingly, VLM signaling targets hypothalamic regions critical in anxiety- and depression-related pathologies and the spinal cord to drive sympathetic outflow to the periphery (i.e., cardiovascular system) (Guyenet et al., 2020). Together, the VLM can promote HPA axis output and trigger the SAM system. Although the VLM is critical to organismal survival, medullary adaptations to chronic stress exposure are unknown. To date, no previous studies have investigated changes in VLM function after a chronic stress paradigm. Moreover, a plausible hypothesis for physiological outcomes after chronic stress may involve RVLM adaptations that modulate VLM Epi/NE signaling and facilitate sympathetic predominance into pathology development. Therefore, the initial experiments presented here measured transcript changes in the VLM after chronic stress. Our search focused on genes involved in pre-and post-synaptic signal transmission and neuromodulators in the brainstem. Additionally, this hypothesis-driven investigation included male and female rats and determined if chronic stress drives different signaling machinery in each sex.

Next, we investigated the necessity of the vmPFC-RVLM circuit to limit stress reactivity after chronic stress. Viral constructs that encode retrograde-transported Cre recombinase were injected in the RVLM and Cre-dependent tetanus toxin light-chain (TeLC) in the vmPFC, which induced TeLC expression in RVLM-projecting vmPFC neurons. TeLC cleaves an obligatory synaptic transmission protein to disrupt neurotransmitter release from RVLM-projecting vmPFC neurons. Therefore, we hypothesized that disruption of vmPFC-RVLM signaling in CVS-

exposed rats to increase comprehensive stress responses in male and female rats. Lastly, a separate set of experiments determined if RVLM-projecting vmPFC output is necessary to prevent the increased expression of RVLM Epi/NE synthesis enzymes after chronic stress. Epi/NE synthesis enzyme expression was examined in chronic variable stress (CVS)-exposed and stress-naïve female rats. In neurons, tyrosine hydroxylase (TH) and phenylamine-N-methyltransferase (PNMT) were probed by fluorescent in situ hybridization. Notably, TH is the rate-limiting enzyme for Epi/NE, which are primary signaling molecules from pre-sympathetic RVLM neurons. Other catecholamine synthesis enzymes include dopamine beta-hydroxylase (DBH), which converts dopamine into norepinephrine, and phenylethanolamine-N-methyltransferase (PNMT) which converts norepinephrine into epinephrine. To understand how chronic stress and vmPFC-RVLM circuit status impact RVLM transcriptional processes involved in neurogenic-driven sympathetic output, we examined TH and PNMT expression throughout the VLM. We hypothesized that vmPFC-RVLM circuit disruption and chronic stress would lead to increased expression of enzymes related to the synthesis of Epi/NE in the RVLM of female rats.

3.2 Methods

3.2.1 Animals

Male and female Sprague-Dawley rats (Envigo Denver, CO) were used for this study. The male rats weighed between 250-300g, while the female rats weighed between 150-200g. Each rat was individually housed in a vivarium with controlled temperature and humidity settings. The male rats for Experiment 1 were procured from Harlan (Indianapolis, IN) but were cared for under the same conditions as the others. In the vivarium, a 12-hour light-dark cycle was maintained, with lights turning on at 0600 and off at 1800. Separate holding rooms were

designated for rats of the same sex. Before the start of the experiment, newly arrived rats underwent a one-week acclimation period in the vivarium. Throughout the entire experiment, the rats had continuous access to both water and chow. All procedures and protocols were approved by the Institutional Animal Care and Use Committee of Colorado State University (protocol: 1392). These protocols adhered to the National Institutes of Health Guidelines for the Care and Use of Laboratory Animals. For Experiment 1 males, the protocols and procedures were approved by the University of Cincinnati Institutional Animal Care and Use Committee (protocol: 04-08-03-01), also in compliance with the National Institutes of Health Guidelines for the Care and Use of Laboratory Animals. The experimental procedures in this study underwent veterinary consultation, and the welfare of all animals was assessed daily by veterinary and/or animal medical service staff.

3.2.2 Experimental design

Experiment 1 used 16 male and 20 female rats. Both sexes were split into stress-naïve or CVS groups and underwent RVLM tissue extraction for gene expression analysis. Somatic data for each group and sex is listed in Table S3. Experiment 2 used an intersectional Tetanus toxin-light chain (TeLC) viral approach on 50 male and 48 female rats. Both sexes were split into stress-naïve or CVS groups and GFP control or TeLC groups. Each sex needed two separately-ran cohorts to reach the required sample size. Neuroendocrine and post-CVS OF measures were garnered from these rats. Likewise, Experiment 3 used an intersectional Tetanus toxin-light chain (TeLC) viral approach on 42 male and 40 female rats. Both sexes were split into stress-naïve or CVS groups, as well as GFP control or TeLC groups. Females required two separately-ran

cohorts to reach the required sample size, while males needed 3 cohorts. Pre-CVS OF and cardiovascular measures were recorded from these rats.

3.2.3 Stereotaxic surgery

Male and female rats were anesthetized with aerosolized isoflurane (1-5%) and administered an analgesic (0.6 mg/kg buprenorphine-SR, subcutaneous). For Experiments 1 and 2, rats received 2 sets of intracranial microinjections: unilateral microinjection (males 0.6 μ L, females 0.5 μ L) of a retrograde-traveling adeno-associated virus construct encoding for Cre recombinase conjugated to mCherry (AAVretro-EF1 α -Cre) targeting the RVLM (males: 1.88 mm lateral to midline, 12.25 mm anterior to bregma, and 10.4 mm ventral from bregma; females: 1.82 mm lateral to midline, 12.1 mm anterior to bregma, and 10.1 mm ventral from dura) and a bilateral microinjection (males 0.7 μ L, females 0.6 μ L) of an adeno-associated virus construct encoding for Cre-dependent tetanus toxin-light chain conjugated to GFP (AAV-DIO-TeLC) or Cre-dependent GFP (AAV-DIO-GFP) constructs (Stanford Vector Core, Chapel Hill, NC) in the vmPFC (males: 0.6 mm lateral to midline, 2.7 mm anterior to bregma, and 4.2 mm ventral from dura; females: 0.5 mm lateral to midline, 2.3 mm anterior to bregma, and 4 mm ventral from dura). All microinjections used a 25-gauge, 2- μ L microsyringe (Hamilton, Reno, NV) using a microinjector (Kopf, Tujunga, CA) at a rate of 5 minutes/ μ L for vmPFC injections and a rate of 10 minutes/ μ L for RVLM and CVLM injections. For RVLM injections, the needle was lowered ventrally to -6 mm from the skull and then reduced in -0.5 mm increments every 4 minutes to avoid damage to the respiratory column. The needle was left in place for 8 minutes before and after injections to facilitate viral diffusion. The skin was closed with wound clips and removed

after 2 weeks of recovery. 6 weeks of incubation were given to ensure appropriate viral construct expression (Wallace et al., 2021).

3.2.4 Telemetry implantations

As previously described (Schaeuble et al., 2019; Wallace et al., 2021), rats were equipped with ECG-enabled radiotelemetry transmitters (HD-S11 F0, Data Sciences International, St. Paul, MN). The rats were prepared for the implantation procedure under aerosolized isoflurane anesthesia (1–5%). They received a subcutaneous injection of analgesic (0.6 mg/kg Buprenorphine-SR) and an intramuscular antibiotic (5 mg/kg gentamicin) to manage pain. An abdominal incision allowed access to the descending aorta, where a catheter connected to the transmitter was implanted. Tissue adhesive (Vetbond; 3 M Animal Care Products, St. Paul, MN) was applied over a cellulose patch to secure the catheter. ECG leads were passed through the abdominal musculature and subcutaneously sutured above the rib cage and pectoral muscles. The transmitter body was then sutured to the abdominal musculature, and the abdominal incision and skin were closed with sutures and wound clips, respectively. Following the procedure, the rats were allowed a recovery period of 2 weeks before removing wound clips.

3.2.5 Estrous cycle cytology

For each experiment, female rats were simultaneously conducted, and they were housed together in the same room. Estrous cycle cytology was performed by swabbing the vaginal canal. After completing the experimental assays, vaginal cytology was examined to estimate the estrous cycle stage. A cotton swab moistened with deionized water was used to collect cells from the vaginal canal and transfer them onto a glass slide. The slides were allowed to dry and then

observed under a light microscope with a 10x objective by at least two independent observers unaware of the experimental conditions. The observers categorized the slides into four stages: proestrus, estrus, metestrus, or diestrus, following the protocols established in previous studies (Cora et al., 2015; Solomon et al., 2007). In cases where discrepancies were in the assigned estrous stages, a third independent observer was consulted to resolve the differences. The distribution of rats in each estrous phase is presented in Table S3 for Experiment 1, Table S6 for Experiment 2 and Table S7 for Experiment 3.

3.2.6 Restraint stress

Restraint stress was used Experiment 2 for evaluate stress reactivity. To induce restraint stress, rats were placed inside plastic decapicones (Braintree Scientific, Braintree, MA), with a small window cut in the plastic to expose the cannula. Fiber-optic patch cords were attached to enable optic stimulation during the 30-minute restraint period. Blood samples were collected via tail clip at the onset of restraint, followed by sequential samples at 15- and 30-minute intervals (Myers et al., 2017). At the 30-minute, the patch cords were detached, and the rats were returned to their home cages for recovery. Additional blood samples were collected at 60- and 90-minute time points. Blood glucose measurement served as an indicator of sympathetic outflow to the periphery, as acute glucose mobilization is dependent on epinephrine and is triggered by RVLM catecholaminergic stimulation (Zhao et al., 2017). Blood glucose levels were determined using Contour Next EZ glucometers (Bayer, Parsippany, NJ), and an average of two readings was recorded at each timepoint. The blood samples were centrifuged at $3000 \times g$ for 15 minutes at 4°C , and the resulting plasma was stored at -20°C until further analysis using an ENZO Corticosterone ELISA kit (ENZO Life Sciences, Farmingdale, NY). The intra-assay coefficient

of variation was 8.4%, and the inter-assay coefficient of variation was 8.2% (Dearing et al., 2021).

3.2.7 Chronic Variable Stress

The chronic variable stress (CVS) protocol involved twice daily stressors, presented randomized during morning and evening sessions. These stressors included exposure to a cold room set at 4 °C for 1 hour, shaker stress at 90 rpm for 1 hour, exposure to fox or coyote urine for 1 hour, forced swim for 10 min, tilted home cages for 3-4 hours, and overnight exposure to wet bedding or lights on (Flak et al., 2014; Ghosal et al., 2014; Wallace et al., 2021). Behavioral tests were incorporated as stressors at the beginning and end of the CVS protocol.

3.2.8 VLM microdissection

The brains were frozen and sectioned into coronal slabs using a CM3050 S Cryostat (Leica, Wetzlar, Germany) to maintain the appropriate temperature conditions. Histological landmarks such as the facial cranial nerve were utilized to determine the rostral boundary of the VLM. Micropunches were obtained from two bilateral sections per animal using a sharp, heavy wall stainless steel dermal biopsy punch with an internal diameter of 2 mm (Miltex, Bethpage, NY). The tissue punches were kept frozen and stored at -80 °C.

3.2.9 Nanostring nCounter

The punched tissue was kept at -80 °C until it was sent to the University of Arizona Genetics Core, where subsequent methods were performed. A RNeasy mini kit (Qiagen, Germantown, MD) was used following the manufacturer's instructions to isolate total RNA from

the tissue punches. The RNA concentrations were measured using a Qubit 4 Fluorometer (Invitrogen, Carlsbad, CA). A NanoString nCounter Custom CodeSet (Seattle, WA) was employed for multiplexed mRNA quantification. This CodeSet included bar-coded hybridization probes that targeted specific mRNAs listed in Table S3. Gene expression analysis was conducted using the nSolver Analysis 4.0 software (Nanostring, Seattle, WA). Transcript counts for each gene were normalized to the geometric mean expression of three housekeeping genes: regulator of G-protein signaling 14, peptidylprolyl isomerase H, and succinate dehydrogenase complex flavoprotein subunit A. To determine background expression levels and normalize each sample, the geometric mean plus the standard deviation of raw counts were calculated for eight synthetic negative control probes (Heck et al., 2020).

3.2.10 in situ hybridization and immunohistochemistry

To examine the density of tyrosine hydroxylase (TH) and phenylethanolamine N-methyl transferase (PNMT) transcripts in RVLM neurons, in situ hybridization (ISH) was conducted on brain tissue collected from rats using the RNAscope multiplex platform (Advanced Cell Diagnostics, Hayward, CA). An adapted protocol to utilize fixed tissue was executed (Sumners et al., 2020). The brains of the rats were perfused as described earlier and coronally sectioned into a 1:12 series at a thickness of 20 μm . These sections were then stored in cryoprotectant solution at -20°C for long-term preservation. Tissue collection, sectioning, and mounting procedures were performed under RNase-free conditions. Once prepared, slides were washed with PBS, hydrogen peroxide, and PBS again before being mounted onto SuperfrostPlus Gold slides, following the manufacturer's protocol (Advanced Cell Diagnostics, Hayward, CA).

The RNAscope ISH technique employed a positive control probe targeting Ubc and a negative control probe targeting DapB. In addition, probes for TH (C1-TH probe, probe sequence, 1:1 dilution, Advanced Cell Diagnostics) and PNMT (C2-PNMT probe, probe sequence, 1:50 dilution, Advanced Cell Diagnostics) were utilized. After ISH, immunohistochemistry (IHC) was performed to label neurons. Sections on slides were rinsed with PBS at room temperature and transferred to a blocking solution (PBS, 0.1% bovine serum albumin, 0.2% Triton X-100) for 1 hour. Subsequently, the sections were incubated overnight with mouse anti-NeuN primary antibody (1:1000 in blocking solution, MAB394, RRID: AB_94983; MilliporeSigma, Burlington, MA). Following a rinse in PBS, the sections were incubated with donkey anti-rabbit Cy3 secondary antibody (1:500 in PBS, 715-165-020, RRID: AB_2340811; Jackson ImmunoResearch, West Grove, PA) for 1 hour. The tissue was washed in PBS, mounted in a polyvinyl medium, and cover-slipped for imaging.

3.2.11 Open Field Assay

The open-field test was employed, following the methodology described in a previous study by Pace et al. (2020). This assessment aimed to evaluate general locomotor activity and approach/avoidance behavior, as Belzung and Griebel (2001) outlined. Rats were individually placed in a square field made of black acrylic, measuring 1 square meter and with walls standing at a height of 30 centimeters. The rats were allowed to explore the field for a duration of 5 minutes freely. Noldus behavioral analysis software was utilized to measure the total distance traveled by the rats, the time spent in the central area of the field, the number of entries into the center, and the latency of the first entry. The center of the arena was defined as the central 0.5 square meter.

3.2.12 Tissue collection

Following the completion of the experiments, all rodents were administered sodium pentobarbital intraperitoneally at a dosage of at least 100 mg/kg for anesthesia. They were then transcardially perfused with 0.9% saline solution, followed by 4% paraformaldehyde in phosphate buffer. The brains were carefully extracted and post-fixed in paraformaldehyde overnight. Subsequently, they were stored in a 30% sucrose solution at 4 °C to facilitate cryoprotection. The brains were later sectioned into coronal slices, each measuring 30 µm thick, with a 1:12 serial sectioning ratio. These sections were preserved in a cryoprotectant solution at -20 °C until further processing for immunohistochemistry.

3.2.13 Immunohistochemistry

To examine the coexpression of synaptobrevin-2 (SynB2) and RVLM-projecting vmPFC neurons, immunohistochemistry was performed to label SynB2 and amplify GFP signal on vmPFC-projecting terminals. Free-floating sections were rinsed with PBS at room temperature and transferred to a blocking solution (PBS, 0.1% bovine serum albumin, 0.2% Triton X-100) for 1 hour. Subsequently, the sections were incubated overnight with mouse anti-GFP primary antibody (1:1000 in blocking solution, ab6556; Abcam, Waltham, MA). Following a rinse in PBS, the sections were incubated with goat anti-rabbit Alexa Fluor 488 secondary antibody (1:500 in PBS, 111-547-003; Jackson ImmunoResearch, West Grove, PA) for 1 hour. The tissue was then washed in PBS, transferred to blocking solution (PBS, 4% bovine serum albumin, 3% of donkey serum, 0.1% of Triton X-100) for 1 hour, then left to incubate overnight with anti-SynB2 (1:200 in blocking solution, 104 211C3; Synaptic Systems, Goettingen, Germany).

Following a rinse in PBS, the sections were incubated with goat anti-mouse Cy5 secondary antibody (1:500 in PBS, 115-175-166; Jackson ImmunoResearch) for 1 hour. After a final PBS rinse, sections were mounted in a polyvinyl medium, and cover-slipped for imaging.

3.2.14 Microscopy

Fluorescent imaging utilized a Zeiss Axio Imager Z2 microscope (Carl Zeiss Microscopy, Jena, Germany) and the corresponding ZEN 2.6 blue edition software (Carl Zeiss Microscopy). To determine injection placement, GFP and m was imaged using the 5x objective. For GFP and Cy5 dual fluorescence imaging, a 63x objective at 0.5- μm thick optical sectioning to produce Z-stacks. Co-localization was defined as signal overlap between GFP terminals and SynB2-Cy5. Further, an off-channel filter was used to identify auto-fluorescent signals that may affect results. To image ISH transcripts and IHC-labeled cells, TH-GFP, PNMT-Cy5, NeuN-Cy3, and DAPI as an off channel, were all imaged using a 63x objective at 1- μm thick optical sectioning to produce 5 z-planes of image stacks. Apotome processing proceeded after the initial imaging. Co-localization was defined as magenta or green fluorescence from the overlap between fluorophores.

3.2.15 Image analysis

ZEN software was used for GFP/SynB2 colocalization experiments to quantify the number of pixels expressing GFP and SynB2-Cy5 separately or together. Colocalization was defined using the colocalization tool to identify GFP and Cy5 pixels present at the exact location. Regions of interest were restricted to terminal-specific areas in male cortical tissue. 3 separate axons per rat were analyzed. Axons were 500-100- μm long. For ISH, image analysis protocols

were adapted from prior fluorescent ISH methods to quantify RNAscope multiplexed probes (Li et al., 2021; Mueller et al., 2013). For ISH experiments (Experiment 2), Carl Zeiss Images (CZIs) were opened using ZEN 2.6 blue software. A colocalization module was used to analyze TH-GFP and PNMT-Cy5. Regions of interest were drawn around NeuN-Cy3-labeled cells. A Pearson correlation coefficient was used to objectively determine a threshold for the fluorescent signal based on the probe and the NeuN fluorescent signal. Precisely, this automated thresholding will fit a line to all pixels and specify where on the line all pixels below it have a 0 value of the correlation.

3.2.16 Neuroanatomy

To anatomically delineate mPFC, each tissue section's bregma location and area delineations were defined according to Brain Maps III: Structure of the Rat Brain (Swanson, 2004). The atlas was used to identify the anterior forceps of the corpus callosum as the lateral boundary and the coronal midline as the medial boundary. The rostral-caudal emergence of the corpus callosum was used to divide the subregions from dorsal to ventral, and the subependymal zone guided the identification of the ventral vmPFC boundary. To delineate the RVLM, The Rat Brain atlas (Paxinos & Watson, 2006) was used for area delineations and landmark identification throughout the brainstem. The RVLM lacks distinct cytoarchitecture; therefore, landmarks such as the facial nucleus served as the rostral boundary, the spinal trigeminal nucleus as the lateral boundary, and lateral portions of the inferior olive guided distinguishing the medial edge. Regarding VLM subregions, The Rat Brain atlas (Paxinos and Watson, 2007) defines the whole VLM as -12.00 to -15.00 mm from bregma, with catecholaminergic populations transitioning from C1, C1/A1, and A1 in a rostro-caudal orientation. We used the C1 population to define

what we considered RVLM (-12.00 to -13.56 mm posterior to bregma) (Li et al., 2018). Notably, our classification regards the RVLM as containing catecholaminergic neurons with bulbospinal and ascending projections. Further, publicly available templates of rat brain coronal sections from Brain Maps III (Swanson, 2004) were used to illustrate virus placement.

3.4.14 Data analysis

Data are expressed as mean \pm standard error of the mean. Data were analyzed using Prism 9 (GraphPad, San Diego, CA), with statistical significance set at $p < 0.05$ for all tests. SynB2 colocalization used an unpaired t-test with Welch's correction. A three-way ANOVA was used to analyze bodyweight changes throughout the experiment. Fisher's post hoc was further executed to identify differences at time points. A one-way ANOVA was used to analyze adrenal weight changes, while multiple comparisons used Fisher's post-hoc test. Corticosterone and glucose measured during restraint stress were analyzed using a repeated mixed-effects analysis with treatment, sex, and time as factors. If significant main or interaction effects are present, then a Fisher's post-hoc test would be used. For chronic circadian recordings of hemodynamic measures and Novel Environment recordings, a mixed-effects analysis with treatment, sex, and time was utilized. Fisher's post-hoc test was used for multiple comparisons. Lastly, a one-way ANOVA was used for normalized area under the curve (AUC) datasets to investigate cumulative changes after chronic recordings and Novel Environment. Normalized AUC sets were corrected to baseline measurements and represented as a percent change from No CVS GFP controls. Multiple comparisons used Fisher's post-hoc test to identify further differences. Multiple t-tests were used to analyze the transcripts probed in the VLM. A mixed-effects ANOVA was run using VLM subregion, circuit treatment, and stress as variables on TH and PNMT transcript density. A

Fisher's post-hoc test was used to analyze ISH data, although male data was excluded due to low sample sizes. Data points are from individual rats.

3.3 Results

3.3.1 VLM gene expression changes after CVS

To better understand the effects of chronic stress on the RVLM, we used a NanoString gene analysis platform to quantify transcript expression of excised medullary tissue from CVS-exposed and -naïve rats of both sexes (Figure 4.1A) Both male and female CVS rats had increased heart weights, a common somatic marker of cardiovascular hypertrophy (n = 7-12/group, unpaired t-test: male heart weights $t(10) = 4.531$, $p = 0.001$; female heart weights $t(19) = 4.467$, $p = 0.0003$) (Dickhout et al., 2011) (Figure S3). We profiled 70+ gene transcripts related to pre-and post-synaptic transmission, steroid signaling, and intracellular signal transduction (Table S8). Within male rats, CVS caused significant differences in only 2 transcripts, the gamma subunit of protein kinase C and tyrosine hydroxylase (TH) (n = 7/group, unpaired t-test: PKC $t(12) = 2.190$, $p = 0.0489$); TH $t(12) = 2.229$, $p = 0.0456$) (Figure 4.4B,C, Table S4).. In female rats, over 40+ transcripts were significantly different in CVS animals relative to No CVS (Figure 4.4D, Table S6). Similar to males, the catecholamine synthesis enzymes TH significantly increased in CVS rats relative to stress-naïve controls (n = 8-12/group, unpaired t-test: TH $t(17) = 2.581$, $p = 0.0194$) (Figure 4.4E). Although TH expression is increased in both sexes, the number of transcripts significantly different after CVS and the magnitude of those changes is intensified in females compared to males (Figure 3.1B,D). This qualitative effect of stress in females suggest the female VLM is highly stress-reactive. Nonetheless, these results suggest that CVS in both sexes may augment VLM catecholamine synthesis, thereby expanding the capacity

and capability of VLM signaling output to nuclei that induce neuroendocrine and sympathetic stress reactivity (i.e., Epi/NE output to the PVN and IML).

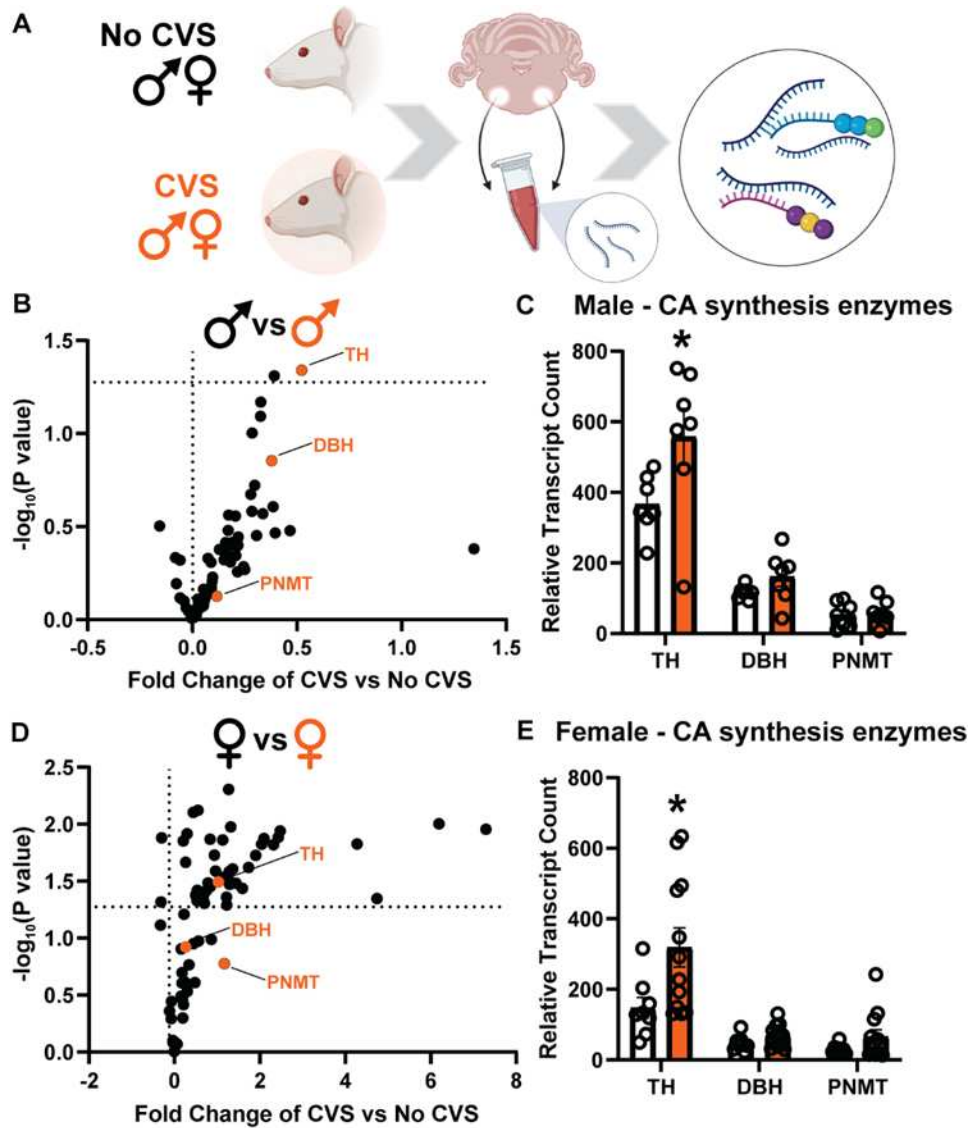


Figure 3.1 Gene expression profile of male and female rats exposed to chronic stress. Male and female ventrolateral medulla tissue from No CVS and CVS groups underwent gene expression analysis (A). 70+ transcripts were targeted with only 2 genes differing significantly in CVS vs No CVS analysis (B). Transcripts for CA synthesis enzymes trended upwards in CVS males with TH significantly increasing compared to stress-naïve animals (C). 70+ transcripts were targeted in female rats (D). CA synthesis enzyme transcripts were up in CVS females with TH increasing significantly relative to controls (E). DBH: dopamine-beta hydroxylase, PNMT: phenylethanolamine N-methyltransferase, TH: tyrosine hydroxylase. Effect of CVS within sex and transcript * $p < 0.05$

3.3.2 vmPFC-RVLM Circuit Disruption Approach While Measuring Physiological Endpoints

Next, we examined the role of RVLM-projecting vmPFC neurons in the context of chronic stress. Chronic stress-induced PFC dysfunction is well established, yet pathways targeting the medulla are in an optimal position to exert physiological effects. To investigate, Experiment 2 adult male and female rats received multiple microinjections: a unilateral injection of retrograde-traveling AAV encoding for Cre recombinase and mCherry (AAVretro-Cre) targeted the RVLM and a bilateral injection of AAV encoding for tetanus toxin light-chain conjugated to GFP (TeLC) or GFP alone targeted the vmPFC (Figure 3.2A-D, Figure S1A). TeLC is an attenuated version of tetanus toxin that cleaves synaptobrevin-2 (SynB2) and thereby obstructs neurotransmitter release. Injection placements were mapped using a rat brain atlas (Figure S1B,D). To determine the efficacy of our circuit disruption approach, RVLM-projecting vmPFC terminals co-expressing SynB2 and TeLC-GFP were compared to GFP controls by analyzing the overlap of fluorescent pixels. TeLC-expressing terminals colocalized with SynB2 less than GFP terminals ($n = 3/\text{group}$, unpaired t-test: GFP vs TeLC $t(4.834) = 2.004$, $p = 0.0401$). Therefore, RVLM-projecting vmPFC terminals expressing TeLC have an attenuated synaptic infrastructure to properly signal (Figure 3.1E).

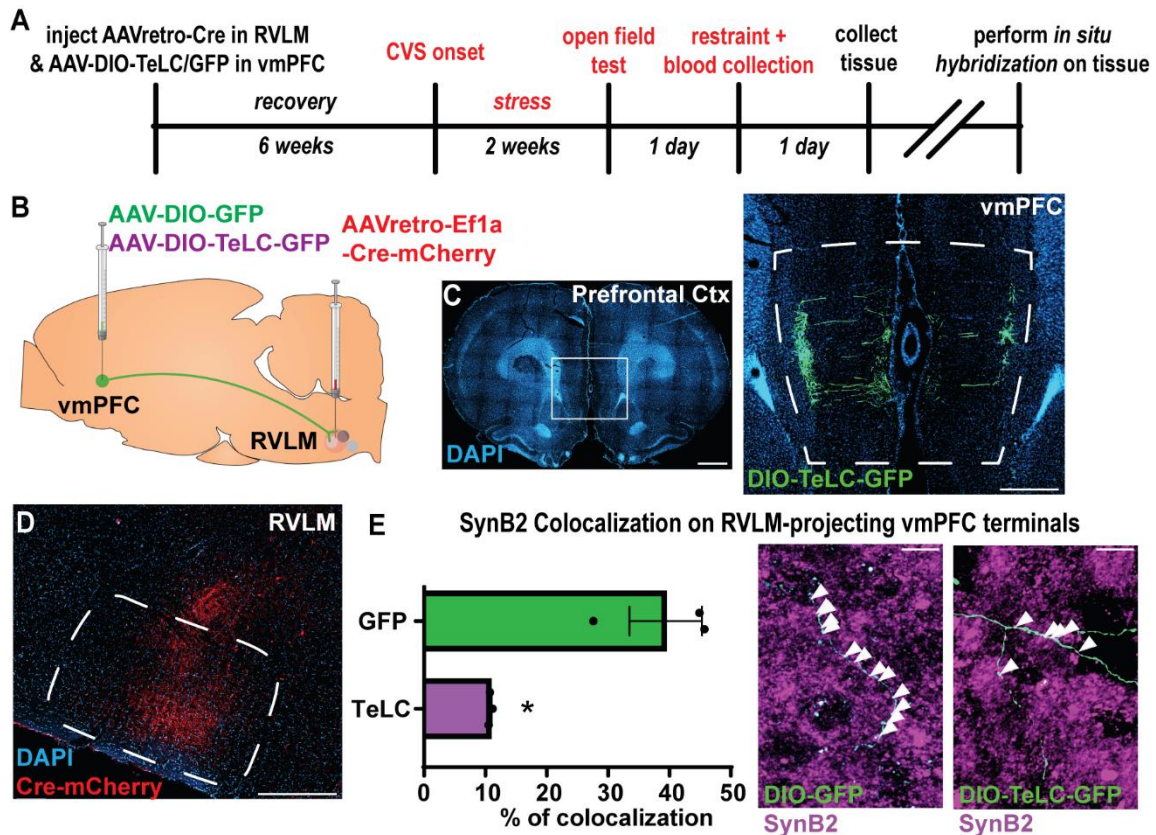


Figure 3.2 Intersectional TeLC approach reduces SynB2 expression on RVLM-projecting vmPFC fibers. vmPFC-RVLM circuit disruption experiment timeline (A). AAV-DIO-GFP or AAV-DIO-TeLC-GFP were injected into the vmPFC and AAVretro-EF1 α -Cre-mCherry was injected into the RVLM, scale bar (C): 1 mm, scale bar (C zoom-in): 500 μ m, scale bar (D): 500 μ m (B-D). Quantification and representative image of TeLC-expressing RVLM-projecting vmPFC terminals that colocalized less with SynB2 relative to controls, scale bars: 250 μ m (E). AAV-DIO-GFP: Cre-dependent adeno-associated virus encoding GFP expression, AAV-DIO-TeLC-GFP: Cre-dependent adeno-associated virus encoding TeLC and GFP expression, AAVretro-Ef1 α -Cre-mCherry: retrograde traveling adeno-associated virus encoding Cre under the promoter eukaryotic translation elongation factor 1 α , CVS: chronic variable stress, GFP: green fluorescent protein, Prefrontal Ctx: prefrontal cortex, RVLM: rostral ventrolateral medulla, SynB2: synaptobrevin-2, TeLC: tetanus toxin light-chain, vmPFC: ventromedial prefrontal cortex. * $p < 0.05$.

3.3.3 vmPFC-RVLM Circuit is Crucial for Regulating Neuroendocrine Stress Responses in Females and Males following CVS

Next, we examined the necessity of vmPFC-RVLM function for stress responses in male rats. Sympathetic and neuroendocrine stress responses were recorded by measuring blood

glucose and plasma corticosterone during and after restraint stress. For glycemic responsivity, only an interaction effect of time and treatment was observed [n = 8–13/group; 3-way ANOVA: time x treatment $F(4,188) = 2.898$, $p = 0.0233$]. Post-hoc analysis revealed no significant differences within No CVS rats (Figure 3.3A). Conversely, CVS TeLC rats had increased blood glucose relative to CVS GFP rats during recovery post-restraint (60 min TeLC, $p = 0.0092$) (Figure 3.3B). For glucocorticoid stress reactivity, there was a main effect of stress and an interaction effect of time and stress [n = 8–13/group; 3-way ANOVA: stress $F(1,174) = 5.064$, $p = 0.0257$; time x stress $F(4,174) = 2.645$, $p = 0.0352$]. Post-hoc analysis showed no differences in corticosterone levels within stress-naïve groups (Figure 3.3C). In CVS rats, the TeLC group had decreased plasma corticosterone at 30 minutes (30 min TeLC, $p = 0.0092$) (Figure 3.3D). Here, vmPFC-RVLM signaling after CVS is critical for appropriating glucocorticoid stress responses and post-stress glycemia maintenance.

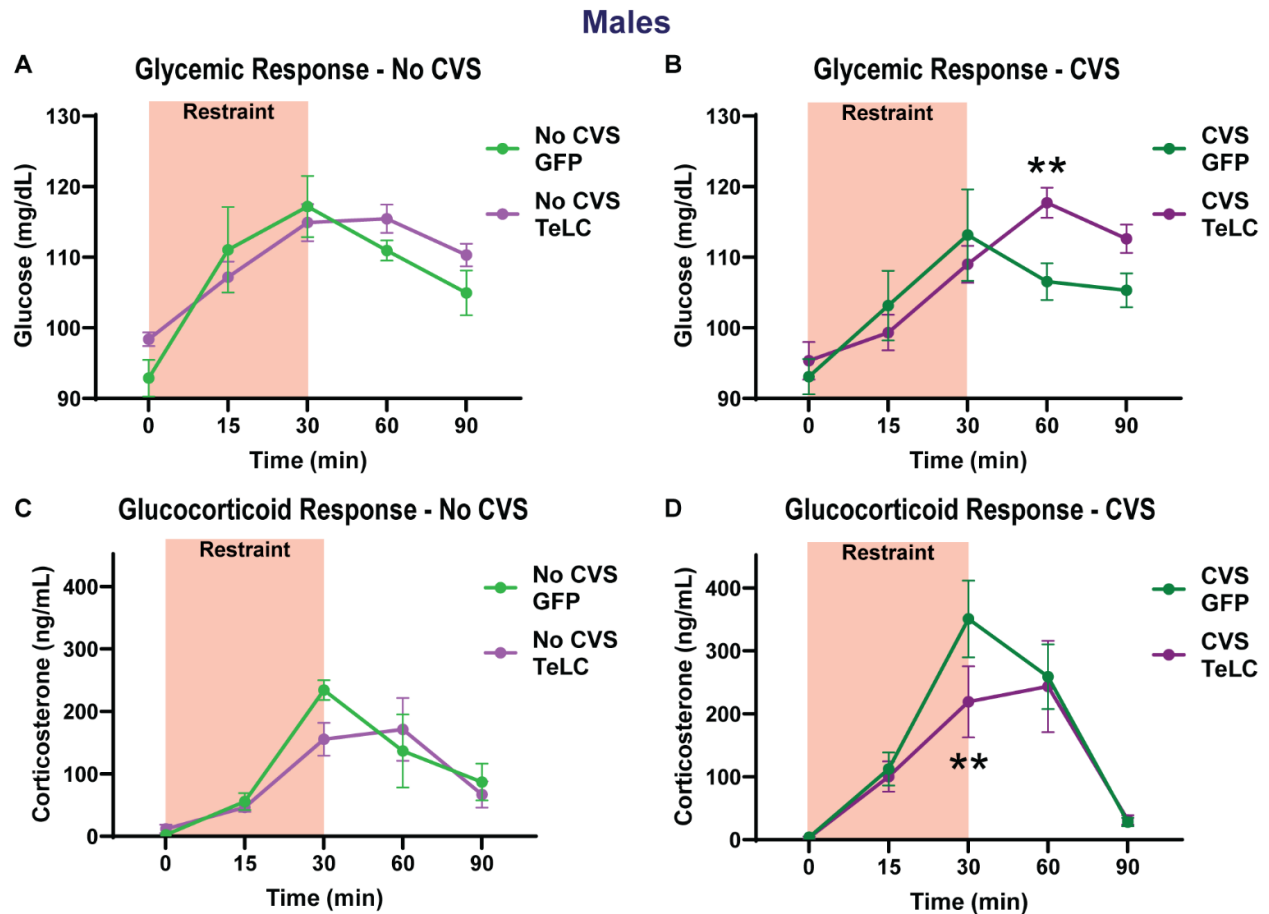


Figure 3.3 Disrupting the vmPFC-RVLM circuit affects male rats exposed to CVS. No CVS GFP and TeLC rats had similar glycemic responses to stress (A). CVS TeLC rats had increased glucose levels after restraint stress relative to CVS GFP rats (B). No significant differences were found in glucocorticoid responses within stress-naïve groups (C). CVS TeLC rats had reduced glucocorticoid responses compared to conspecific GFP controls (D). * $p < 0.05$, ** $p < 0.01$

Next, we investigated the essentialness of the vmPFC-RVLM pathway in regulating stress responses in female rats. We measured blood glucose and plasma corticosterone levels during and after restraint stress to assess sympathetic and neuroendocrine stress responses. Regarding glycemic responsivity, interaction effects of stress and treatment, then time by stress by treatment, were evident. [$n = 8-12/\text{group}$; 3-way ANOVA: stress x treatment $F(1,200) = 27.03$, $p < 0.0001$; time x stress x treatment $F(4,200) = 3.409$, $p = 0.0101$]. At 15 minutes, TeLC glucose levels were reduced relative to No CVS GFP rats (60 min TeLC, $p = 0.0092$) (Figure 3.4A). Inversely, CVS TeLC rats had augmented glycemic responses to controls at 15,

30, and 90 minute marks throughout restraint (15 min TeLC, $p = 0.0029$; 30 min TeLC, $p = 0.0182$; 90 min TeLC, $p = 0.0102$) (Figure 3.4B). With glucocorticoid responses to restraint, there was an effect of stress and interaction effects of time and stress, as well as stress and treatment [$n = 8-13$ /group; 3-way ANOVA: stress $F(1,192) = 9.659$, $p = 0.0022$; time x stress $F(4,192) = 5.974$, $p = 0.0001$; stress x treatment $F(1,192) = 6.302$, $p = 0.0129$]. No differences in corticosterone levels were observed in stress-naïve rats (Figure 3.4C). In CVS-exposed rats, the TeLC group had augmented plasma corticosterone at 15 and 30 minutes (15 min TeLC, $p = 0.0216$; 30 min TeLC, $p = 0.0029$) (Figure 3.4D). Together, these studies demonstrate that the vmPFC-RVLM circuit is needed to limit neuroendocrine stress reactivity after CVS in female rats.

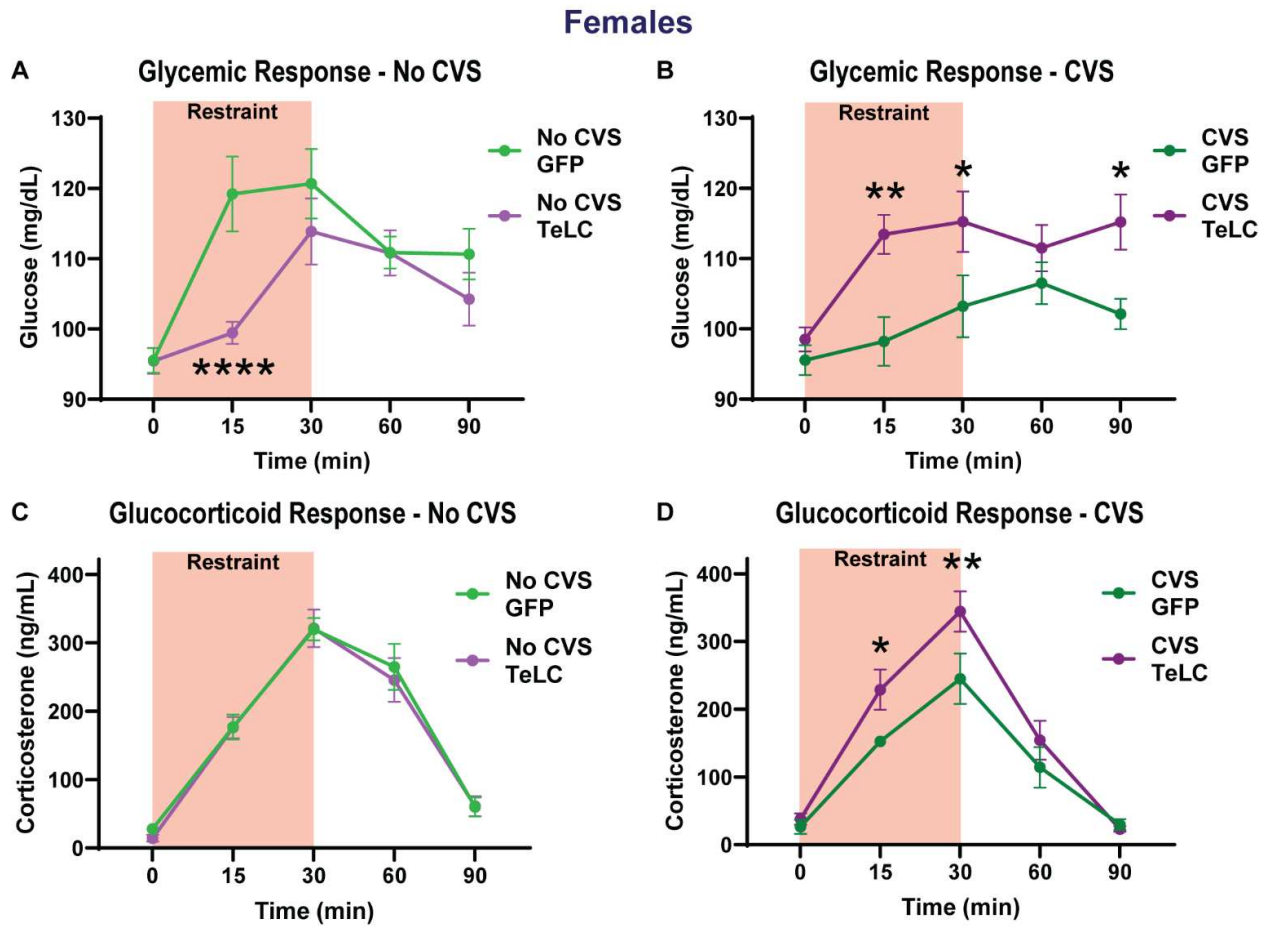


Figure 3.4 Disrupting the vmPFC-RVLM circuit augments the stress reactivity of CVS female rats. No CVS TeLC rats had diminished stress-induced glycaemic responses compared to GFP controls (A). CVS TeLC rats had higher glucose levels than GFP rats (B). No CVS GFP and TeLC rats had similar glucocorticoid responses to stress (C). CVS TeLC rats had increased corticosterone levels during restraint stress relative to CVS GFP rats (D). * $p < 0.05$, ** $p < 0.01$, **** $p < 0.0001$.

3.3.4 vmPFC-RVLM Circuit is Necessary to Limit CVS Effects on Behavior in Females, But Not Males

To investigate the necessity of vmPFC-RVLM signaling on stress responding, open field (OF) behavioral patterns were examined before and after CVS in separate experiments and multiple cohorts of rats. OF is a well-established behavioral assay to assess approach vs. avoidance during exploration (Prut & Belzung, 2003). Critically, avoidant behavioral patterns are linked to anxiety-like phenotypes in multiple psychiatric disorders (Lister, 1990). All pre-CVS OF assays were run in Experiment 3 (Figure S2), and all post-CVS OF assays in Experiment 2 (Figure 3.2) to avoid repeated testing in the same subjects. This study design led to treatment effects being evaluated within sex and stress conspecifics. Before and after CVS in male rats, there were no significant effects on total distance traveled in the open field, indicating no TeLC effects on general locomotion in males (Figure 3.5A,B). Furthermore, no change in time spent in the center of the open field was observed in pre- or post-CVS males (Figure 3.5C,D). Notably, pre-CVS TeLC males are considerably close to being statistically different [pre-CVS ($n = 13$ /group, unpaired t-test: TeLC vs GFP $t(13) = 2.132$, $p = 0.0521$)]. In females, distance traveled throughout the OF assay was not significantly different in TeLC rats compared to GFP controls in pre- and post-CVS cohorts (Figure 3.5E,F). Time spent in the center did not differ by treatment in pre-CVS females (Figure 3.5G). However, post-CVS TeLC rats spent less time in the center of the OF relative to GFP controls [post-CVS ($n = 9-11$ /group, unpaired t-test: TeLC

vs GFP $t(11) = 2.336, p = 0.0394$] (Figure 3.5H). These results suggest that vmPFC-RVLM signaling primarily does not affect male behavior patterns during stress but does mediate avoidance in females exposed to CVS.

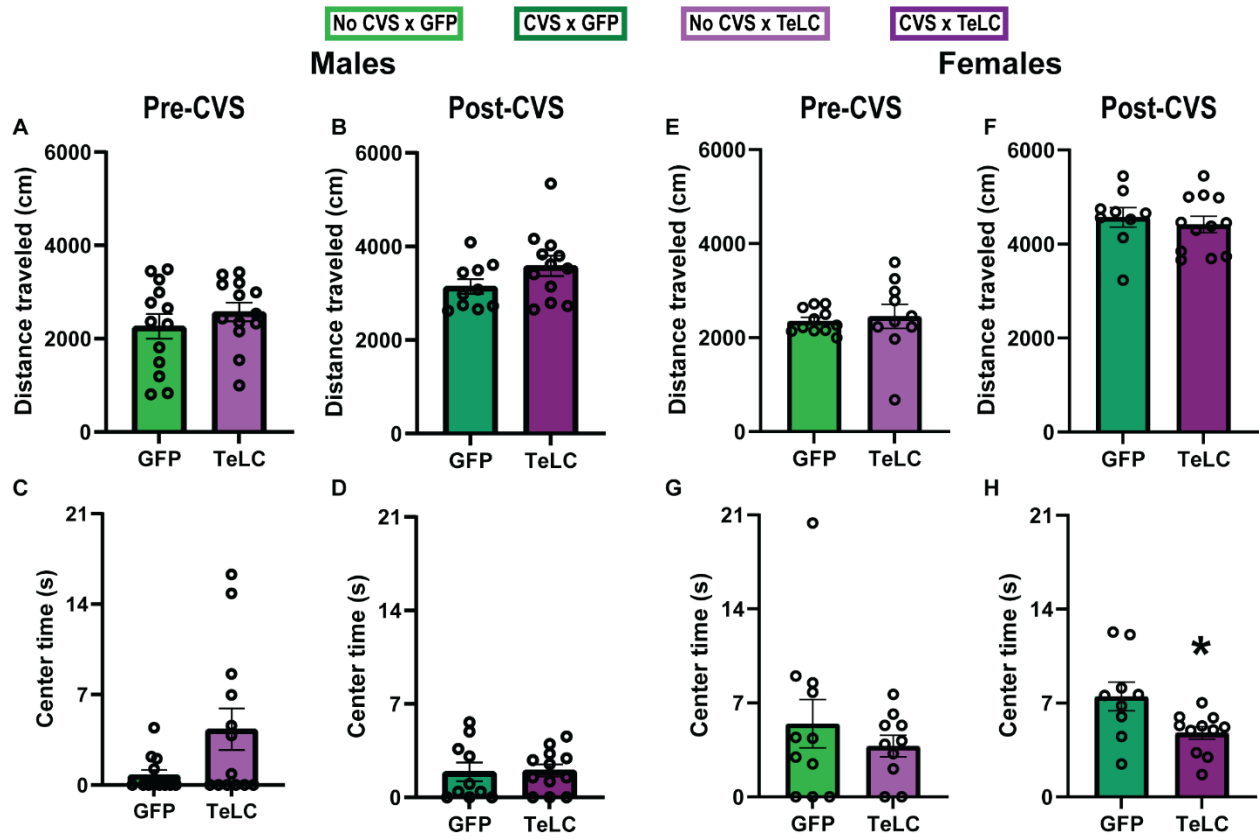


Figure 3.5 Interfering with vmPFC-RVLM signaling induces avoidance in CVS females but not males during OF. Male pre-CVS TeLC rats and GFP controls had similar locomotive levels (A). Post-CVS TeLC rats did not travel significantly different distances than GFP rats (B). Pre-CVS rats did not have significantly different times in the center of the OF arena (C). Post-CVS TeLC rats did not have any approach-avoidant phenotypes (D). Female pre-CVS TeLC rats and GFP controls had similar locomotive levels (E). Post-CVS TeLC rats did not travel significantly different distances than control rats (F). Pre-CVS rats did not have significantly different times in the center of the OF arena (G). Post-CVS TeLC rats spent less time in the OF arena's center than GFP conspecifics (H). * $p < 0.05$.

3.3.5 vmPFC-RVLM Circuit is Needed to Appropriate Cardiovascular Function in Males and Females After CVS

As with Experiment 2, Experiment 3 male and female rats received intracranial injections targeting the vmPFC and RVLM (Figure S2A), vmPFC received bilateral AAV injections encoding for TeLC or GFP, and the RVLM received counterbalanced unilateral AAVretro-Cre (Figure S2B). Throughout the experiment, bodyweights was recorded, and an effect of treatment was seen in males [n = 8–11/group; 3-way ANOVA: day x stress $F(1,251) = 8.504$, $p = 0.0039$] (Figure S2C). Significant differences were not seen in male adrenal weights (Figure S2C). In female rats, an interaction effect of experimental day and stress was seen in bodyweight change throughout the experiment [n = 8–11/group; 3-way ANOVA: day x stress $F(6,231) = 2.673$, $p = 0.0158$] (Figure S2D). Additionally, CVS GFP rats had an increased adrenal weight relative to stress and treatment conspecifics [n=8–11/group; 1-way ANOVA: $F(3,31) = 24.51$, $p < 0.0001$; No CVS GFP v CVS GFP, $p < 0.0001$; CVS GFP v CVS TeLC, $p < 0.0001$] (Figure S2D).

Throughout the 2 weeks of CVS homecage, circadian radiotelemetry data was measured to examine the effects of chronic stress and disrupted vmPFC-RVLM circuit function. A mixed-effects analysis in males of systolic arterial pressure (SAP) revealed interaction effects of treatment and stress, separately [n = 6–10/group; mixed-effects ANOVA: treatment $F(1,455) = 28.59$, $p < 0.0001$; stress $F(1,455) = 8.405$, $p = 0.0039$] (Figure S3A). Area under the curve (AUC) normalized to No CVS GFP rats was taken from these chronic recordings to evaluate cumulative effects. Additionally, all recordings were normalized to baseline values to interpret percent changes that occurred through the 2 weeks of recordings. Here, we saw normalized AUC of SAP circadian hemodynamics reveal significant differences, increases explicitly of CVS TeLC relative to CVS controls [n=6–9/group; 1-way ANOVA: $F(3,24) = 4.200$, $p = 0.0160$; CVS

GFP v CVS TeLC, $p=0.0211$] (Figure 3.6A). Analysis of diastolic arterial pressure (DAP) revealed an effect of treatment and treatment by stress [$n = 6-10/\text{group}$; mixed-effects ANOVA: treatment $F(1,439) = 17.94$, $p<0.0001$; treatment x stress $F(1,439) = 24.81$, $p<0.0001$] (Figure S3B). Aggregate measurements of normalized AUC for DAP did not exhibit significant differences (Figure 3.6B). Mean arterial pressure (MAP) analysis demonstrated the effects of treatment and treatment by stress [$n = 6-10/\text{group}$; mixed-effects ANOVA: treatment $F(1,439) = 26.60$, $p<0.0001$; treatment x stress $F(1,439) = 14.16$, $p=0.0002$] (Figure S3C). Cumulative measurements of normalized AUC for MAP unveiled significant differences, particularly between CVS and no CVS TeLC animal controls [$n=6-9/\text{group}$; 1-way ANOVA: $F(3,24) = 4.924$, $p=0.0083$; CVS GFP v CVS TeLC, $p=0.0193$] (Figure 3.6C). Lastly, analysis of long-term heart rate measurements revealed effects of treatment, stress, and time by stress interactions [$n = 6-10/\text{group}$; mixed-effects ANOVA: treatment $F(1,455) = 14.08$, $p<0.0001$; stress $F(1,455) = 5.753$, $p=0.0169$; treatment x stress $F(15,455) = 2.266$, $p=0.0043$] (Figure S3D). Aggregate HR analysis using the normalized AUC also showed significant differences and revealed CVS GFP to be increased compared to no CVS GFP rats controls [$n=6-9/\text{group}$; 1-way ANOVA: $F(3,25) = 6.378$, $p=0.0023$; CVS GFP v CVS TeLC, $p=0.0456$] (Figure 3.6D). Together, these results demonstrate that disrupted vmPFC-RVLM function predisposes male rats to CVS-induced increases of SAP and MAP.

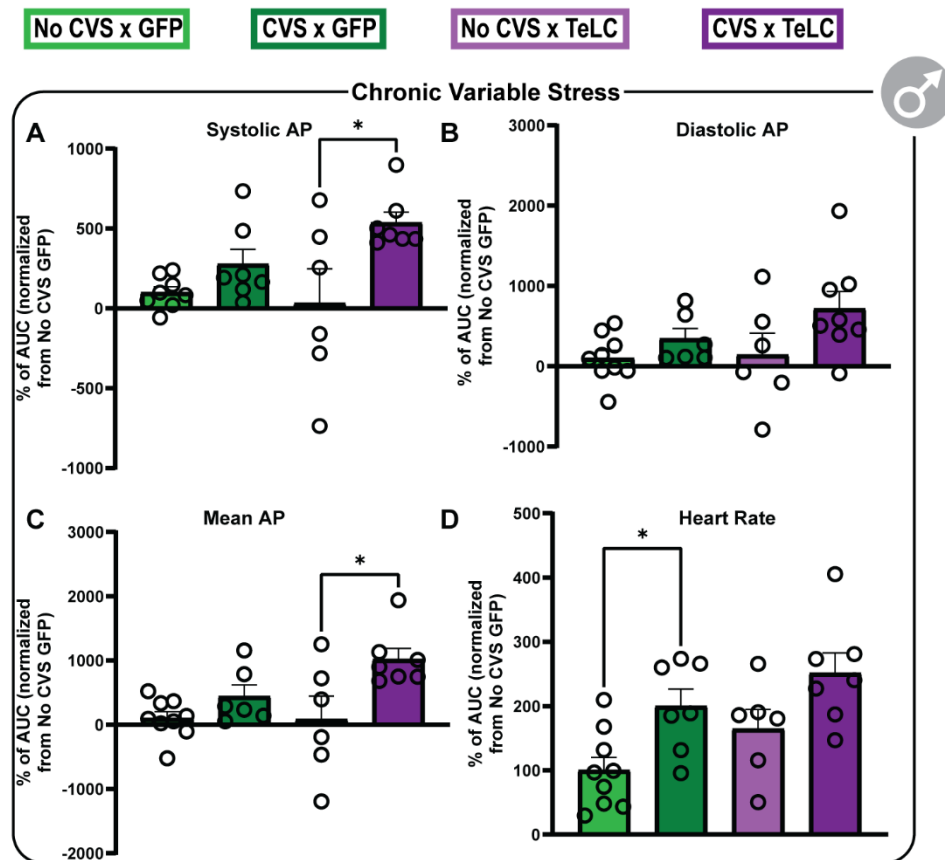


Figure 3.6 CVS and vmPFC-RVLM disruption altered cumulative hemodynamic levels in males after long-term recordings. Analysis of cumulative SAP revealed CVS-induced increases in TeLC rats (A). No changes were seen in DAP (B). Increased MAP was seen in TeLC rats after CVS exposure (C). CVS caused HR increases in GFP controls (D). AUC: Area Under the Curve, AP: Arterial Pressure. * $p < 0.05$.

As with males, female hemodynamics were recorded over the 2 weeks of CVS while rats were in home cages. These radiotelemetry recordings were used to examine the effects of CVS and TeLC in females. SAP was analyzed using a mixed effects model to reveal an interaction effect of time by stress [$n = 6-10$ /group; mixed-effects ANOVA: time x stress $F(15,416) = 3.168$, $p < 0.0001$] (Figure S5A). An aggregate of SAP changes during long-term recordings was analyzed using the AUC of SAP normalized to No CVS GFP controls and baseline recordings. Significant increases were seen in both CVS groups compared to no CVS conspecifics in each treatment group [$n = 6-9$ /group; 1-way ANOVA: $F(3,22) = 5.475$, $p = 0.0058$; no CVS GFP v CVS

GFP, $p=0.0104$; no CVS TeLC v CVS TeLC, $p=0.0079$] (Figure 3.7A). Next, analyzed chronic DAP recordings unveiled significant interaction effects in time by treatment and time by stress [$n = 6-10$ /group; mixed-effects ANOVA: time x treatment $F(15,420) = 2.108$, $p=0.0089$; time x stress $F(15,420) = 3.351$, $p=0.0001$] (Figure S5B). An analysis of normalized DAP AUCs did not identify any differences (Figure 3.7B). Circadian MAP was analyzed and interactions between time and stress were revealed [$n = 6-10$ /group; mixed-effects ANOVA: time x stress $F(15,420) = 3.363$, $p<0.0001$] (Figure S5C). AUC of MAP recordings was significantly different based on a 1-way ANOVA [$n=6-9$ /group; 1-way ANOVA: $F(3,21) = 4.361$, $p=0.0155$] (Figure 3.7C). Further, CVS increases were seen in GFP and TeLC groups (no CVS GFP v CVS GFP, $p=0.0107$; no CVS TeLC v CVS TeLC, $p=0.0361$) (Figure 3.6C). Next, A multi-effects ANOVA on chronic HR recordings unveiled an interaction effect of time by stress [$n = 6-10$ /group; mixed-effects ANOVA: time x stress $F(15,421) = 5.990$] (Figure S5D). Lastly, the AUC of HR was analyzed with an ANOVA and found differences [$n=6-9$ /group; 1-way ANOVA: $F(3,21) = 6.178$, $p=0.0035$] (Figure 3.7D). Additionally, CVS GFP was increased compared to no CVS GFP (no CVS GFP v CVS GFP, $p=0.0005$). Collectively, treatment effects were only evident during interactions with time when analyzing female hemodynamics. Therefore, these data powerfully illustrate the effects of CVS on female rats regardless of circuit status.

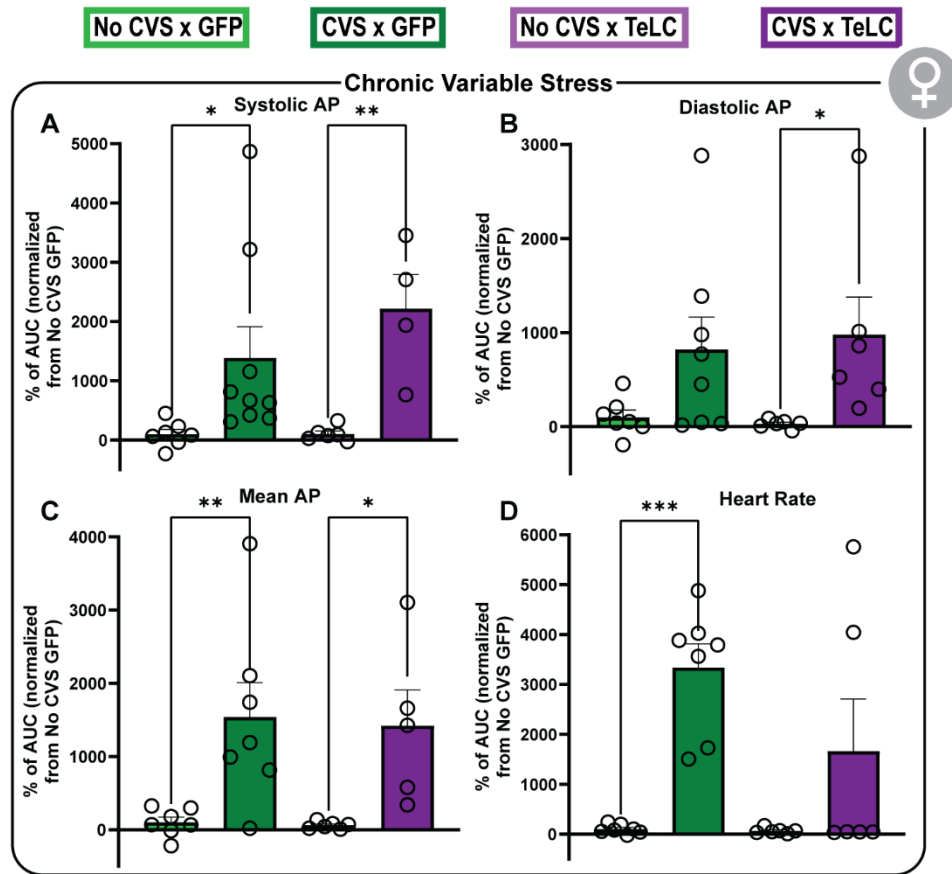


Figure 3.7 Cumulative female hemodynamic levels are altered with CVS and circuit disruption during chronic recordings. Analysis of cumulative SAP revealed increases in CVS rats regardless of treatment (A). No changes were seen in DAP (B). Cumulative MAP was increased in CVS rats regardless of treatment (C). HR was increased only in GFP controls (D). * $p < 0.05$, ** $p < 0.01$, **** $p < 0.0001$.

After CVS, rats underwent a Novel Environment assay to measure acute hemodynamic reactivity (Figure S3A). Minute-to-minute time points of this assay were analyzed by stress, treatment, and time. Here, male SAP was analyzed using a multi-effects ANOVA, and effects of treatment and treatment by stress were found [$n = 6-9$ /group; mixed-effects ANOVA: treatment $F(1,496) = 21.99$, $p < 0.0001$; treatment x stress $F(1,279) = 176.7$, $p < 0.0001$] (Figure S3E). A cumulative representation of SAP using AUC normalized to No CVS GFP controls. Percent changes of AUC were analyzed with an ANOVA, yet no differences were found (Figure 3.8A). Similarly, effects of treatment and treatment by stress were seen in DAP recordings [$n = 6-$

9/group; mixed-effects ANOVA: treatment $F(1,496) = 11.65$, $p=0.0007$; treatment x stress $F(1,279) = 126.6$, $p<0.0001$] (Figure S3F). A 1-way ANOVA of normalized DAP AUC values did not reveal any significant differences (Figure 3.8B). A multi-effects analysis of MAP revealed effects of treatment, stress, and treatment by stress [$n = 6-9$ /group; mixed-effects ANOVA: treatment $F(1,406) = 35.32$, $p<0.0001$; stress $F(1,249) = 11.65$, $p=0.0054$; treatment x stress $F(1,249) = 9.337$, $p=0.0025$] (Figure S3G). Analyzed aggregate MAP values did not detect any significant changes (Figure 3.8C). Lastly, HR during Novel Environment was analyzed. Likewise, effects of treatment and treatment by stress were identified [$n = 6-9$ /group; mixed-effects ANOVA: treatment $F(1,496) = 16.38$, $p<0.0001$; treatment x stress $F(1,279) = 67.37$, $p<0.0001$] (Figure S3E). Normalized percent changes of HR AUC during Novel Environment was not significantly different (Figure 3.8D). Together, hemodynamic activity recorded throughout Novel Environment revealed effects of treatment on vasopressor and heart rate reactivity. However, analysis of cumulative measures did not indicate any changes, suggesting that minute-to-minute effects of vmPFC-RVLM circuit disruption did not summate to larger changes in stress responding.

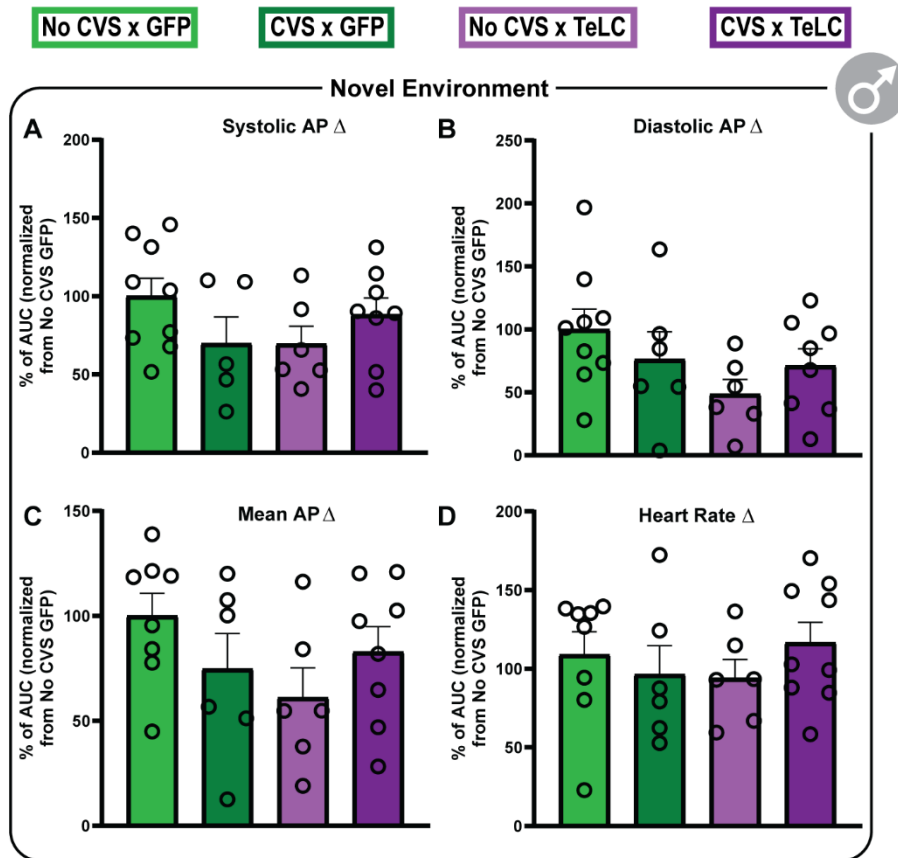


Figure 3.8 Cumulative male hemodynamic levels during Novel Environment showed no significant changes due to stress or treatment. Regardless of stress history or vmPFC-RVLM function, no significant differences were seen in SAP (A), DAP (B), MAP (C), and HR (D).

Following the administration of CVS, female rats were subjected to a Novel Environment assay to assess their immediate hemodynamic responses (Figure S3A). We conducted a mixed-effects analysis of this assay, considering factors such as stress, treatment, and time. In the case of female SAP, we used an ANOVA to reveal significant effects attributable to treatment and stress, and interaction effects between time by treatment and time by stress [n = 6–9/group; mixed-effects ANOVA: treatment $F(1,24) = 11.51, p=0.0024$; stress $F(1,24) = 11.56, p=0.0024$, time x treatment $F(30,720) = 2.375, p<0.0001$; time x stress $F(30,720) = 1.479, p=0.0488$] (Figure S4E). Additionally, we used an ANOVA to examine the cumulative representation of SAP using the percent change of normalized AUC to No CVS GFP controls. Here, significant

differences of aggregate SAP measurements were discovered [n=6–9/group; 1-way ANOVA: $F(3,25) = 8.130, p=0.0006$] (Figure 3.9A). Additionally, CVS groups were higher in GFP and TeLC cohorts (no CVS GFP v CVS GFP, $p=0.0209$; no CVS TeLC v CVS TeLC, $p=0.0116$) (Figure 3.8A). Similarly, when analyzing diastolic arterial pressure (DAP) recordings, we observed effects related to treatment and the interactions between time by treatment, time by stress, treatment by stress, and time by treatment by stress [n = 6–9/group; mixed-effects ANOVA: treatment $F(1,24) = 19.34, p=0.0002$; time x treatment $F(30,720) = 7.128, p=0.0024$, time x stress $F(30,720) = 1.862, p=0.0037$; treatment x stress $F(1,24) = 8.751, p=0.0069$; time x treatment x stress $F(30,720) = 3.121, p<0.0001$] (Figure S4F). Further, a 1-way ANOVA of normalized DAP AUC values did reveal statistically significant distinctions [n=5–9/group; 1-way ANOVA: $F(3,25) = 8.130, p=0.0158$] (Figure 3.8B). CVS TeLC was significantly increased relative to CVS conspecifics (no CVS TeLC v CVS TeLC, $p=0.0344$) (Figure 3.9B). Moving on to MAP, our analysis detected effects associated with treatment, time by treatment, time by stress, treatment by stress, and time by treatment by stress [n = 6–9/group; mixed-effects ANOVA: treatment $F(1,24) = 15.69, p=0.0006$; time x treatment $F(30,720) = 7.351, p<0.0001$, time x stress $F(30,720) = 1.912, p=0.0025$; treatment x stress $F(1,24) = 8.154, p=0.0087$; time x treatment x stress $F(30,720) = 3.599, p<0.0001$] (Figure S4G). When we examined the aggregated MAP values, we found significant differences in normalized MAP AUCs [n=5–9/group; 1-way ANOVA: $F(3,21) = 4.361, p=0.0155$] (Figure 3.9C). Again, CVS TeLC was significantly increased relative to CVS conspecifics (no CVS TeLC v CVS TeLC, $p=0.0344$) (Figure 3.9C).

Finally, we analyzed HR during the Novel Environment assay. Similarly, we observed effects related to treatment and the interactions between time by treatment, treatment by stress, and time by treatment by stress [n = 6–9/group; mixed-effects ANOVA: treatment $F(1,25) = 6.443$ $p=0.0177$; time x treatment $F(30,750) = 2.790$, $p<0.0001$, treatment x stress $F(1,25) = 4.878$, $p=0.0366$; time x treatment x stress $F(30, 750) = 2.418$, $p<0.0001$] (Figure S4H). Normalized AUCs of HR during the Novel Environment did not exhibit significant differences (Figure 3.9D). In summary, the assessment of female hemodynamic activity throughout the Novel Environment consistently revealed effects associated with the treatment. Specifically, vmPFC-RVLM disruption induces increased vasopressor reactivity in chronically stressed rats.

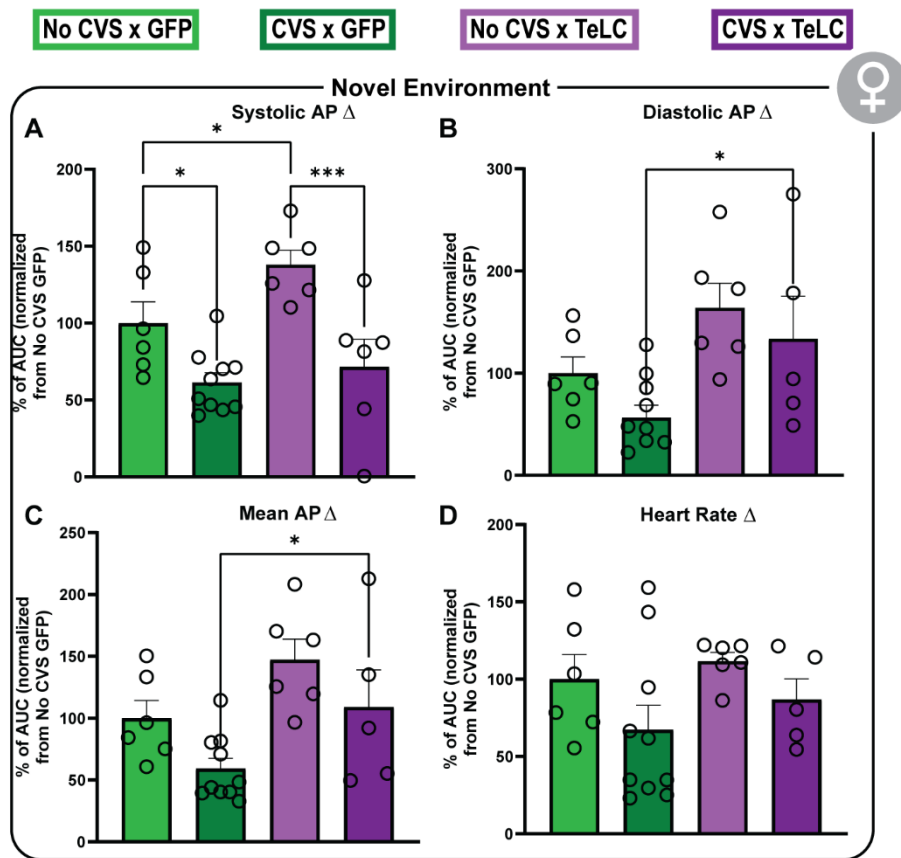


Figure 3.9 Aggregate female hemodynamics during Novel Environment were altered based on stress history and circuit status. SAP was reduced in CVS rats in both treatment groups (A). TeLC rats after CVS had increased DAP (B) and MAP (C). No changes were seen in HR (D). * $p<0.05$.

3.3.6 RVLM-projecting vmPFC Neurons Have Collaterals Throughout the Brain

Throughout Chapter 3 an intersectional TeLC approach was used to disrupt the vmPFC-RVLM circuit (Figure S3A). This technique transduced TeLC expression on RVLM-projecting vmPFC neurons (Figure 3.9A). Sparse extra-medullary vmPFC collaterals were seen in the posterior hypothalamus (B), lateral hypothalamus (C), lateral preoptic area (D), medial amygdala (E), nucleus tract of the solitary (F), and the medial dorsal thalamus (G). Therefore, each of these downstream vmPFC regions could be affected during our TeLC approach.

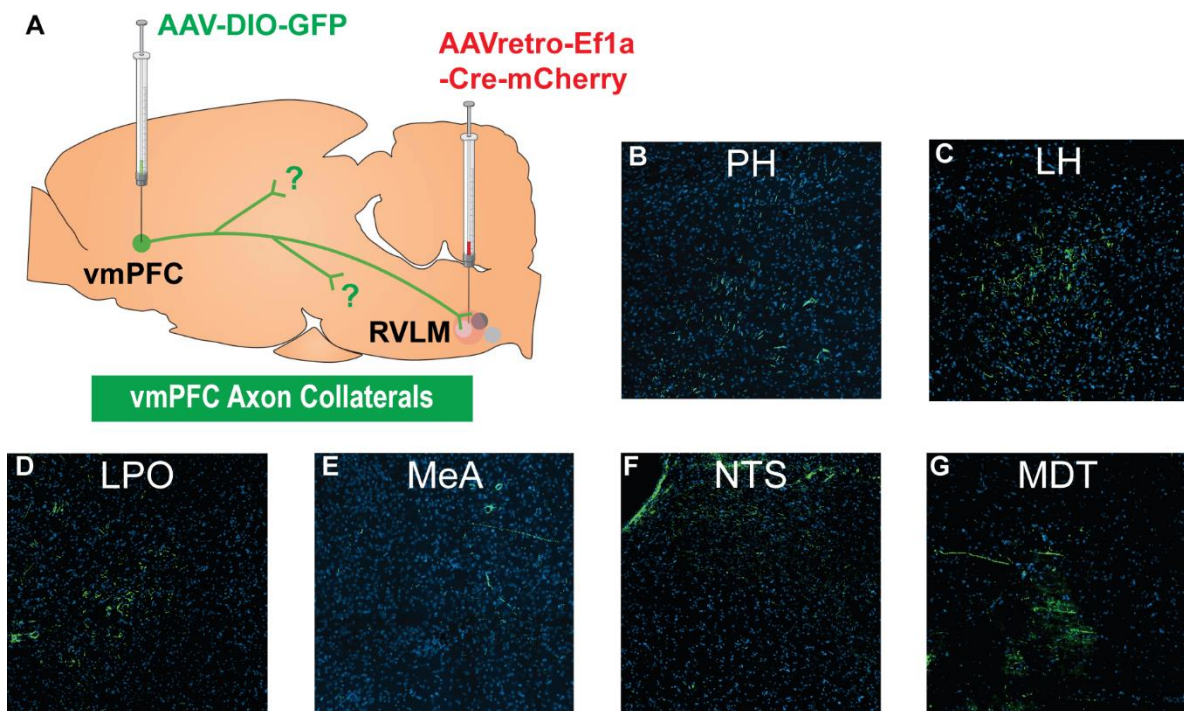


Figure 3.10 RVLM-projecting vmPFC collaterals are present in select regions. Multi-virus schema utilized to express GFP on RVLM-projecting vmPFC neurons (A). vmPFC collaterals were observed in the PH (B), LH (C), LPO (D), MeA (E), NTS (F), MDT (G). LH: lateral hypothalamus, LPO: lateral preoptic area, PH: posterior hypothalamus, MeA: medial amygdala, MDT: medial dorsal thalamus, NTS: nucleus tract of the solitary.

3.3.7 vmPFC-RVLM Circuit is Necessary to Reduce PNMT Expression in Females

Due to the consistent effects of vmPFC-RVLM circuit disruption and CVS, TH and PNMT transcript density was quantified in female VLM neurons using ISH. In TH transcripts, we observed effects by VLM subregion and an interaction effect of treatment by stress [n = 4/group; mixed-effects ANOVA: subregion $F(2,36) = 2.787$, $p=0.0178$; treatment x stress $F(1,36) = 13.95$, $p=0.0006$] (Figure 3.11A). Post-hoc analysis indicated that CVS increased TH transcript density in rostral and caudal subregions (Rostral: no CVS GFP v CVS GFP, $p=0.0189$; Caudal: no CVS GFP v CVS TeLC, $p=0.0122$). Additionally, TeLC treatment reduced TH density in the RVLM of CVS animals (Rostral: CVS GFP v CVS TeLC, $p=0.0377$), yet increased transcript density in CVLM of no CVS (Caudal: No CVS GFP v No CVS TeLC, $p=0.0300$). Analysis of PNMT transcript density revealed subregional VLM differences, effects of treatment, and an interaction effect between VLM regions x treatment [n = 4/group; mixed-effects ANOVA: subregion $F(2,36) = 23.81$, $p<0.0001$; treatment $F(1,36) = 17.60$, $p=0.0002$; subregion x treatment $F(2,36) = 6.439$, $p=0.0041$] (Figure 3.11B). Specifically, we observed TeLC treatment to increase PNMT density in rostral and intermediate VLM regions in no CVS and CVS groups (Rostral: No CVS GFP vs. No CVS TeLC, $p<0.0001$; Rostral: CVS GFP v CVS TeLC $p=0.0095$; Intermediate: CVS GFP v No CVS TeLC $p=0.0444$). Further, no CVS TeLC PNMT cell density was increased relative to CVS TeLC transcripts (Intermediate: No CVS TeLC v CVS TeLC, $p=0.0362$). These data suggest that vmPFC-RVLM circuit disruption via TeLC transduction increases PNMT transcript expression in no CVS and CVS rats.

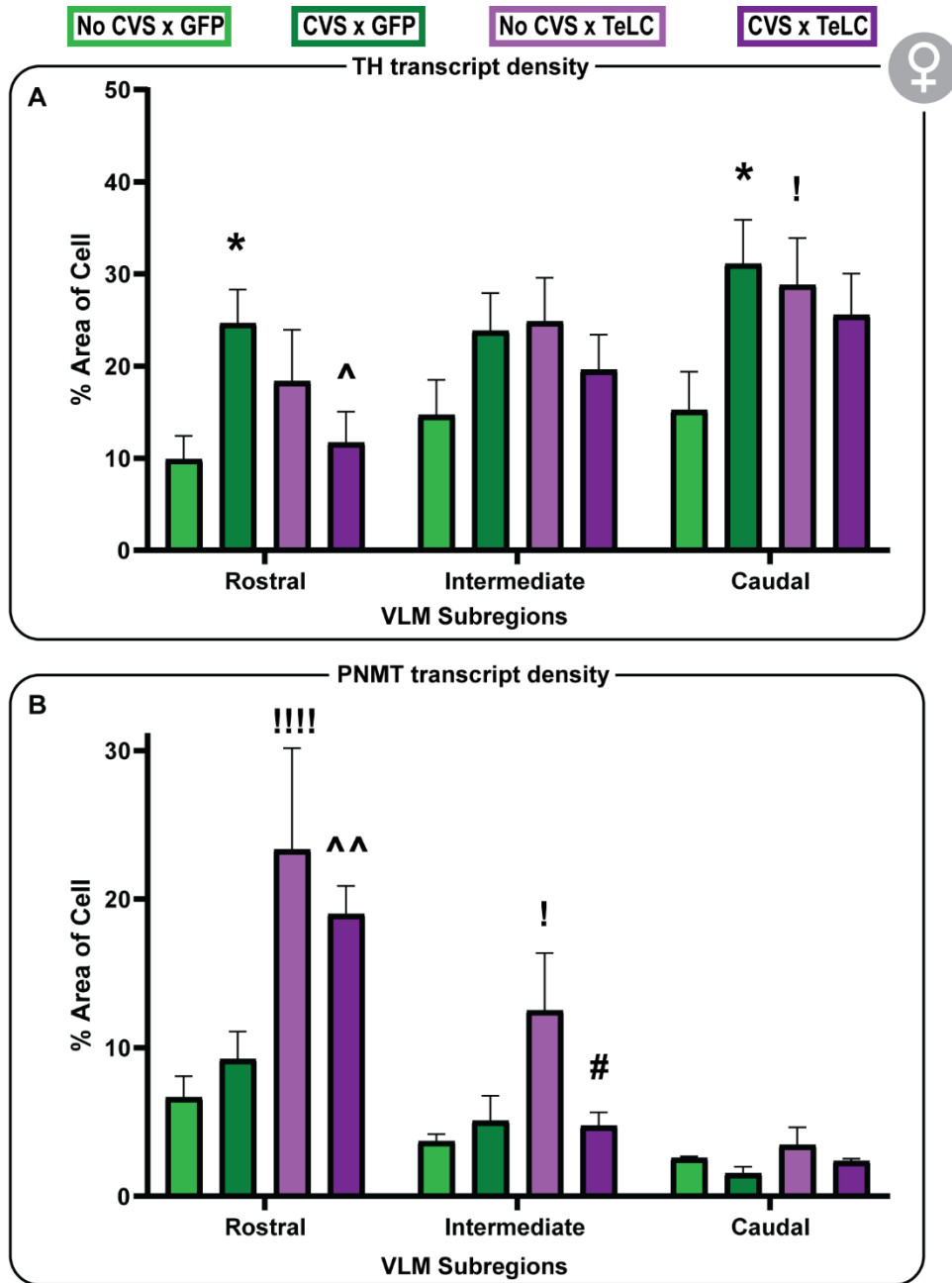


Figure 3.11 Female TH and PNMT transcript density were altered by stress and circuit status in VLM subregions. CVS increased TH transcripts in GFP groups (A). PNMT transcripts were increased in TeLC rats (B). No CVS x GFP vs CVS x GFP: * $p < 0.05$; No CVS x TeLC vs CVS x TeLC: # $p < 0.05$; No CVS x GFP vs no CVS x TeLC: ! $p < 0.05$, !!!! $p < 0.0001$; CVS x GFP vs CVS x TeLC: ^ $p < 0.05$, ^^ $p < 0.01$.

3.4 Discussion

Experiments executed throughout Chapter 3 demonstrated the effects of chronic stress on augmenting Epi/NE synthesis enzymes and the involvement of the vmPFC-RVLM circuit. First, gene expression analysis of the male and female VLM yielded data highlighting increased catecholamine synthesis enzyme transcripts following CVS. These data aided in the design of subsequent spatial transcriptomics experiments by identifying a candidate signaling system related to sympathoexcitation. To determine the role of the vmPFC-RVLM circuit during chronic stress, an intersectional viral strategy was used to express TeLC in RVLM-projecting vmPFC neurons, thereby disrupting vmPFC-RVLM signaling. TeLC-expressing vmPFC neurons had less synaptobrevin-2 protein located on terminals in the RVLM demonstrating that TeLC expression was effectively cleaving a synaptic vesicle protein needed for neurotransmitter release. This chronic circuit disruption approach was evaluated in a 2-week CVS paradigm in male and female rats. In males, CVS-exposed TeLC rats displayed decreased corticosterone levels in response to a novel stressor compared to control rats. CVS-naïve males showed no significant changes to TeLC treatment. In females, we similarly observed decreased glucose responding in TeLC vs GFP rats in no CVS groups. However, CVS TeLC female rats had increased glycemic and corticosterone stress responses compared to CVS control animals. Additionally, female CVS TeLC rats had increased behavioral avoidance, as indicated by less time spent in the center of an open field arena than CVS control rats. This behavioral effect was not present in males, demonstrating that the vmPFC-RVLM circuit is critical for approach-avoidant behaviors in CVS-exposed females but not males.

During radiotelemetry experiments, TeLC males and females had increased SAP and MAP in CVS groups throughout long-term basal recordings compared to no CVS TeLC rats.

When recording hemodynamics during Novel Environment, males displayed no differences regardless of stress or circuit status, yet females had increased hemodynamic stress reactivity. These results suggest the vmPFC-RVLM circuit is essential for preventing stress responses after chronic stress in female rats but not males. Further, this circuit regulation is necessary only after chronic stress exposure. To better understand this female-specific mechanism, TH and PNMT were probed using the TeLC circuit strategy to interrupt RVLM-projecting vmPFC output in female rats. Here, CVS-induced TH increases were seen throughout the VLM. Further, TeLC rats had increased PNMT densities in the RVLM. These data demonstrated that the vmPFC-RVLM circuit is also necessary to limit CVS-induced increases in PNMT expression density in females RVLM neurons.

Stress maladaptation is a multilevel biological process contributing to chronic stress-induced disease progression. In pre-sympathetic nuclei like the RVLM, identifying the molecular and cellular mechanisms related to stress adaptation may expand our understanding of how stress-related pathologies develop. Characterization of RVLM transcripts has primarily been limited to identifying neuronal chemoidentities within this region (Stornetta, 2009). These studies carefully audited catecholaminergic neurons and reported coexpression of neuropeptides (Stornetta et al., 2002). Beyond these initial studies, large-scale RVLM gene expression analysis is focused mainly on aging-related studies in various contexts, i.e., estradiol administration, immune system markers, and an acute heat stressor (Balivada et al., 2017; Pawar et al., 2018; Subramanian et al., 2015). Moreover, none of these studies analyzed both sexes although our studies used separate rat suppliers for male and female rats. This variable may contribute to differences between males and females after chronic stress. Nonetheless, TH was increased in CVS-exposed male and female rats (Figure 3.1). Critically, TH is the rate-limiting enzyme for

NE and Epi, which are synthesized in pre-sympathetic medullary neurons (Carlsson & Waldeck, 1972). Therefore, increased TH can potentially prime VLM neurons for increased catecholaminergic output to areas directly triggering HPA axis and sympathetic outflow.

Clinical neuroimaging studies have revealed a close-knit link between medial prefrontal cortex (mPFC) activity and cardiovascular physiology (Beissner et al., 2013; Brooks et al., 2018; Shoemaker et al., 2015). As a critical autonomic coordinator, mPFC activity can predict HR reactivity to stress, while attenuated mPFC activity correlates with baroreceptor unloading, and augmented mPFC activity correlates with enhanced heart rate variability (Gianaros & Jennings, 2018; Kimmerly et al., 2005; Ziegler et al., 2009). Such a connection epitomizes the influential role of the mPFC in the central autonomic network. Further, deep brain stimulation targeting the vmPFC induces hypotension by decreasing SAP (Lacuey et al., 2018). To better understand these phenomena, our lab stimulated the rodent vmPFC and measured in vivo physiological reactivity during acute and chronic stress using radiotelemetry and echocardiography (Wallace et al., 2021). Stimulating vmPFC projection neurons during an acute stressor induced diminished HR reactivity, MAP, and plasma corticosterone in male rats (Wallace et al., 2021). Further, prior vmPFC stimulation in males reduced the incidence of cardiac sympathetic dominance, ventricle contractility deficits, and hypertrophic remodeling of the left ventricle (Wallace et al., 2021). Remarkably, none of these therapeutic effects were seen in female rodents undergoing the same optogenetic activation of vmPFC neurons (Wallace et al., 2021). To address the sexually divergent regulation of vmPFC output, our lab shifted its focus to vmPFC projection regions responsible for autonomic coordination. Revealing these discrete circuits could be imperative to understanding the therapeutic value of vmPFC stimulation due to the distinct physiological systems that may be leveraged. For example, a study using similar stimulation protocols as our

lab described stimulating separate vmPFC pathways to generate opposing behavioral responses to stress (Warden et al., 2012). Therefore, stimulating a specific vmPFC circuit may develop a therapeutically protective effect in females and males.

The current studies sought to investigate the necessity of the vmPFC-RVLM circuit to reduce cardiovascular deficits caused by chronic stress. This approach utilized an intersectional TeLC approach as a projection-specific loss-of-function tool that functions by ablating synaptobrevin-2. Previous studies have demonstrated that TeLC-expressing neurons are unable to elicit evoked excitatory post-synaptic potentials and have reduced synaptobrevin-2 co-expression (Boehringer et al., 2017; Han et al., 2015; Woods et al., 2020). Here, we recapitulated the latter finding in RVLM-projecting vmPFC neurons (Figure 3.1E). Moreover, using a viral-mediated attenuation of the vmPFC-RVLM circuit allowed us to avoid optic implants or excessive cohorts in rats undergoing radiotelemetry surgeries and chronic stress. Although, using a TeLC approach does introduce certain caveats regarding unknown changes to the intrinsic firing of the affected neurons and post-synaptic modifications in the RVLM. As shown in Chapter 2, vmPFC neurons project to both catecholaminergic and inhibitory medullary neurons (Figure 2.2.7); hence, a change in presynaptic inputs may interrupt vital hindbrain microcircuitries that coordinate neurogenic regulation of hemodynamics and sympathetic outflow. These possible adaptations are a part of understanding the role of vmPFC-RVLM signaling, yet they also introduce additional variables when interpreting of circuit function.

The male outcomes suggest the circuit may not be essential for acute stress reactivity, either before or after chronic stress exposure. Conversely, when the circuit is disrupted and combined with CVS, these variables interact to reduce glucocorticoid stress responses and impede glycemic recovery. This reduced glucocorticoid presence may contribute to elevated

glucose levels, as corticosterone plays a significant role in promoting glycolysis. Importantly, when examining behavioral responses or vascular reactivity during exposure to a novel stressor, there were no observable interaction effects. These findings imply that male vmPFC-RVLM projections predominantly influence neuroendocrine or metabolic responses.

In female rats, the vmPFC-RVLM circuit functions to curb stress reactivity and is essential in dampening stress responses following exposure to chronic stress. Notably, this circuitry is not required to reduce stress reactivity in the absence of CVS. OF assays suggest the vmPFC-RVLM circuit may prevent avoidant behaviors following CVS. Similarly, interrupting RVLM-projecting vmPFC neurons caused an increase of TH density in the caudal VLM and increased PNMT density in the rostral and intermediate VLM of female rats. Therefore, more anatomical TeLC effects were seen when analyzing PNMT data compared to TH data. Notably, no post-hoc stress effects were seen in PNMT data by region. The lack of PNMT increases with CVS is challenging to interpret when PNMT is needed to derive Epi in the RVLM and parts of the intermediate medulla. Observing TeLC-induced increases in these specific subregions suggests that vmPFC-RVLM disruption may affect a particular part of the catecholamine synthesis pathway. The increased PNMT expression after circuit disruption means that VLM neurons could be primed to release more Epi, thereby triggering an increased stress response. Increased RVLM-PNMT expression in CVS TeLC females compared to CVS controls aligns with this hypothesis. These data suggest that after circuit disruption, increased PNMT expression in the RVLM may drive increased physiological and behavioral stress reactivity after CVS.

Lastly, RVLM-projecting vmPFC neurons do not exclusively synapse at the RVLM. Instead, bifurcations along these terminals allow for collaterals to other brain regions. A qualitative inspection of a male rat brain showed these collaterals to be present in stress

response-involved regions like the lateral preoptic area, lateral hypothalamus, posterior hypothalamus, medial dorsal thalamus, medial amygdala, and the nucleus of the solitary tract (Figure 3.9). Therefore, any interpretations regarding RVLM-projecting vmPFC neurons must consider other affected postsynaptic areas.

3.5 Conclusion

The experiments conducted in Chapter 3 shed light on the intricate mechanisms underlying the impact of chronic stress on the vmPFC-RVLM circuit and its potential role in mediating medullary catecholamine synthesis gene expression. Further, these data demonstrate the necessity of the vmPFC-RVLM circuit in limiting stress reactivity after chronic stress in female rats. In male rats, perturbation of the vmPFC-RVLM appears to alter integrated stress response patterns, although a certain level of circuit necessity may be present for cardiovascular function and reactivity. These studies build on prior studies (Chapter 2) that demonstrate the sufficiency of this circuit to reduce glucocorticoid responses after acute stress. This study design explored acute stress reactivity in rats exposed to CVS. CVS is a well-established model of chronic stress capable of generating metabolic, behavioral, and cardiovascular phenotypes that align with many stress-related pathologies. Critically, these stress response phenotypes, such as increased corticosterone, avoidance, and arterial pressure, are precursors to diseases caused by chronic stress, such as major depressive disorder (MDD) and cardiovascular disease (CVD) (Chida & Steptoe, 2010; Steptoe & Kivimäki, 2012). Females are at twice the risk of developing comorbidities like CVD and MDD than males (Eid et al., 2019; Goldstein et al., 2019; Möller-Leimkühler, 2007). With this in mind, our integrative data sets consistently demonstrate that the vmPFC-RVLM circuit is integral for preventing exacerbated physiological responses after

chronic stress in females. Therefore, the vmPFC-RVLM is the first identified corticolimbic circuit necessary for endocrine, behavioral, and cardiovascular reactivity in females. Moreover, these results largely align with circuit activation studies presented in Chapter 2. The female vmPFC-RVLM circuit appears to be a part of the neurogenic sequelae resulting from chronic stress. Further mechanistic studies investigating RVLM-specific changes after stress and in the context of this circuit are still needed to identify a biological mechanism. Identifying and understanding this female-specific mechanism could help identify an avenue to minimize the harmful outcomes caused by chronic stress.

Gene expression findings suggested an augmentation of VLM catecholamine synthesis, potentially expanding the capacity of the VLM to drive neuroendocrine and sympathetic stress responses. Subsequent experiments focused on the vmPFC-RVLM circuit and its role in modulating catecholamine synthesis gene expression. Disrupting this circuit via TeLC transduction resulted in altered TH and PNMT transcript density in different VLM subregions. Notably, TeLC-induced increases in female PNMT expression suggest that vmPFC-RVLM disruption may prime VLM neurons to release more catecholamines, potentially amplifying stress reactivity after CVS. These findings emphasized the importance of the vmPFC-RVLM circuit in regulating VLM function and stress reactivity. Overall, these experiments provide valuable insights into the molecular and circuit-level adaptations that occur in response to chronic stress, with implications for our understanding of stress-related pathologies. The intricate interplay between the vmPFC-RVLM circuit and VLM gene expression highlights the complexity of stress adaptation and its potential contribution to disease progression. Further research in this area may offer new avenues for therapeutic interventions targeting the neural circuits involved in stress-related disorders.

Chapter 4: Discussion

Hindbrain regions characterized by epinephrine and norepinephrine production play a vital role in coordinating stress responses by interpreting internal and external cues to maintain physiological balance. The key sources of epinephrine and norepinephrine in the brain are the NTS, VLM, and LC. These nuclei form an interconnected neural network with forebrain and spinal cord regions, enabling neuroendocrine, behavioral, and autonomic function integration. Despite advances in understanding these stress response systems, questions about the influence of sex, stress history, and circuit mechanisms persist. Here, we identify a prefrontal-medullary circuit that plays a role in inhibiting stress responses. The vmPFC sends signals to catecholaminergic neurons throughout the VLM, and stress-reactive vmPFC neurons project to the RVLM and CVLM. Activation of the vmPFC-RVLM circuit reduces glucocorticoid stress reactivity in both male and female rats, but hyperglycemia is blunted only in males. vmPFC-RVLM circuit stimulation targets non-catecholaminergic neurons in the RVLM. Catecholaminergic neurons in the RVLM are involved in stress responses, with different populations targeting sympathetic and HPA axis pathways. GABAergic and glycinergic neurons in the VLM inhibit these responses. Therefore, the vmPFC-RVLM circuit may leverage these neurons, offering a circuit mechanism for controlling stress responses.

Next, we explored the necessity of the vmPFC-RVLM circuit for limiting comprehensive stress responding and how it may interact with chronic stress. We used an intersectional TeLC approach to selectively reduce synaptobrevin-2 localization on RVLM-projecting vmPFC neuronal terminals. Chronic stress can have lasting effects on health, particularly in females, and the vmPFC-RVLM circuit appears crucial in mitigating these effects. TeLC and chronic stress-exposed male rats showed decreased corticosterone levels during stress and reduced glycem

recovery after stress, yet did not alter behavioral or cardiovascular stress reactivity. In females, circuit disruption and chronic stress resulted in increased glycemic, corticosterone, and arterial pressure stress reactivity and avoidance behaviors. Critically, these studies emphasize that the necessity of the vmPFC-RVLM circuit after chronic stress may be greater in females than males, highlighting the role of this pathway in preventing chronic stress-related outcomes in females but not males.

Lastly, we investigated the effects of chronic stress on signaling machinery within the female RVLM. Our hypothesis-driven survey of specific transcripts revealed increased TH after chronic stress. To better understand the role of vmPFC inputs to the RVLM, we again employed a circuit-based TeLC approach and used ISH combined with IHC to determine the transcript density of TH and PNMT in various VLM subregions. Notably, the TeLC-induced elevation of PNMT expression in females suggests that interrupting this circuit could potentially enhance the release of Epi by RVLM neurons, thereby intensifying stress reactivity after CVS. These results largely align with the observed physiological endpoints and underscore the significance of the vmPFC-RVLM circuit in modulating VLM activity and stress responsiveness.

4.1 Circuit manipulation approaches

Collectively, these findings emphasize the importance of the vmPFC-RVLM circuit in regulating stress responses and suggest potential therapeutic strategies for addressing chronic stress-related health problems. However, a careful interpretation of this data is needed to best apply the gained knowledge to future studies. Notably, the utilized circuit manipulation approaches act to acutely stimulate vmPFC terminals in RVLM or chronically disrupt signaling machinery in RVLM-projecting vmPFC neurons. Although these techniques are gain-of-function

and loss-of-function approaches, they should not be taken as simply ‘turning on or off’ the circuit. Instead, the nuances of each approach must be carefully considered to understand the role of the circuit.

Our experimental approach focused on precise optogenetic stimulation of vmPFC terminals within the RVLM. It is essential to note that this terminal stimulation can lead to downstream activation of targets, as observed in Figure 2.6, where RVLM-specific stimulation resulted in increased c-Fos expression in the caudal VLM, despite cannula placement being more rostral. Consequently, when assessing physiological endpoints using this method, it's crucial to consider the possibility of terminal stimulation. Our histological analysis of vmPFC-RVLM circuit stimulation revealed that the activated medullary cells were predominantly non-catecholaminergic. It is worth noting that this stimulation occurred for 5 minutes in the homecage, 90 minutes before sacrifice. Critically, stress assays used 30 minutes of stimulation. Further, we used a stimulation frequency of 10 Hz based on patch clamp recordings of vmPFC neurons, ensuring continuous activation without concerns of depolarization-block (Wallace et al., 2021). Nevertheless, the spike fidelity of RVLM neurons following 10 Hz vmPFC terminal stimulation remains uncertain. Despite these technical considerations, our data indicate that vmPFC-RVLM signaling effectively reduces glucocorticoid responses in both males and females.

Furthermore, our findings suggest a working hypothesis where vmPFC neurons exploit local inhibitory medullary neurons to inhibit catecholaminergic neurons, thereby modulating the activation of the HPA and SAM axes. While these stimulation experiments show that the vmPFC-RVLM circuit reduces glucocorticoid stress reactivity in both sexes, sex-related differences may still exist. Challenges in direct statistical comparisons between males and

females exist due to variations in experimental parameters. For example, different viral amounts were injected into males and females to account for vmPFC area differences. Because of this, sex-specific differences in circuit strength between males and females would be difficult to identify.

The second circuit manipulation approach was an intersectional viral strategy that transduced TeLC in RVLM-projecting vmPFC neurons. This approach reduces synaptobrevin-2 presence and blocks evoked post-synaptic potentials (Boehringer et al., 2017; Han et al., 2015). However, these prior studies did not report if TeLC expression changes spontaneous post-synaptic potentials or alters projection neuron cellular physiology. Furthermore, unlike optogenetics, this virus transduces expression over 8+ weeks and may cause pre- and post-synaptic adaptations. These adaptations are not limited to the vmPFC or RVLM but include any RVLM-projecting vmPFC neurons with collaterals to other areas. We mapped these collaterals (Figure 3.11) and although they are sparsely present in various areas, these areas are involved in stress response systems. Therefore, this loss-of-function approach can best be interpreted as testing the necessity of RVLM-projecting vmPFC neurons by disrupting presynaptic infrastructure.

4.2 Role of PFC in stress responding

Human neuroimaging studies highlight the vmPFC's role in emotion, cognition, and physiological regulation. Alterations in vmPFC activity are linked to depression and stress-related disorders, particularly in females. The growing focus on females in preclinical research and advances in neurobiological techniques have unveiled distinct sex-specific roles within vmPFC neural populations (Wallace et al., 2021; Wallace & Myers, 2023). In male rodents,

vmPFC glutamate neuron output reduces stress responses and coping and increases affective behaviors (Wallace et al., 2021). While less research has explored stress responding in females, our lab's recent studies suggest the female vmPFC may play a comparatively opposing role in initiating neuroendocrine and autonomic stress responses and driving affective behavior (Wallace et al., 2021). In the studies presented here, female vmPFC neurons can regulate stress responding to the same degree as males, revealing that vmPFC function is dependent on specific downstream circuitries to modulate stress responses. Further, gonadal hormone signaling within the vmPFC neural and glial network may influence many of these distinctions. Broadly, estrogens appear to shield glutamate neurons from the consequences of chronic stress, whereas androgens modulate cortical dopamine function (Almey et al., 2014; Aubele & Kritzer, 2012; Dossat et al., 2018; Handa et al., 1997; Kritzer, 2003; Wallace & Myers, 2023; Yousuf et al., 2019). Furthermore, the impact of chronic stress on vmPFC activity and cellular excitability varies for both sexes (Wallace & Myers, 2023; Wei et al., 2014). Ultimately, the intricate interplay between sex and stress significantly affects numerous aspects of vmPFC local networks and projections from vmPFC glutamate neurons (Wallace & Myers, 2021).

Physiological and behavioral functions associated with the vmPFC are executed through an extensive network of downstream projections (Saper & Stornetta, 2014). These glutamatergic pyramidal neurons are seen to project throughout the brain, with the densest projections being the posterior hypothalamus (PH) and the nucleus reuniens of the thalamus (Vertes, 2004; M. Wood et al., 2019). Notably, relatively no projections are seen in the PVN, indicating an intermediate relay is necessary to influence PVN-derived stress responding (Ulrich-Lai & Herman, 2009; Vertes, 2004; Wood et al., 2019). Teasing out specific vmPFC downstream circuits can leverage differential stress responses (Warden et al., 2012). Furthermore, vmPFC

projection-specific vulnerabilities can be seen after chronic stress (Shansky et al., 2009). Collectively, this evidence suggests that specific vmPFC projections can alter facets of stress responses and that chronic stress can influence circuit-specific effects.

How specific vmPFC projections differ between sex may spell out the intricacies of cortical coordination of physiological stress responses. Prior research has suggested that projection-specific circuits can be sex hormone-sensitive (Shansky et al., 2010), yet any sex differences within vmPFC downstream circuitries have only been reported by our lab. A recent study from our lab probed the vmPFC-PH circuit to reveal largely sex-specific results (Schaeuble et al., 2023). Here, the male vmPFC-PH circuitry actively enhances positive affective states and effectively reduces sympathetic-mediated stress responses. In contrast, the female vmPFC-PH circuit does not modulate social or preference behaviors. However, it is sufficient and necessary to elevate neuroendocrine stress responses. These findings underscore the intricate sex-specific modulation of stress reactivity and behavior through cortical projections to the hypothalamus. Further, these results predominately align with sex-specific effects after vmPFC somatic stimulation (Wallace et al., 2021). Together, these prior studies provide contextual and intellectual background surrounding our rationale to pursue an understanding of the vmPFC-RVLM circuit. In addition, it points out the uniqueness of observing sex-similar results when stimulating the vmPFC-RVLM circuit.

4.3 Role of RVLM in stress

Catecholaminergic neurons in the RVLM are pivotal in driving stress responses and maintaining physiological homeostasis. RVLM Epi and NE orchestrate sympathetic stress responses, often called the ‘fight or flight’ response. These hindbrain catecholaminergic neurons

are activated in response to stressors and lead to postganglionic sympathetic neurons to mediate peripheral neural responses. Notably, while catecholaminergic neurons are instrumental in initiating the stress response, they also play a critical role in maintaining physiological homeostasis. In non-stressful conditions, these neurons release norepinephrine to regulate blood pressure, heart rate, and digestive processes, ensuring the body operates within its optimal parameters. This delicate balance between stress response activation and homeostasis maintenance is essential for overall health and adaptability to environmental challenges.

Brain areas projecting to the RVLM are crucial in orchestrating the stress response. These areas include the hypothalamus, amygdala, prefrontal cortex, and dorsal brainstem (Rinaman, 2011; Saha et al., 2005; Saper, 2002; Shafton et al., 1998). First, hypothalamic projections from the PVN are the most characterized hypothalamic afferent. PVN-derived inputs to the RVLM originate in the pre-sympathetic magnocellular cells (Ziegler et al., 2005). Notably, the quantity of PVN neurons engaged in RVLM projections, surpasses those projecting to the spinal cord by approximately sevenfold (Shafton et al., 1998). Further, PVN-RVLM activity correlates with renal sympathetic nerve activity alterations (Chen & Toney, 2010). Limbic inputs to the RVLM are less understood. Although limbic-RVLM circuits were identified decades ago (Gabbott et al., 2007; Gabbott et al., 2005; Hurley et al., 1991; Yasui et al., 1991), little progress has been made in investigating the circuit until recent technological advancements made targeting this circuit possible. Thus far, these circuitries are canonically considered a systems-level mechanism providing cognitive control over stress reactions or a structural path to psychosomatic coordination (Dum et al., 2019; Saper & Stornetta, 2014). Lastly, dorsal medullary inputs from the NTS innervate local VLM inhibitory neurons to modulate VLM Epi/NE output (Gao et al., 2019; Guyenet et al., 1990; Heesch et al., 2006). This microcircuitry is recruited by the

baroreflex to regulate sympathetic output and maintain cardiovascular homeostasis, underscoring the pivotal support these nuclei provide (Guyenet, 2006). From our studies, we describe a stress-sensitive vmPFC-RVLM circuitry that can recruit this local inhibitory circuitry. These data provide a cellular mechanism of how cortical inputs can regulate various components of the RVLM-derived stress response.

Unfortunately, not much is known about RVLM, specifically, in the context of preclinical models of chronic stress. However, many lines of research have used rodent models of elevated blood pressure (e.g. spontaneously hypertensive, obese, or salt-sensitive) and revealed elevated tonic activity of C1/RVLM neurons to be substrate for sympathetic-mediated hypertension (Huber & Schreihof, 2011; Ito et al., 2000, 2001; Minson et al., 1996; Stocker et al., 2007). Further, chronic homotypic stressors are seen to increase TH expression in the male RVLM (Tóth et al., 2008). These studies align with our gene expression results and together indicate the RVLM is primed to release more Epi/NE and thereby drive sympathoexcitation after chronic stress. Keeping in mind that RVLM output is needed for sympathetic-induced vascular changes (Madden & Sved, 2003), identifying RVLM adaptations to chronic stress denote a fundamental step in understanding resulting physiological adaptations. Furthermore, understanding how the male and female RVLM differently adapt could help elucidate physiological sex differences relating to chronic stress.

4.4 Male vmPFC-RVLM function

Findings from males reveal the vmPFC-RVLM circuit to have intricate roles in acute stress reactivity and physiological regulation in the context of chronic stress. Optogenetic stimulation experiments demonstrated that the circuit is sufficient at reducing acute stress

responses. However, the results from TeLC experiments suggest the circuit is not necessary for acute stress reactivity in no CVS rats. Conversely, circuit disruption and CVS interact to reduce glucocorticoid stress responses and glycemic recovery. Decreased circulating glucocorticoids may account for the increased glucose levels because corticosterone drives glycolysis (Kuo et al., 2015). Notably, no circuit or stress interaction effects were seen when observing exploratory behavior or cardiovascular reactivity during novel stressors. In the context of stress responding, these data suggest that vmPFC-RVLM projections may predominately affect glucocorticoid stress responses as seen in optogenetic stimulation and TeLC studies. As previously described, intermediate and caudal regions of the VLM project to the PVN to influence HPA axis output and drive glucocorticoid secretion (Ritter et al., 2019a). These data suggest that vmPFC-RVLM function after CVS may preferentially affect neurons with ascending projections. As described in Figure 2.2, stress-sensitive vmPFC neurons have parallel and divergent projections to the RVLM and CVLM, thereby confirming a possible structural circuit mechanism.

Homecage radiotelemetry recordings revealed an interaction of CVS and vmPFC-RVLM signaling on basal cardiovascular measures. Here, systolic and mean AP was increased after CVS in TeLC rats. Although no effects were observed on stress reactivity, a disrupted vmPFC-RVLM circuit unmasked effects of CVS on resting AP suggesting that circuit function may predominately affect maintenance of baseline AP rather than vasopressor reactivity during stress. RVLM Epi/NE neurons are vital to tonic and reflexive control of cardiovascular function (Madden et al., 2006; Madden & Sved, 2003). How these catecholaminergic medullary neurons can differentiate between those functions remains to be determined. However, it is possible that vmPFC-RVLM function after CVS mainly impacts Epi/NE neurons with ascending projections, as previously proposed. Ascending projections to other regions with pre-sympathetic bulbospinal

projections, like the LC, could account for baseline increases in AP (Crawley et al., 1980; Sved & Felsten, 1987; Wood & Valentino, 2017). This hypothesized male-specific mechanism for vmPFC-RVLM projections can also be supported by gene expression data revealing increased TH expression after CVS. Together, these data underscore the contribution of vmPFC-RVLM circuit function after CVS on specific stress response systems.

4.5 Female vmPFC-RVLM function

From both circuit manipulation approaches, each finding in female rats indicated that the vmPFC-RVLM circuit is sufficient to reduce stress reactivity and necessary to blunt stress responses after chronic stress exposure. Critically, TeLC-induced increases of glucocorticoid, glycemic, and AP reactivity to stress are unveiled with CVS. CVS in females augments the number and magnitude of synaptic machinery transcripts that could interact with a vmPFC-RVLM circuit (Figure 3.1). Notably, increases of TH expression are seen after CVS implying an increased capacity to synthesize and release Epi/NE. Therefore, if CVS-exposed rats are predisposed to facilitate stress responses, disrupted vmPFC-RVLM function identifies the necessity of the circuit to reduce physiological stress responses. However, the exact mechanism underlying vmPFC-RVLM function and CVS interactions may be more complicated. Gene expression data identified numerous transcripts altered by CVS (48 of 74 transcripts). Moreover, these transcripts are involved in excitatory, inhibitory, and steroid signaling, thereby clouding a clear or simple interpretation of medullary adaptations after CVS. Although, increased expression of signaling machinery can indicate an added level of regulation within the VLM. Regardless, more studies are needed to best understand how the female VLM changes after chronic stress and how those changes impact physiological outcomes.

Notably, CVS-induced increases on baseline cardiovascular measures occur in vmPFC-RVLM disrupted and circuit-intact rats. Therefore, the weight of vmPFC-RVLM signaling occurs primarily during stress responding. This observation is in line with RTPP data, where rats are habituated to the arena to reduce neophobia. Critically, circuit stimulation did not show any preference or avoidance for vmPFC-RVLM activation during the RTPP assay. OF assays from TeLC experiments indicate that the vmPFC-RVLM circuit may drive avoidant behaviors after CVS. It is plausible that a lack of affective effect in RTPP may be driven by stress-history or by the specific behavioral phenotype we are probing. The role of vmPFC-RVLM function may be minimized in no CVS rats, thus leading to no effect in stimulation studies compared to TeLC assays. Future vmPFC-RVLM stimulation experiments on CVS animals could test this hypothesis. Further, RTPP and OF assays probe affective motivation and exploration, respectively. vmPFC-RVLM function could drive exploration avoidance yet have no effect on affective motivation. However, we need more behavioral tests to gain a clearer understanding of the role of vmPFC-RVLM function. We also need to determine whether this function directly influences behaviors or if it interacts with other physiological systems that shape behavior.

4.6 Conclusion

The reported collection of studies provides valuable insights into the role of the vmPFC-RVLM circuit in regulating stress responses and how function differs between sexes. In all, the data collected through the described experiments highlight the significance of hindbrain regions responsible for epinephrine and norepinephrine production in coordinating stress responses, with vmPFC-RVLM circuit stimulation being sufficient to inhibit stress responses in male and female rats. To a degree, these stimulation studies recapitulate ongoing clinical work utilizing deep brain

stimulation (DBS). For the past 20 years, DBS of the vmPFC provided symptom relief for treatment-resistant depression (Crowell et al., 2019). However, this line of studies had difficulty achieving a stable recovery in patients, leading to trial-and-error stimulation adjustments. Recently, this research group utilized an AI model to modify stimulation parameters based on imaging of structural and functional connectivity within the vmPFC white matter network while also matching facial expression changes during stimulation sessions (Alagapan et al., 2023). Albeit preliminary, these adjustments have been able to reduce clinical symptoms in 90% of participants and achieve long-term remission in 70% (Alagapan et al., 2023). From clinical studies like these, our results can assist in providing a circuit-level mechanism of vmPFC-mediated effects on stress-related health outcomes. Furthermore, these clinical studies indicate that employing dynamic circuit stimulation methods can help us gain a deeper understanding of the complete range of behavioral and physiological effects related to vmPFC-RVLM regulation.

Additionally, this circuit appears necessary for reducing neuroendocrine, behavioral, and cardiovascular stress responses in female rats exposed to chronic stress. This sex-bias of circuit function and stress history to females, emphasizes the role of the vmPFC-RVLM in preventing chronic stress-related outcomes. Critically, pathologies associated with chronic stress predominately affect women, adding interest to this neural pathway. Additionally, these experiments emphasize the complexity of manipulating this circuit and the need for a nuanced interpretation of the results. The comprehensive analysis of multiple physiological stress responses emphasize the importance of considering various factors, such as stimulation duration, circuit strength, and sex-specific variations in experimental parameters. The resulting data underscore the need for future studies to understand how the vmPFC-RVLM circuit interacts with multiple physiological systems and the interplay between these systems in the context of

chronic stress. Overall, the research reported offers valuable insights into the intricate mechanisms underlying stress regulation and the potential therapeutic implications of targeting the vmPFC-RVLM circuit.

References

- Alagapan, S., Choi, K. S., Heisig, S., Riva-Posse, P., Crowell, A., Tiruvadi, V., Obatusin, M., Veerakumar, A., Waters, A. C., Gross, R. E., Quinn, S., Denison, L., O'Shaughnessy, M., Connor, M., Canal, G., Cha, J., Hershenberg, R., Nauvel, T., Isbaine, F., ... Rozell, C. J. (2023). Cingulate dynamics track depression recovery with deep brain stimulation. *Nature*, *622*(7981), 1–9. <https://doi.org/10.1038/s41586-023-06541-3>
- Alfinito, P. D., Chen, X., Mastroeni, R., Pawlyk, A. C., & Deecher, D. C. (2009). Estradiol increases catecholamine levels in the hypothalamus of ovariectomized rats during the dark-phase. *European Journal of Pharmacology*, *616*(1–3), 334–339. <https://doi.org/10.1016/j.ejphar.2009.06.045>
- Almey, A., Cannell, E., Bertram, K., Filardo, E., Milner, T. A., & Brake, W. G. (2014). Medial prefrontal cortical estradiol rapidly alters memory system bias in female rats: Ultrastructural analysis reveals membrane-associated estrogen receptors as potential mediators. *Endocrinology (United States)*, *155*(11), 4422–4432. <https://doi.org/10.1210/en.2014-1463>
- Anderson, R. M., Johnson, S. B., Lingg, R. T., Hinz, D. C., Romig-Martin, S. A., & Radley, J. J. (2019). Evidence for Similar Prefrontal Structural and Functional Alterations in Male and Female Rats Following Chronic Stress or Glucocorticoid Exposure. *Cerebral Cortex*. <https://doi.org/10.1093/cercor/bhz092>
- Andresen, M. C., Doyle, M. W., Jin, Y. H., & Bailey, T. W. (2001). Cellular mechanisms of baroreceptor integration at the nucleus tractus solitarius. *Annals of the New York Academy of Sciences*, *940*(1), 132–141. <https://doi.org/10.1111/j.1749-6632.2001.tb03672.x>
- Arnsten, A. F. T. (2009). Stress signalling pathways that impair prefrontal cortex structure and function. In *Nature Reviews Neuroscience* (Vol. 10, Issue 6, pp. 410–422). Nature

Publishing Group. <https://doi.org/10.1038/nrn2648>

Arnsten, A. F. T. (2011). Catecholamine influences on dorsolateral prefrontal cortical networks.

In *Biological Psychiatry* (Vol. 69, Issue 12, pp. e89–e99). Elsevier.

<https://doi.org/10.1016/j.biopsych.2011.01.027>

Arnsten, A. F. T. (2015). Stress weakens prefrontal networks: Molecular insults to higher

cognition. In *Nature Neuroscience* (Vol. 18, Issue 10, pp. 1376–1385). Nature Publishing

Group. <https://doi.org/10.1038/nn.4087>

Aubele, T., & Kritzer, M. F. (2012). Androgen influence on prefrontal dopamine systems in

adult male rats: Localization of cognate intracellular receptors in medial prefrontal

projections to the ventral tegmental area and effects of gonadectomy and hormone

replacement on glutamate-stimulated. *Cerebral Cortex*, 22(8), 1799–1812.

<https://doi.org/10.1093/cercor/bhr258>

Bains, J. S., Cusulin, J. I. W., & Inoue, W. (2015). Stress-related synaptic plasticity in the

hypothalamus. In *Nature Reviews Neuroscience* (Vol. 16, Issue 7, pp. 377–388).

<https://doi.org/10.1038/nrn3881>

Balivada, S., Ganta, C. K., Zhang, Y., Pawar, H. N., Ortiz, R. J., Becker, K. G., Khan, A. M., &

Kenney, M. J. (2017). Microarray analysis of aging-associated immune system alterations

in the rostral ventrolateral medulla of F344 rats. *Physiological Genomics*, 49(8), 400–415.

<https://doi.org/10.1152/physiolgenomics.00131.2016>

Bangasser, D. A., Curtis, A., Reyes, B. A. S., Bethea, T. T., Parastatidis, I., Ischiropoulos, H.,

Van Bockstaele, E. J., & Valentino, R. J. (2010). Sex differences in corticotropin-releasing

factor receptor signaling and trafficking: Potential role in female vulnerability to stress-

related psychopathology. *Molecular Psychiatry*, 15(9), 896–904.

<https://doi.org/10.1038/mp.2010.66>

- Bangasser, D. A., Reyes, B. A. S., Piel, D., Garachh, V., Zhang, X. Y., Plona, Z. M., Van Bockstaele, E. J., Beck, S. G., & Valentino, R. J. (2013). Increased vulnerability of the brain norepinephrine system of females to corticotropin-releasing factor overexpression. *Molecular Psychiatry*, *18*(2), 166–173. <https://doi.org/10.1038/mp.2012.24>
- Bangasser, Debra A., & Valentino, R. J. (2012). Sex differences in molecular and cellular substrates of stress. In *Cellular and Molecular Neurobiology* (Vol. 32, Issue 5, pp. 709–723). Springer. <https://doi.org/10.1007/s10571-012-9824-4>
- Bangasser, Debra A., Wiersielis, K. R., & Khantsis, S. (2016). Sex differences in the locus coeruleus-norepinephrine system and its regulation by stress. In *Brain Research* (Vol. 1641, pp. 177–188). Elsevier. <https://doi.org/10.1016/j.brainres.2015.11.021>
- Bangasser, Debra A., Zhang, X., Garachh, V., Hanhauser, E., & Valentino, R. J. (2011). Sexual dimorphism in locus coeruleus dendritic morphology: A structural basis for sex differences in emotional arousal. *Physiology and Behavior*, *103*(3–4), 342–351. <https://doi.org/10.1016/j.physbeh.2011.02.037>
- Banihashemi, L., & Rinaman, L. (2006). Noradrenergic inputs to the bed nucleus of the stria terminalis and paraventricular nucleus of the hypothalamus underlie hypothalamic-pituitary-adrenal axis but not hypophagic or conditioned avoidance responses to systemic yohimbine. *Journal of Neuroscience*, *26*(44), 11442–11453. <https://doi.org/10.1523/JNEUROSCI.3561-06.2006>
- Bechtold, A. G., Patel, G., Hochhaus, G., & Scheuer, D. A. (2009). Chronic blockade of hindbrain glucocorticoid receptors reduces blood pressure responses to novel stress and attenuates adaptation to repeated stress. *American Journal of Physiology - Regulatory*

Integrative and Comparative Physiology, 296(5), 1445–1454.

<https://doi.org/10.1152/ajpregu.00095.2008>

Beissner, F., Meissner, K., Bär, K. J., & Napadow, V. (2013). The autonomic brain: An activation likelihood estimation meta-analysis for central processing of autonomic function. *Journal of Neuroscience*, 33(25), 10503–10511. <https://doi.org/10.1523/JNEUROSCI.1103-13.2013>

Benarroch, E. E. (2008). The arterial baroreflex: Functional organization and involvement in neurologic disease. *Neurology*, 71(21), 1733–1738.

<https://doi.org/10.1212/01.wnl.0000335246.93495.92>

Bienkowski, M. S., & Rinaman, L. (2008). Noradrenergic inputs to the paraventricular hypothalamus contribute to hypothalamic-pituitary-adrenal axis and central Fos activation in rats after acute systemic endotoxin exposure. *Neuroscience*, 156(4), 1093–1102.

<https://doi.org/10.1016/j.neuroscience.2008.08.011>

Boehringer, R., Polygalov, D., Huang, A. J. Y., Middleton, S. J., Robert, V., Wintzer, M. E., Piskorowski, R. A., Chevaleyre, V., & McHugh, T. J. (2017). Chronic Loss of CA2 Transmission Leads to Hippocampal Hyperexcitability. *Neuron*, 94(3), 642-655.e9.

<https://doi.org/10.1016/j.neuron.2017.04.014>

Boudaba, C., Di, S., & Tasker, J. G. (2003). Presynaptic noradrenergic regulation of glutamate inputs to hypothalamic magnocellular neurones. In *Journal of Neuroendocrinology* (Vol. 15, Issue 8, pp. 803–810). John Wiley & Sons, Ltd.

<https://doi.org/10.1046/j.1365-2826.2003.01063.x>

Brooks, S. D., Hileman, S. M., Chantler, P. D., Milde, S. A., Lemaster, K. A., Frisbee, S. J., Shoemaker, J. K., Jackson, D. N., & Frisbee, J. C. (2018). Protection from vascular

dysfunction in female rats with chronic stress and depressive symptoms. *American Journal of Physiology - Heart and Circulatory Physiology*, 314(5), H1070–H1084.

<https://doi.org/10.1152/ajpheart.00647.2017>

Bruinstroop, E., Cano, G., Vanderhorst, V. G. J. M., Cavalcante, J. C., Wirth, J., Sena-Esteves, M., & Saper, C. B. (2012). Spinal projections of the A5, A6 (locus coeruleus), and A7 noradrenergic cell groups in rats. *Journal of Comparative Neurology*, 520(9), 1985–2001.

<https://doi.org/10.1002/cne.23024>

Bundzikova-Osacka, J., Ghosal, S., Packard, B. A., Ulrich-Lai, Y. M., & Herman, J. P. (2015). Role of nucleus of the solitary tract noradrenergic neurons in post-stress cardiovascular and hormonal control in male rats. *Stress*, 18(2), 221–232.

<https://doi.org/10.3109/10253890.2015.1013531>

Burke, P. G. R., Abbott, S. B. G., Coates, M. B., Viar, K. E., Stornetta, R. L., & Guyenet, P. G. (2014). Optogenetic stimulation of adrenergic C1 neurons causes sleep state-dependent cardiorespiratory stimulation and arousal with sighs in rats. *American Journal of Respiratory and Critical Care Medicine*, 190(11), 1301–1310.

<https://doi.org/10.1164/rccm.201407-1262OC>

Card, J. P., Sved, J. C., Craig, B., Raizada, M., Vazquez, J., & Sved, A. F. (2006). Efferent projections of rat rostroventrolateral medulla C1 catecholamine neurons: Implications for the central control of cardiovascular regulation. *Journal of Comparative Neurology*, 499(5), 840–859.

<https://doi.org/10.1002/cne.21140>

Carlsson, A., & Waldeck, B. (1972). Formation of dopamine from 3-methoxytyrosine - Fact or artifact? *Naunyn-Schmiedeberg's Archives of Pharmacology*, 272(4), 441–446.

<https://doi.org/10.1007/BF00501250>

- Chappell, P. B., Smith, M. A., Kilts, C. D., Bissette, G., Ritchie, J., Anderson, C., & Nemeroff, C. B. (1986). Alterations in corticotropin-releasing factor-like immunoreactivity in discrete rat brain regions after acute and chronic stress. *Journal of Neuroscience*, *6*(10), 2908–2914. <https://doi.org/10.1523/jneurosci.06-10-02908.1986>
- Chen, C., Jiang, Z. Y., Fu, X., Yu, D., Huang, H., & Tasker, J. G. (2019). Astrocytes Amplify Neuronal Dendritic Volume Transmission Stimulated by Norepinephrine. *Cell Reports*, *29*(13), 4349–4361.e4. <https://doi.org/10.1016/j.celrep.2019.11.092>
- Chen, Q. H., & Toney, G. M. (2010). In vivo discharge properties of hypothalamic paraventricular nucleus neurons with axonal projections to the rostral ventrolateral medulla. *Journal of Neurophysiology*, *103*(1), 4–15. <https://doi.org/10.1152/jn.00094.2009>
- Cheng, Z., Powley, T. L., Schwaber, J. S., & Doyle, F. J. (1999). Projections of the dorsal motor nucleus of the vagus to cardiac ganglia of rat atria: An anterograde tracing study. *Journal of Comparative Neurology*, *410*(2), 320–341. [https://doi.org/10.1002/\(SICI\)1096-9861\(19990726\)410:2<320::AID-CNE12>3.0.CO;2-5](https://doi.org/10.1002/(SICI)1096-9861(19990726)410:2<320::AID-CNE12>3.0.CO;2-5)
- Chida, Y., & Steptoe, A. (2010). Greater Cardiovascular Responses to Laboratory Mental Stress Are Associated With Poor Subsequent Cardiovascular Risk Status. *Hypertension*, *55*(4), 1026–1032. <https://doi.org/10.1161/HYPERTENSIONAHA.109.146621>
- Cora, M. C., Kooistra, L., & Travlos, G. (2015). Vaginal Cytology of the Laboratory Rat and Mouse: Review and Criteria for the Staging of the Estrous Cycle Using Stained Vaginal Smears. *Toxicologic Pathology*, *43*(6), 776–793. <https://doi.org/10.1177/0192623315570339>
- Crawley, J. N., Maas, J. W., & Roth, R. H. (1980). Evidence against specificity of electrical stimulation of the nucleus locus coeruleus in activating the sympathetic nervous system in

- the rat. *Brain Research*, 183(2), 301–311. [https://doi.org/10.1016/0006-8993\(80\)90466-7](https://doi.org/10.1016/0006-8993(80)90466-7)
- Crowell, A. L., Riva-Posse, P., Holtzheimer, P. E., Garlow, S. J., Kelley, M. E., Gross, R. E., Denison, L., Quinn, S., & Mayberg, H. S. (2019). Long-term outcomes of subcallosal cingulate deep brain stimulation for treatment-resistant depression. *American Journal of Psychiatry*, 176(11), 949–956. <https://doi.org/10.1176/appi.ajp.2019.18121427>
- Cullinan, W. E., Herman, J. P., Battaglia, D. F., Akil, H., & Watson, S. J. (1995). Pattern and time course of immediate early gene expression in rat brain following acute stress. *Neuroscience*, 64(2), 477–505. [https://doi.org/10.1016/0306-4522\(94\)00355-9](https://doi.org/10.1016/0306-4522(94)00355-9)
- Cummings, S., & Seybold, V. (1988). Relationship of alpha-1- and alpha-2-adrenergic-binding sites to regions of the paraventricular nucleus of the hypothalamus containing corticotropin-releasing factor and vasopressin neurons. *Neuroendocrinology*, 47(6), 523–532. <https://doi.org/10.1159/000124965>
- Cunningham, E. T., & Sawchenko, P. E. (1988). Anatomical specificity of noradrenergic inputs to the paraventricular and supraoptic nuclei of the rat hypothalamus. *Journal of Comparative Neurology*, 274(1), 60–76. <https://doi.org/10.1002/cne.902740107>
- Curtis, A L, Grigoriadis, D. E., Page, M. E., Rivier, J., & Valentino, R. J. (1994). Pharmacological comparison of two corticotropin-releasing factor antagonists: In vivo and in vitro studies. *Journal of Pharmacology and Experimental Therapeutics*, 268(1), 359–365.
- Curtis, Andre L., Bethea, T., & Valentino, R. J. (2005). Sexually Dimorphic Responses of the Brain Norepinephrine System to Stress and Corticotropin-Releasing Factor. *Neuropsychopharmacology 2006 31:3*, 31(3), 544–554. <https://doi.org/10.1038/sj.npp.1300875>
- Dallman, M. F. (2005). Fast glucocorticoid actions on brain: Back to the future. In *Frontiers in*

Neuroendocrinology (Vol. 26, Issues 3–4, pp. 103–108). Academic Press.

<https://doi.org/10.1016/j.yfrne.2005.08.001>

Dampney, R. A.L., Coleman, M. J., Fontes, M. A. P., Hirooka, Y., Horiuchi, J., Li, Y. W., Polson, J. W., Potts, P. D., & Tagawa, T. (2002). Central mechanisms underlying short- and long-term regulation of the cardiovascular system. *Clinical and Experimental Pharmacology and Physiology*, 29(4), 261–268. <https://doi.org/10.1046/j.1440-1681.2002.03640.x>

Dampney, Roger A.L. (2015). Central mechanisms regulating coordinated cardiovascular and respiratory function during stress and arousal. In *American Journal of Physiology - Regulatory Integrative and Comparative Physiology* (Vol. 309, Issue 5, pp. R429–R443). American Physiological Society. <https://doi.org/10.1152/ajpregu.00051.2015>

Daskalakis, N. P., Meijer, O. C., & de Kloet, E. R. (2022). Mineralocorticoid receptor and glucocorticoid receptor work alone and together in cell-type-specific manner: Implications for resilience prediction and targeted therapy. *Neurobiology of Stress*, 18, 100455. <https://doi.org/10.1016/j.ynstr.2022.100455>

Dayas, C. V, Buller, K. M., Crane, J. W., Xu, Y., & Day, T. a. (2001). Stressor categorization: acute physical and psychological stressors elicit distinctive recruitment. *Eur J Neurosci*, 14(7), 1143–1152. <https://doi.org/10.1046/j.0953-816x.2001.01733.x>

Dearing, C., Morano, R., Ptaskiewicz, E., Mahbod, P., Scheimann, J. R., Franco-Villanueva, A., Wulsin, L., & Myers, B. (2021). Glucoregulation and coping behavior after chronic stress in rats: Sex differences across the lifespan. *Hormones and Behavior*, 136, 105060. <https://doi.org/10.1016/j.yhbeh.2021.105060>

DePuy, S. D., Stornetta, R. L., Bochorishvili, G., Deisseroth, K., Witten, I., Coates, M., &

- Guyenet, P. G. (2013). Glutamatergic neurotransmission between the C1 neurons and the parasympathetic preganglionic neurons of the dorsal motor nucleus of the vagus. *Journal of Neuroscience*, *33*(4), 1486–1497. <https://doi.org/10.1523/JNEUROSCI.4269-12.2013>
- Dickhout, J. G., Carlisle, R. E., & Austin, R. C. (2011). Interrelationship between cardiac hypertrophy, heart failure, and chronic kidney disease: Endoplasmic reticulum stress as a mediator of pathogenesis. In *Circulation Research* (Vol. 108, Issue 5, pp. 629–642). Lippincott Williams & Wilkins Hagerstown, MD.
<https://doi.org/10.1161/CIRCRESAHA.110.226803>
- Dossat, A. M., Wright, K. N., Strong, C. E., & Kabbaj, M. (2018). Behavioral and biochemical sensitivity to low doses of ketamine: Influence of estrous cycle in C57BL/6 mice. *Neuropharmacology*, *130*, 30–41. <https://doi.org/10.1016/j.neuropharm.2017.11.022>
- Drevets, W. C., Price, J. L., Furey, M. L., Ae, J. L. P., Furey, M. L., & Price, J. L. (2008). Brain structural and functional abnormalities in mood disorders: implications for neurocircuitry models of depression. *Brain Struct Funct*, *213*(1–2), 93–118.
<https://doi.org/10.1007/s00429-008-0189-x>
- Drevets, W. C., Savitz, J., & Trimble, M. (2008). The subgenual anterior cingulate cortex in mood disorders. *CNS Spectrums*, *13*(8), 663–681.
<https://doi.org/10.1017/S1092852900013754>
- Dum, R. P., Levinthal, D. J., & Strick, P. L. (2019). The mind-body problem: Circuits that link the cerebral cortex to the adrenal medulla. *Proceedings of the National Academy of Sciences of the United States of America*, *116*(52), 26321–26328.
<https://doi.org/10.1073/pnas.1902297116>
- Eid, R. S., Gobinath, A. R., & Galea, L. A. M. (2019). Sex differences in depression: Insights

- from clinical and preclinical studies. In *Progress in Neurobiology* (Vol. 176, pp. 86–102). Pergamon. <https://doi.org/10.1016/j.pneurobio.2019.01.006>
- Fan, Y., Chen, P., Li, Y., & Zhu, M. Y. (2013). Effects of chronic social defeat on expression of dopamine β -hydroxylase in rat brains. *Synapse*, *67*(6), 300–312.
<https://doi.org/10.1002/syn.21641>
- Fan, Y., Chen, P., Raza, M. U., Szebeni, A., Szebeni, K., Ordway, G. A., Stockmeier, C. A., & Zhu, M. Y. (2018). Altered Expression of Phox2 Transcription Factors in the Locus Coeruleus in Major Depressive Disorder Mimicked by Chronic Stress and Corticosterone Treatment In Vivo and In Vitro. *Neuroscience*, *393*, 123–137.
<https://doi.org/10.1016/J.NEUROSCIENCE.2018.09.038>
- Firmino, E. M. S., Kuntze, L. B., Lagatta, D. C., Dias, D. P. M., & Resstel, L. B. M. (2019). Effect of chronic stress on cardiovascular and ventilatory responses activated by both chemoreflex and baroreflex in rats. *Journal of Experimental Biology*, *222*(20).
<https://doi.org/10.1242/jeb.204883>
- Flak, J. N., Myers, B., Solomon, M. B., Mcklveen, J. M., Krause, E. G., & Herman, J. P. (2014a). Role of paraventricular nucleus-projecting norepinephrine/epinephrine neurons in acute and chronic stress. *European Journal of Neuroscience*, *39*(11), 1903–1911.
<https://doi.org/10.1111/ejn.12587>
- Flak, J. N., Myers, B., Solomon, M. B., Mcklveen, J. M., Krause, E. G., & Herman, J. P. (2014b). Role of paraventricular nucleus-projecting norepinephrine/epinephrine neurons in acute and chronic stress. *European Journal of Neuroscience*, *39*(11), 1903–1911.
<https://doi.org/10.1111/ejn.12587>
- Flak, J. N., Myers, B., Solomon, M. B., Mcklveen, J. M., Krause, E. G., & Herman, J. P.

- (2014c). Role of paraventricular nucleus-projecting norepinephrine/epinephrine neurons in acute and chronic stress. *European Journal of Neuroscience*, 39(11), 1903–1911.
<https://doi.org/10.1111/ejn.12587>
- Flak, J. N., Ostrander, M. M., Tasker, J. G., & Herman, J. P. (2009). Chronic stress-induced neurotransmitter plasticity in the PVN. *Journal of Comparative Neurology*, 517(2), 156–165. <https://doi.org/10.1002/cne.22142>
- Flak, J. N., Solomon, M. B., Jankord, R., Krause, E. G., & Herman, J. P. (2012). Identification of Chronic Stress Activated Regions Reveals a Potential Recruited Circuit in Rat Brain. *The European Journal of Neuroscience*, 36(4), 2547. <https://doi.org/10.1111/J.1460-9568.2012.08161.X>
- Franco, A. J., Chen, C., Scullen, T., Zsombok, A., Salahudeen, A. A., Di, S., Herman, J. P., & Tasker, J. G. (2016). Sensitization of the hypothalamic-pituitary-adrenal axis in a male rat chronic stress model. *Endocrinology*, 157(6), 2346–2355. <https://doi.org/10.1210/en.2015-1641>
- Fritschy, J. -M., & Grzanna, R. (1990). Demonstration of two separate descending noradrenergic pathways to the rat spinal cord: Evidence for an intragriseal trajectory of locus coeruleus axons in the superficial layers of the dorsal horn. *Journal of Comparative Neurology*, 291(4), 553–582. <https://doi.org/10.1002/cne.902910406>
- Fuxe, K. (1965). Evidence for the existence of monoamine neurons in the central nervous system - III. The monoamine nerve terminal. *Zeitschrift Für Zellforschung Und Mikroskopische Anatomie*, 65(4), 573–596. <https://doi.org/10.1007/BF00337069>
- Fuxe, K., Dahlström, A. B., Jonsson, G., Marcellino, D., Guescini, M., Dam, M., Manger, P., & Agnati, L. (2010). The discovery of central monoamine neurons gave volume transmission

- to the wired brain. In *Progress in Neurobiology* (Vol. 90, Issue 2, pp. 82–100). Pergamon.
<https://doi.org/10.1016/j.pneurobio.2009.10.012>
- Füzesi, T., Wittmann, G., Liposits, Z., Lechan, R. M., & Fekete, C. (2007). Contribution of noradrenergic and adrenergic cell groups of the brainstem and agouti-related protein-synthesizing neurons of the arcuate nucleus to neuropeptide-Y innervation of corticotropin-releasing hormone neurons in hypothalamic paraventricular nucle. *Endocrinology*, *148*(11), 5442–5450. <https://doi.org/10.1210/en.2007-0732>
- Gabbott, P. L.A., Warner, T., & Busby, S. J. (2007). Catecholaminergic neurons in medullary nuclei are among the post-synaptic targets of descending projections from infralimbic area 25 of the rat medial prefrontal cortex. *Neuroscience*, *144*(2), 623–635.
<https://doi.org/10.1016/j.neuroscience.2006.09.048>
- Gabbott, Paul L.A., Warner, T. A., Jays, P. R. L., Salway, P., & Busby, S. J. (2005). Prefrontal cortex in the rat: Projections to subcortical autonomic, motor, and limbic centers. *Journal of Comparative Neurology*, *492*(2), 145–177. <https://doi.org/10.1002/cne.20738>
- Gao, H., Korim, W. S., Yao, S. T., Heesch, C. M., & Derbenev, A. V. (2019). Glycinergic neurotransmission in the rostral ventrolateral medulla controls the time course of baroreflex-mediated sympathoinhibition. *Journal of Physiology*, *597*(1), 283–301.
<https://doi.org/10.1113/JP276467>
- Ghosal, S., Bundzikova-Osacka, J., Dolgas, C. M., Myers, B., & Herman, J. P. (2014). Glucocorticoid receptors in the nucleus of the solitary tract (NTS) decrease endocrine and behavioral stress responses. *Psychoneuroendocrinology*, *45*, 142–153.
<https://doi.org/10.1016/j.psyneuen.2014.03.018>
- Gianaros, P. J., & Jennings, J. R. (2018). Host in the machine: A neurobiological perspective on

psychological stress and cardiovascular disease. *American Psychologist*, 73(8), 1031–1044.
<https://doi.org/10.1037/amp0000232>

Goldstein, J. M., Hale, T., Foster, S. L., Tobet, S. A., & Handa, R. J. (2019). Sex differences in major depression and comorbidity of cardiometabolic disorders: impact of prenatal stress and immune exposures. In *Neuropsychopharmacology* (Vol. 44, Issue 1, pp. 59–70). Nature Publishing Group. <https://doi.org/10.1038/s41386-018-0146-1>

Gos, T., Krell, D., Biela, H., Brisch, R., Trübner, K., Steiner, J., Bernstein, H. G., Jankowski, Z., & Bogerts, B. (2008). Tyrosine hydroxylase immunoreactivity in the locus coeruleus is elevated in violent suicidal depressive patients. *European Archives of Psychiatry and Clinical Neuroscience*, 258(8), 513–520. <https://doi.org/10.1007/s00406-008-0825-8>

Gouws, J. M., Sherrington, A., Zheng, S., Kim, J. S., & Iremonger, K. J. (2022). Regulation of corticotropin-releasing hormone neuronal network activity by noradrenergic stress signals. *Journal of Physiology*, 600(19), 4347–4359. <https://doi.org/10.1113/JP283328>

Grippo, A. J., Moffitt, J. A., & Johnson, A. K. (2002). Cardiovascular alterations and autonomic imbalance in an experimental model of depression. *American Journal of Physiology - Regulatory Integrative and Comparative Physiology*, 282(5 51-5).
<https://doi.org/10.1152/ajpregu.00614.2001>

Guillamón, A., de Blas, M. R., & Segovia, S. (1988). Effects of sex steroids on the development of the locus coeruleus in the rat. *Developmental Brain Research*, 40(2), 306–310.
[https://doi.org/10.1016/0165-3806\(88\)90143-5](https://doi.org/10.1016/0165-3806(88)90143-5)

Guyenet, P. G., Darnall, R. A., & Riley, T. A. (1990). Rostral ventrolateral medulla and sympathorespiratory integration in rats. *American Journal of Physiology - Regulatory Integrative and Comparative Physiology*, 259(5 28-5).

<https://doi.org/10.1152/ajpregu.1990.259.5.r1063>

Guyenet, Patrice G. (2006). The sympathetic control of blood pressure. In *Nature Reviews Neuroscience* (Vol. 7, Issue 5, pp. 335–346). Nature Publishing Group.

<https://doi.org/10.1038/nrn1902>

Guyenet, Patrice G., Stornetta, R. L., Bochorishvili, G., DePuy, S. D., Burke, P. G. R., & Abbott, S. B. G. (2013). C1 neurons: The body's EMTs. In *American Journal of Physiology - Regulatory Integrative and Comparative Physiology* (Vol. 305, Issue 3).

<https://doi.org/10.1152/ajpregu.00054.2013>

Guyenet, Patrice G., Stornetta, R. L., Souza, G. M. P. R., Abbott, S. B. G., & Brooks, V. L. (2020). Neuronal Networks in Hypertension: Recent Advances. In *Hypertension* (pp. 300–311). Lippincott Williams & Wilkins Hagerstown, MD.

<https://doi.org/10.1161/HYPERTENSIONAHA.120.14521>

Han, S., Soleiman, M., Soden, M., Zweifel, L., & Palmiter, R. D. (2015). Elucidating an Affective Pain Circuit that Creates a Threat Memory. *Cell*, *162*(2), 363–374.

<https://doi.org/10.1016/j.cell.2015.05.057>

Handa, R. J., Hejna, G. M., & Lorens, S. A. (1997). Androgen inhibits neurotransmitter turnover in the medial prefrontal cortex of the rat following exposure to a novel environment. *Brain Research*, *751*(1), 131–138. [https://doi.org/10.1016/S0006-8993\(96\)01394-7](https://doi.org/10.1016/S0006-8993(96)01394-7)

Handa, R. J., Sheng, J. A., Castellanos, E. A., Templeton, H. N., & McGivern, R. F. (2022). Sex Differences in Acute Neuroendocrine Responses to Stressors in Rodents and Humans. *Cold Spring Harbor Perspectives in Biology*, *14*(9), a039081.

<https://doi.org/10.1101/cshperspect.a039081>

Hay, M. (2016). Sex, the brain and hypertension: Brain oestrogen receptors and high blood

- pressure risk factors. In *Clinical Science* (Vol. 130, Issue 1, pp. 9–18). Portland Press.
<https://doi.org/10.1042/CS20150654>
- Heck, A. L., Thompson, M. K., Uht, R. M., & Handa, R. J. (2020). Sex-dependent mechanisms of glucocorticoid regulation of the mouse hypothalamic corticotropin-releasing hormone gene. *Endocrinology (United States)*, *161*(1). <https://doi.org/10.1210/endo/bqz012>
- Heesch, C. M., Laiprasert, J. D., & Kvochina, L. (2006). RVLM glycine receptors mediate GABAA and GABAB independent sympathoinhibition from CVLM in rats. *Brain Research*, *1125*(1), 46–59. <https://doi.org/10.1016/j.brainres.2006.09.090>
- Hegarty, A. A., & Felder, R. B. (1997). Vasopressin and V1-receptor antagonists modulate the activity of NTS neurons receiving baroreceptor input. *American Journal of Physiology - Regulatory Integrative and Comparative Physiology*, *273*(1 42-1).
<https://doi.org/10.1152/ajpregu.1997.273.1.r143>
- Herman, J. P., Adams, D., & Prewitt, C. (1995). Regulatory changes in neuroendocrine stress-integrative circuitry produced by a variable stress paradigm. *Neuroendocrinology*, *61*(2), 180–190. <https://doi.org/10.1159/000126839>
- Herman, J. P., McKlveen, J. M., Ghosal, S., Kopp, B., Wulsin, A., Makinson, R., Scheimann, J., & Myers, B. (2016). Regulation of the hypothalamic-pituitary- adrenocortical stress response. *Comprehensive Physiology*, *6*(2), 603–621. <https://doi.org/10.1002/cphy.c150015>
- Herman, J. P., & Tasker, J. G. (2016). Paraventricular hypothalamic mechanisms of chronic stress adaptation. In *Frontiers in Endocrinology* (Vol. 7, Issue OCT).
<https://doi.org/10.3389/fendo.2016.00137>
- Hernández-Pérez, O. R., Hernández, V. S., Nava-Kopp, A. T., Barrio, R. A., Seifi, M., Swinny, J. D., Eiden, L. E., & Zhang, L. (2019). A Synaptically Connected Hypothalamic

- Magnocellular Vasopressin-Locus Coeruleus Neuronal Circuit and Its Plasticity in Response to Emotional and Physiological Stress. *Frontiers in Neuroscience*, 13.
<https://doi.org/10.3389/fnins.2019.00196>
- Hokfelt, T. (1984). Distribution maps of tyrosine-hydroxylase-immunoreactive neurons in the rat brain. *Classical Transmitters in the CNS*, 277–379.
<https://cir.nii.ac.jp/crid/1573950399921715456>
- Huber, D. A., & Schreihöfer, A. M. (2011). Altered regulation of the rostral ventrolateral medulla in hypertensive obese Zucker rats. *https://doi.org/10.1152/Ajphheart.00075.2011*, 301(1), 230–240. <https://doi.org/10.1152/AJPHEART.00075.2011>
- Hurley, K. M., Herbert, H., Moga, M. M., & Saper, C. B. (1991). Efferent projections of the infralimbic cortex of the rat. *Journal of Comparative Neurology*, 308(2), 249–276.
<https://doi.org/10.1002/cne.903080210>
- Ito, S., Komatsu, K., Tsukamoto, K., & Sved, A. F. (2000). Excitatory amino acids in the rostral ventrolateral medulla support blood pressure in spontaneously hypertensive rats. *Hypertension*, 35(1 II), 413–417. <https://doi.org/10.1161/01.hyp.35.1.413>
- Ito, S., Komatsu, K., Tsukamoto, K., & Sved, A. F. (2001). Tonic excitatory input to the rostral ventrolateral medulla in Dahl salt-sensitive rats. *Hypertension*, 37(2 II), 687–691.
<https://doi.org/10.1161/01.hyp.37.2.687>
- Jiang, Z., Chen, C., Weiss, G. L., Fu, X., Stelly, C. E., Sweeten, B. L. W., Tirrell, P. S., Pursell, I., Stevens, C. R., Fisher, M. O., Begley, J. C., Harrison, L. M., & Tasker, J. G. (2022). Stress-induced glucocorticoid desensitizes adrenoreceptors to gate the neuroendocrine response to somatic stress in male mice. *Cell Reports*, 41(3), 111509.
<https://doi.org/10.1016/j.celrep.2022.111509>

- Kanbar, R., Stornetta, R. L., Cash, D. R., Lewis, S. J., & Guyenet, P. G. (2010). Photostimulation of Phox2b Medullary Neurons Activates Cardiorespiratory Function in Conscious Rats. *American Journal of Respiratory and Critical Care Medicine*, 182(9), 1184.
<https://doi.org/10.1164/RCCM.201001-0047OC>
- Khan, A. M., Kaminski, K. L., Sanchez-Watts, G., Ponzio, T. A., Brent Kuzmiski, J., Bains, J. S., & Watts, A. G. (2011). MAP kinases couple hindbrain-derived catecholamine signals to hypothalamic adrenocortical control mechanisms during glycemia-related challenges. *Journal of Neuroscience*, 31(50), 18479–18491. <https://doi.org/10.1523/JNEUROSCI.4785-11.2011>
- Kimmerly, D. S., O’Leary, D. D., Menon, R. S., Gati, J. S., & Shoemaker, J. K. (2005). Cortical regions associated with autonomic cardiovascular regulation during lower body negative pressure in humans. *Journal of Physiology*, 569(1), 331–345.
<https://doi.org/10.1113/jphysiol.2005.091637>
- Kivimäki, M., & Steptoe, A. (2017). Effects of stress on the development and progression of cardiovascular disease. *Nature Reviews Cardiology*.
<https://doi.org/10.1038/nrcardio.2017.189>
- Kritzer, M. F. (2003). Long-term gonadectomy affects the density of tyrosine hydroxylase- but not dopamine- β -hydroxylase-, choline acetyltransferase- or serotonin-immunoreactive axons in the medial prefrontal cortices of adult male rats. *Cerebral Cortex*, 13(3), 282–296.
<https://doi.org/10.1093/cercor/13.3.282>
- Kuo, T., McQueen, A., Chen, T. C., & Wang, J. C. (2015). Regulation of glucose homeostasis by glucocorticoids. *Advances in Experimental Medicine and Biology*, 872, 99–126.
https://doi.org/10.1007/978-1-4939-2895-8_5

- Kvetnansky, R., Bodnar, I., Shahar, T., Uhereczky, G., Krizanova, O., & Mravec, B. (2006). Effect of lesion of A5 and A7 brainstem noradrenergic areas or transection of brainstem pathways on sympathoadrenal activity in rats during immobilization stress. *Neurochemical Research*, 31(2), 267–275. <https://doi.org/10.1007/s11064-005-9016-4>
- Lacuey, N., Hampson, J. P., Theeranaew, W., Zonjy, B., Vithala, A., Hupp, N. J., Loparo, K. A., Miller, J. P., & Lhatoo, S. D. (2018). Cortical structures associated with human blood pressure control. *JAMA Neurology*, 75(2), 194–202. <https://doi.org/10.1001/jamaneurol.2017.3344>
- Li, A. J., Wang, Q., & Ritter, S. (2018). Selective pharmacogenetic activation of catecholamine subgroups in the ventrolateral medulla elicits key glucoregulatory responses. *Endocrinology*, 159(1), 341–355. <https://doi.org/10.1210/en.2017-00630>
- Li, H. Y., Ericsson, A., & Sawchenko, P. E. (1996). Distinct mechanisms underlie activation of hypothalamic neurosecretory neurons and their medullary catecholaminergic afferents in categorically different stress paradigms. *Proceedings of the National Academy of Sciences of the United States of America*, 93(6), 2359–2364. <https://doi.org/10.1073/pnas.93.6.2359>
- Li, X., Eadara, S., Jeon, S., Liu, Y., Muwanga, G., Qu, L., Caterina, M. J., & Meffert, M. K. (2021). Combined single-molecule fluorescence in situ hybridization and immunohistochemistry analysis in intact murine dorsal root ganglia and sciatic nerve. *STAR Protocols*, 2(2). <https://doi.org/10.1016/j.xpro.2021.100555>
- Lister, R. G. (1990). Ethologically-based animal models of anxiety disorders. In *Pharmacology and Therapeutics* (Vol. 46, Issue 3, pp. 321–340). Pergamon. [https://doi.org/10.1016/0163-7258\(90\)90021-S](https://doi.org/10.1016/0163-7258(90)90021-S)
- Littlejohn, E. L., Fedorchak, S., & Boychuk, C. R. (2020). Sex-steroid-dependent plasticity of

- brain-stem autonomic circuits. In *American Journal of Physiology - Regulatory Integrative and Comparative Physiology* (Vol. 319, Issue 1, pp. R60–R68). American Physiological Society. <https://doi.org/10.1152/ajpregu.00357.2019>
- Loewy, A. D., & Burton, H. (1978). Nuclei of the solitary tract: Efferent projections to the lower brain stem and spinal cord of the cat. *Journal of Comparative Neurology*, *181*(2), 421–449. <https://doi.org/10.1002/cne.901810211>
- Lubbers, L. S., Zafian, P. T., Gautreaux, C., Gordon, M., Alves, S. E., Correa, L., Lorrain, D. S., Hickey, G. J., & Luine, V. (2010). Estrogen receptor (ER) subtype agonists alter monoamine levels in the female rat brain. *Journal of Steroid Biochemistry and Molecular Biology*, *122*(5), 310–317. <https://doi.org/10.1016/j.jsbmb.2010.08.005>
- Ma, X. M., Lightman, S. L., & Aguilera, G. (1999). Vasopressin and corticotropin-releasing hormone gene responses to novel stress in rats adapted to repeated restraint. *Endocrinology*, *140*(8), 3623–3632. <https://doi.org/10.1210/endo.140.8.6943>
- Machhada, A., Ang, R., Ackland, G. L., Ninkina, N., Buchman, V. L., Lythgoe, M. F., Trapp, S., Tinker, A., Marina, N., & Gourine, A. V. (2015). Control of ventricular excitability by neurons of the dorsal motor nucleus of the vagus nerve. *Heart Rhythm*, *12*(11), 2285–2293. <https://doi.org/10.1016/j.hrthm.2015.06.005>
- Madden, C. J., Stocker, S. D., & Sved, A. F. (2006). Attenuation of homeostatic responses to hypotension and glucoprivation after destruction of catecholaminergic rostral ventrolateral medulla neurons. *American Journal of Physiology - Regulatory Integrative and Comparative Physiology*, *291*(3), R751–R759. <https://doi.org/10.1152/ajpregu.00800.2005>
- Madden, C. J., & Sved, A. F. (2003). Cardiovascular regulation after destruction of the C1 cell group of the rostral ventrolateral medulla in rats. *American Journal of Physiology-Heart*

and Circulatory Physiology, 285(6), H2734–H2748.

<https://doi.org/10.1152/ajpheart.00155.2003>

Makino, S., Smith, M. A., & Gold, P. W. (1995). Increased expression of corticotropin-releasing hormone and vasopressin messenger ribonucleic acid (mrna) in the hypothalamic paraventricular nucleus during repeated stress: Association with reduction in glucocorticoid receptor mrna levels. *Endocrinology*, 136(8), 3299–3309.

<https://doi.org/10.1210/endo.136.8.7628364>

Makino, S., Smith, M. A., & Gold, P. W. (2002). Regulatory role of glucocorticoids and glucocorticoid receptor mRNA levels on tyrosine hydroxylase gene expression in the locus coeruleus during repeated immobilization stress. *Brain Research*, 943(2), 216–223.

[https://doi.org/10.1016/S0006-8993\(02\)02647-1](https://doi.org/10.1016/S0006-8993(02)02647-1)

Marina, N., Abdala, A. P. L., Korsak, A., Simms, A. E., Allen, A. M., Paton, J. F. R., & Gourine, A. V. (2011). Control of sympathetic vasomotor tone by catecholaminergic C1 neurones of the rostral ventrolateral medulla oblongata. *Cardiovascular Research*, 91(4), 703–710.

<https://doi.org/10.1093/cvr/cvr128>

McCall, J. G., Al-Hasani, R., Siuda, E. R., Hong, D. Y., Norris, A. J., Ford, C. P., & Bruchas, M. R. (2015). CRH Engagement of the Locus Coeruleus Noradrenergic System Mediates Stress-Induced Anxiety. *Neuron*, 87(3), 605–620.

<https://doi.org/10.1016/j.neuron.2015.07.002>

Mccall, J. G., Siuda, E. R., Bhatti, D. L., & Lamley, A. (2017). *Locus coeruleus to basolateral amygdala noradrenergic projections promote anxiety - like behavior*. 1–23.

<https://doi.org/10.7554/eLife.18247>

McKlveen, J. M., Myers, B., & Herman, J. P. (2015). The Medial Prefrontal Cortex: Coordinator

- of Autonomic, Neuroendocrine and Behavioural Responses to Stress. *Journal of Neuroendocrinology*, 27(6), 446–456. <https://doi.org/10.1111/jne.12272>
- Melia, K. R., Nestler, E. J., & Duman, R. S. (1992). Chronic imipramine treatment normalizes levels of tyrosine hydroxylase in the locus coeruleus of chronically stressed rats. *Psychopharmacology*, 108(1–2), 23–26. <https://doi.org/10.1007/BF02245280>
- Minson, J., Arnolda, L., Llewellyn-Smith, I., Pilowsky, P., & Chalmers, J. (1996). Altered c-fos in rostral medulla and spinal cord of spontaneously hypertensive rats. *Hypertension*, 27(3 D), 433–441. <https://doi.org/10.1161/01.HYP.27.3.433>
- Mitra, S. W., Hoskin, E., Yudkovitz, J., Pear, L., Wilkinson, H. A., Hayashi, S., Pfaff, D. W., Ogawa, S., Rohrer, S. P., Schaeffer, J. M., McEwen, B. S., & Alves, S. E. (2003). Immunolocalization of estrogen receptor β in the mouse brain: Comparison with estrogen receptor α . *Endocrinology*, 144(5), 2055–2067. <https://doi.org/10.1210/en.2002-221069>
- Möller-Leimkühler, A. M. (2007). Gender differences in cardiovascular disease and comorbid depression. *Dialogues in Clinical Neuroscience*, 9(1), 71–83. <https://doi.org/10.31887/dcns.2007.9.1/ammoeller>
- Morrison, S. F., Milner, T. A., & Reis, D. J. (1988). Reticulospinal vasomotor neurons of the rat rostral ventrolateral medulla: Relationship to sympathetic nerve activity and the C1 adrenergic cell group. *Journal of Neuroscience*, 8(4), 1286–1301. <https://doi.org/10.1523/jneurosci.08-04-01286.1988>
- Mueller, F., Senecal, A., Tantale, K., Marie-Nelly, H., Ly, N., Collin, O., Basyuk, E., Bertrand, E., Darzacq, X., & Zimmer, C. (2013). FISH-quant: Automatic counting of transcripts in 3D FISH images. In *Nature Methods* (Vol. 10, Issue 4, pp. 277–278). Nature Publishing Group. <https://doi.org/10.1038/nmeth.2406>

- Myers, B., Mark Dolgas, C., Kasckow, J., Cullinan, W. E., & Herman, J. P. (2014). Central stress-integrative circuits: Forebrain glutamatergic and GABAergic projections to the dorsomedial hypothalamus, medial preoptic area, and bed nucleus of the stria terminalis. *Brain Structure and Function*, 219(4), 1287–1303. <https://doi.org/10.1007/s00429-013-0566-y>
- Myers, B., McKlveen, J. M., & Herman, J. P. (2014). Glucocorticoid actions on synapses, circuits, and behavior: Implications for the energetics of stress. In *Frontiers in Neuroendocrinology* (Vol. 35, Issue 2, pp. 180–196). <https://doi.org/10.1016/j.yfrne.2013.12.003>
- Myers, B., McKlveen, J. M., Morano, R., Ulrich-Lai, Y. M., Solomon, M. B., Wilson, S. P., & Herman, J. P. (2017). Vesicular glutamate transporter 1 knockdown in infralimbic prefrontal cortex augments neuroendocrine responses to chronic stress in male rats. *Endocrinology*, 158(10), 3579–3591. <https://doi.org/10.1210/en.2017-00426>
- Myers, B., Scheimann, J. R., Franco-Villanueva, A., & Herman, J. P. (2017). Ascending mechanisms of stress integration: Implications for brainstem regulation of neuroendocrine and behavioral stress responses. In *Neuroscience and Biobehavioral Reviews* (Vol. 74, pp. 366–375). <https://doi.org/10.1016/j.neubiorev.2016.05.011>
- Owens, N. C., & Verberne, A. J. M. (2001). Regional haemodynamic responses to activation of the medial prefrontal cortex depressor region. *Brain Research*, 919(2), 221–231. [https://doi.org/10.1016/S0006-8993\(01\)03017-7](https://doi.org/10.1016/S0006-8993(01)03017-7)
- Pawar, H. N., Balivada, S., & Kenney, M. J. (2018). Does acute heat stress differentially-modulate expression of ionotropic neurotransmitter receptors in the RVLM of young and aged F344 rats? *Neuroscience Letters*, 687, 223–233.

<https://doi.org/10.1016/j.neulet.2018.09.062>

Paxinos, G., & Watson, C. (2006). *The Rat Brain in Stereotaxic Coordinates*.

[https://doi.org/10.1016/0143-4179\(83\)90049-5](https://doi.org/10.1016/0143-4179(83)90049-5)

Pezzone, M. A., Lee, W. Sen, Hoffman, G. E., Pezzone, K. M., & Rabin, B. S. (1993).

Activation of brainstem catecholaminergic neurons by conditioned and unconditioned aversive stimuli as revealed by c-Fos immunoreactivity. *Brain Research*, 608(2), 310–318.

[https://doi.org/10.1016/0006-8993\(93\)91472-5](https://doi.org/10.1016/0006-8993(93)91472-5)

Plotsky, P. M., Cunningham, E. T., & Cunningham, E. T. (1989). Catecholaminergic modulation

of corticotropin-releasing factor and adrenocorticotropin secretion. *Endocrine Reviews*, 10(4), 437–458. <https://doi.org/10.1210/edrv-10-4-437>

Prut, L., & Belzung, C. (2003). The open field as a paradigm to measure the effects of drugs on

anxiety-like behaviors: A review. In *European Journal of Pharmacology* (Vol. 463, Issues 1–3, pp. 3–33). Elsevier. [https://doi.org/10.1016/S0014-2999\(03\)01272-X](https://doi.org/10.1016/S0014-2999(03)01272-X)

Raby, W. N., & Renaud, L. P. (1989). Nucleus tractus solitarius innervation of supraoptic

nucleus: Anatomical and electrophysiological studies in the rat suggest differential innervation of oxytocin and vasopressin neurons. *Progress in Brain Research*, 81(C), 319–327. [https://doi.org/10.1016/S0079-6123\(08\)62020-8](https://doi.org/10.1016/S0079-6123(08)62020-8)

Radley, J. J., Sisti, H. M., Hao, J., Rocher, A. B., McCall, T., Hof, P. R., McEwen, B. S., &

Morrison, J. H. (2004). Chronic behavioral stress induces apical dendritic reorganization in pyramidal neurons of the medial prefrontal cortex. *Neuroscience*, 125(1), 1–6.

<https://doi.org/10.1016/j.neuroscience.2004.01.006>

Radley, Jason J., Williams, B., & Sawchenko, P. E. (2008). Noradrenergic innervation of the

dorsal medial prefrontal cortex modulates hypothalamo-pituitary-adrenal responses to acute

emotional stress. *Journal of Neuroscience*, 28(22), 5806–5816.

<https://doi.org/10.1523/JNEUROSCI.0552-08.2008>

Ragozzino, F. J., Arnold, R. A., Kowalski, C. W., Savenkova, M. I., Karatsoreos, I. N., & Peters, J. H. (2020). Corticosterone inhibits vagal afferent glutamate release in the nucleus of the solitary tract via retrograde endocannabinoid signaling. *American Journal of Physiology - Cell Physiology*, 319(6), C1097–C1106. <https://doi.org/10.1152/ajpcell.00190.2020>

Reul, J. M. H. M., & De Kloet, E. R. (1985). Two receptor systems for corticosterone in rat brain: Microdistribution and differential occupation. *Endocrinology*, 117(6), 2505–2511. <https://doi.org/10.1210/endo-117-6-2505>

Reyes, B. A. S., Fox, K., Valentino, R. J., & Van Bockstaele, E. J. (2006). Agonist-induced internalization of corticotropin-releasing factor receptors in noradrenergic neurons of the rat locus coeruleus. *European Journal of Neuroscience*, 23(11), 2991–2998. <https://doi.org/10.1111/j.1460-9568.2006.04820.x>

Reyes, B. A. S., Valentino, R. J., & Van Bockstaele, E. J. (2008). Stress-induced intracellular trafficking of corticotropin-releasing factor receptors in rat locus coeruleus neurons. *Endocrinology*, 149(1), 122–130. <https://doi.org/10.1210/en.2007-0705>

Rinaman, L. (2011). Hindbrain noradrenergic A2 neurons: Diverse roles in autonomic, endocrine, cognitive, and behavioral functions. In *American Journal of Physiology - Regulatory Integrative and Comparative Physiology* (Vol. 300, Issue 2, pp. 222–235). American Physiological Society Bethesda, MD. <https://doi.org/10.1152/ajpregu.00556.2010>

Ritter, S., Bugarith, K., & Dinh, T. T. (2001). Immunotoxic destruction of distinct catecholamine subgroups produces selective impairment of glucoregulatory responses and neuronal activation. *Journal of Comparative Neurology*, 432(2), 197–216.

<https://doi.org/10.1002/cne.1097>

- Ritter, S., Li, A. J., & Wang, Q. (2019a). Hindbrain glucoregulatory mechanisms: Critical role of catecholamine neurons in the ventrolateral medulla. In *Physiology and Behavior* (Vol. 208, p. 112568). Elsevier. <https://doi.org/10.1016/j.physbeh.2019.112568>
- Ritter, S., Li, A. J., & Wang, Q. (2019b). Hindbrain glucoregulatory mechanisms: Critical role of catecholamine neurons in the ventrolateral medulla. In *Physiology and Behavior* (Vol. 208, p. 112568). NIH Public Access. <https://doi.org/10.1016/j.physbeh.2019.112568>
- Ritter, S., Watts, A. G., Dinh, T. T., Sanchez-Watts, G., & Pedrow, C. (2003). Immunotoxin lesion of hypothalamically projecting norepinephrine and epinephrine neurons differentially affects circadian and stressor-stimulated corticosterone secretion. *Endocrinology*, *144*(4), 1357–1367. <https://doi.org/10.1210/en.2002-221076>
- Russell, J. A., Leng, G., & Douglas, A. J. (2003). The magnocellular oxytocin system, the fount of maternity: Adaptations in pregnancy. In *Frontiers in Neuroendocrinology* (Vol. 24, Issue 1, pp. 27–61). Academic Press. [https://doi.org/10.1016/S0091-3022\(02\)00104-8](https://doi.org/10.1016/S0091-3022(02)00104-8)
- Saha, S., Drinkhill, M. J., Moore, J. P., & Batten, T. F. C. (2005). Central nucleus of amygdala projections to rostral ventrolateral medulla neurones activated by decreased blood pressure. *European Journal of Neuroscience*, *21*(7), 1921–1930. <https://doi.org/10.1111/j.1460-9568.2005.04023.x>
- Saleh, T. M., & Connell, B. J. (2000). 17beta-estradiol modulates baroreflex sensitivity and autonomic tone of female rats. *Journal of Autonomic Nervous System*, *80*(3), 148–161. [https://doi.org/10.1016/S0165-1838\(00\)00087-4](https://doi.org/10.1016/S0165-1838(00)00087-4)
- Saper, C. B. (2002). The central autonomic nervous system: Conscious visceral perception and autonomic pattern generation. In *Annual Review of Neuroscience* (Vol. 25, pp. 433–469).

Annual Reviews 4139 El Camino Way, P.O. Box 10139, Palo Alto, CA 94303-0139, USA.

<https://doi.org/10.1146/annurev.neuro.25.032502.111311>

Saper, C. B., & Stornetta, R. L. (2014). Central Autonomic System. In *The Rat Nervous System: Fourth Edition* (pp. 629–673). Elsevier. <https://doi.org/10.1016/B978-0-12-374245-2.00023-1>

Sawchenko, P. E. (1988). Effects of Catecholamine-Depleting Medullary Knife Cuts on Corticotropin-Releasing Factor and Vasopressin Immunoreactivity in the Hypothalamus of Normal and Steroid-Manipulated Rats. *Neuroendocrinology*, *48*(5), 459–470. <https://doi.org/10.1159/000125050>

Schaeuble, D., Packard, A. E. B., McKlveen, J. M., Morano, R., Fourman, S., Smith, B. L., Scheimann, J. R., Packard, B. A., Wilson, S. P., James, J., Hui, D. Y., Ulrich-Lai, Y. M., Herman, J. P., & Myers, B. (2019). Prefrontal Cortex Regulates Chronic Stress-Induced Cardiovascular Susceptibility. *Journal of the American Heart Association*, *8*(24), e014451. <https://doi.org/10.1161/JAHA.119.014451>

Schaeuble, D., Wallace, T., Pace, S. A., Hentges, S. T., & Myers, B. (2023). Sex-specific prefrontal-hypothalamic control of behavior and stress responding. *BioRxiv*, 2023.07.09.548297. <https://doi.org/10.1101/2023.07.09.548297>

Scheuer, D. A. (2010). Regulation of the stress response in rats by central actions of glucocorticoids. *Experimental Physiology*, *95*(1), 26–31. <https://doi.org/10.1113/expphysiol.2008.045971>

Scheuer, D. A., Bechtold, A. G., Shank, S. S., & Akana, S. F. (2004). Glucocorticoids act in the dorsal hindbrain to increase arterial pressure. *American Journal of Physiology - Heart and Circulatory Physiology*, *286*(1 55-1), 458–467. <https://doi.org/10.1152/ajpheart.00824.2003>

- Scheuer, D. A., Bechtold, A. G., & Vernon, K. A. (2007). Chronic activation of dorsal hindbrain corticosteroid receptors augments the arterial pressure response to acute stress. *Hypertension*, *49*(1), 127–133. <https://doi.org/10.1161/01.HYP.0000250088.15021.c2>
- Schreihofe, A. M., & Guyenet, P. G. (2002). The baroreflex and beyond: Control of sympathetic vasomotor tone by gabaergic neurons in the ventrolateral medulla. *Clinical and Experimental Pharmacology and Physiology*, *29*(5–6), 514–521. <https://doi.org/10.1046/j.1440-1681.2002.03665.x>
- Selmanoff, M. K., Pramik-Holdaway, M. J., & Weiner, R. I. (1976). Concentrations of dopamine and norepinephrine in discrete hypothalamic nuclei during the rat estrous cycle. *Endocrinology*, *99*(1), 326–329. <https://doi.org/10.1210/endo-99-1-326>
- Seo, D. oh, Zhang, E. T., Piantadosi, S. C., Marcus, D. J., Motard, L. E., Kan, B. K., Gomez, A. M., Nguyen, T. K., Xia, L., & Bruchas, M. R. (2021). A locus coeruleus to dentate gyrus noradrenergic circuit modulates aversive contextual processing. *Neuron*, *109*(13), 2116–2130.e6. <https://doi.org/10.1016/j.neuron.2021.05.006>
- Serova, L. I., Maharjan, S., Huang, A., Sun, D., Kaley, G., & Sabban, E. L. (2004). Response of tyrosine hydroxylase and GTP cyclohydrolase I gene expression to estrogen in brain catecholaminergic regions varies with mode of administration. *Brain Research*, *1015*(1–2), 1–8. <https://doi.org/10.1016/j.brainres.2004.04.002>
- Serova, L., Rivkin, M., Nakashima, A., & Sabban, E. L. (2002). Estradiol stimulates gene expression of norepinephrine biosynthetic enzymes in rat locus coeruleus. *Neuroendocrinology*, *75*(3), 193–200. <https://doi.org/10.1159/000048237>
- Shafton, A. D., Ryan, A., & Badoer, E. (1998). Neurons in the hypothalamic paraventricular nucleus send collaterals to the spinal cord and to the rostral ventrolateral medulla in the rat.

- Brain Research*, 801(1–2), 239–243. [https://doi.org/10.1016/S0006-8993\(98\)00587-3](https://doi.org/10.1016/S0006-8993(98)00587-3)
- Shansky, R. M., Hamo, C., Hof, P. R., Lou, W., McEwen, B. S., & Morrison, J. H. (2010). Estrogen Promotes Stress Sensitivity in a Prefrontal Cortex-Amygdala Pathway. *Cerebral Cortex*, 20(11), 2560–2567. <https://doi.org/10.1093/cercor/bhq003>
- Shansky, Rebecca M, Hamo, C., Hof, P. R., McEwen, B. S., Morrison, J. H., & Milliken, M. (2009). Stress-Induced Dendritic Remodeling in the Prefrontal Cortex is Circuit Specific. *Cerebral Cortex October*, 19, 2479–2484. <https://doi.org/10.1093/cercor/bhp003>
- Shih, C. D. (2009). Activation of estrogen receptor -dependent nitric oxide signaling mediates the hypotensive effects of estrogen in the rostral ventrolateral medulla of anesthetized rats. *Journal of Biomedical Science*, 16(1), 60. <https://doi.org/10.1186/1423-0127-16-60>
- Shoemaker, J. K., Norton, K. N., Baker, J., & Luchyshyn, T. (2015). Forebrain organization for autonomic cardiovascular control. *Autonomic Neuroscience: Basic and Clinical*, 188, 5–9. <https://doi.org/10.1016/j.autneu.2014.10.022>
- Shughrue, P. J., Lane, M. V, & Merchenthaler, I. (1997). Comparative distribution of estrogen receptor- α and - β mRNA in the rat central nervous system. *Journal of Comparative Neurology*, 388(4), 507–525. [https://doi.org/10.1002/\(SICI\)1096-9861\(19971201\)388:4<507::AID-CNE1>3.0.CO;2-6](https://doi.org/10.1002/(SICI)1096-9861(19971201)388:4<507::AID-CNE1>3.0.CO;2-6)
- Simerly, R. B., Swanson, L. W., Chang, C., & Muramatsu, M. (1990). Distribution of androgen and estrogen receptor mRNA-containing cells in the rat brain: An in situ hybridization study. *Journal of Comparative Neurology*, 294(1), 76–95. <https://doi.org/10.1002/cne.902940107>
- Sofia Beas, B., Gu, X., Leng, Y., Koita, O., Rodriguez-Gonzalez, S., Kindel, M., Matikainen-Ankney, B. A., Larsen, R. S., Kravitz, A. V., Hoon, M. A., & Penzo, M. A. (2020). A

- ventrolateral medulla-midline thalamic circuit for hypoglycemic feeding. *Nature Communications*, 11(1). <https://doi.org/10.1038/s41467-020-19980-7>
- Solomon, M. B., Karom, M. C., & Huhman, K. L. (2007). Sex and estrous cycle differences in the display of conditioned defeat in Syrian hamsters. *Hormones and Behavior*, 52(2), 211–219. <https://doi.org/10.1016/j.yhbeh.2007.04.007>
- Sosa, M. K., Boorman, D. C., & Keay, K. A. (2023). *The Impact of Sciatic Nerve Injury and Social Interactions Testing on Glucocorticoid Receptor Expression in Catecholaminergic Medullary Cell Populations*. <https://doi.org/10.2139/SSRN.4499049>
- Souza, G. M. P. R., Stornetta, D. S., Vitali, A. J., Wildner, H., Zeilhofer, H. U., Campbell, J. N., & Abbott, S. B. G. (2022). Chemogenetic activation of noradrenergic A5 neurons increases blood pressure and visceral sympathetic activity in adult rats. *American Journal of Physiology - Regulatory Integrative and Comparative Physiology*, 323(4), R512–R531. <https://doi.org/10.1152/ajpregu.00119.2022>
- Souza, G. M. P. R., Stornetta, R. L., Stornetta, D. S., Guyenet, P. G., & Abbott, S. B. G. (2022). Adrenergic C1 neurons monitor arterial blood pressure and determine the sympathetic response to hemorrhage. *Cell Reports*, 38(10), 110480. <https://doi.org/10.1016/j.celrep.2022.110480>
- Spary, E. J., Maqbool, A., & Batten, T. F. C. (2009). Oestrogen receptors in the central nervous system and evidence for their role in the control of cardiovascular function. In *Journal of Chemical Neuroanatomy* (Vol. 38, Issue 3, pp. 185–196). Elsevier. <https://doi.org/10.1016/j.jchemneu.2009.05.008>
- Steptoe, A., & Kivimäki, M. (2012). Stress and cardiovascular disease. In *Nature Reviews Cardiology* (Vol. 9, Issue 6, pp. 360–370). <https://doi.org/10.1038/nrcardio.2012.45>

- Stocker, S. D., Meador, R., & Adams, J. M. (2007). Neurons of the rostral ventrolateral medulla contribute to obesity-induced hypertension in rats. *Hypertension*, *49*(3 PART 2 SUPPL.), 640–646. <https://doi.org/10.1161/01.HYP.0000254828.71253.dc>
- Stornetta, R. L., Sevigny, C. P., & Guyenet, P. G. (2002). Vesicular glutamate transporter DNPI/VGLUT2 mRNA is present in C1 and several other groups of brainstem catecholaminergic neurons. *Journal of Comparative Neurology*, *444*(3), 191–206. <https://doi.org/10.1002/cne.10141>
- Stornetta, R. L., Sevigny, C. P., Schreihof, A. M., Rosin, D. L., & Guyenet, P. G. (2002). Vesicular glutamate transporter DNPI/VGLUT2 is expressed by both C1 adrenergic and nonaminergic presympathetic vasomotor neurons of the rat medulla. *Journal of Comparative Neurology*, *444*(3), 207–220. <https://doi.org/10.1002/cne.10142>
- Stornetta, Ruth L. (2009). Neurochemistry of bulbospinal presympathetic neurons of the medulla oblongata. In *Journal of Chemical Neuroanatomy* (Vol. 38, Issue 3, pp. 222–230). NIH Public Access. <https://doi.org/10.1016/j.jchemneu.2009.07.005>
- Stornetta, Ruth L., & Guyenet, P. G. (2018). C1 neurons: a nodal point for stress? *Experimental Physiology*, *103*(3), 332–336. <https://doi.org/10.1113/EP086435>
- Strack, A. M., Sawyer, W. B., Hughes, J. H., Platt, K. B., & Loewy, A. D. (1989). A general pattern of CNS innervation of the sympathetic outflow demonstrated by transneuronal pseudorabies viral infections. *Brain Research*, *491*(1), 156–162. [https://doi.org/10.1016/0006-8993\(89\)90098-X](https://doi.org/10.1016/0006-8993(89)90098-X)
- Subramanian, M., Hahn-Townsend, C., Clark, K. A., Mohankumar, S. M. J., & Mohankumar, P. S. (2015). Chronic estrogen exposure affects gene expression in the rostral ventrolateral medulla of young and aging rats: Possible role in hypertension. *Brain Research*, *1627*, 134–

142. <https://doi.org/10.1016/j.brainres.2015.09.007>

- Sumners, C., Alleyne, A., Rodríguez, V., Pioquinto, D. J., Ludin, J. A., Kar, S., Winder, Z., Ortiz, Y., Liu, M., Krause, E. G., & de Kloet, A. D. (2020). Brain angiotensin type-1 and type-2 receptors: cellular locations under normal and hypertensive conditions. *Hypertension Research*, *43*(4), 281–295. <https://doi.org/10.1038/s41440-019-0374-8>
- Sved, A. F., & Felsten, G. (1987). Stimulation of the locus coeruleus decreases arterial pressure. *Brain Research*, *414*(1), 119–132. [https://doi.org/10.1016/0006-8993\(87\)91332-1](https://doi.org/10.1016/0006-8993(87)91332-1)
- Swanson, L. W., & Sawchenko, P. E. (1980). Paraventricular nucleus: A site for the integration of neuroendocrine and autonomic mechanisms. *Neuroendocrinology*, *31*(6), 410–417. <https://doi.org/10.1159/000123111>
- Swanson, Larry W. (2004). *Brain maps: structure of the rat brain* (Issue 3rd edition). [https://doi.org/10.1016/0166-2236\(93\)90187-q](https://doi.org/10.1016/0166-2236(93)90187-q)
- Tóth, Z. E., Zelena, D., Mergl, Z., Kirilly, E., Várnai, P., Mezey, É., Makara, G. B., & Palkovits, M. (2008). Chronic repeated restraint stress increases prolactin-releasing peptide/tyrosine-hydroxylase ratio with gender-related differences in the rat brain. *Journal of Neurochemistry*, *104*(3), 653–666. <https://doi.org/10.1111/J.1471-4159.2007.05069.X>
- Travagli, R. A., Hermann, G. E., Browning, K. N., & Rogers, R. C. (2006). Brainstem circuits regulating gastric function. In *Annual Review of Physiology* (Vol. 68, pp. 279–305). Annual Reviews. <https://doi.org/10.1146/annurev.physiol.68.040504.094635>
- Ulrich-Lai, Y. M., & Herman, J. P. (2009). Neural regulation of endocrine and autonomic stress responses. *Nature Reviews: Neuroscience*, *10*, 397–409. <http://www.embase.com/search/results?subaction=viewrecord%7B%7Dfrom=export%7B%7D&Did=L70444258%5Cnhttp://dx.doi.org/10.1007/s10286-010-0060->

z%5Cnhttp://sfx.library.uu.nl/utrecht?sid=EMBASE%7B&%7Dissn=09599851%7B&%7D
id=doi:10.1007%7B%25%7D2Fs10286-010-0060

- Valentino, R. J., Foote, S. L., & Page, M. E. (1993). The Locus Coeruleus as a Site for Integrating Corticotropin-Releasing Factor and Noradrenergic Mediation of Stress Responses. *Annals of the New York Academy of Sciences*, 697(1), 173–188.
<https://doi.org/10.1111/j.1749-6632.1993.tb49931.x>
- Valentino, R. J., Page, M. E., & Curtis, A. L. (1991). Activation of noradrenergic locus coeruleus neurons by hemodynamic stress is due to local release of corticotropin-releasing factor. *Brain Research*, 555(1), 25–34. [https://doi.org/10.1016/0006-8993\(91\)90855-P](https://doi.org/10.1016/0006-8993(91)90855-P)
- Valentino, R. J., & Van Bockstaele, E. (2008). Convergent regulation of locus coeruleus activity as an adaptive response to stress. In *European Journal of Pharmacology* (Vol. 583, Issues 2–3, pp. 194–203). Elsevier. <https://doi.org/10.1016/j.ejphar.2007.11.062>
- Verberne, A. J. M. (1996). Medullary sympathoexcitatory neurons are inhibited by activation of the medial prefrontal cortex in the rat. *American Journal of Physiology - Regulatory Integrative and Comparative Physiology*, 270(4 39-4), R713-9.
<https://doi.org/10.1152/ajpregu.1996.270.4.r713>
- Verberne, A. J. M., Sartor, D. M., & Berke, A. (1999). Midline medullary depressor responses are mediated by inhibition of RVLM sympathoexcitatory neurons in rats. *American Journal of Physiology - Regulatory Integrative and Comparative Physiology*, 276(4 45-4).
<https://doi.org/10.1152/ajpregu.1999.276.4.r1054>
- Verkuyl, J. M., Hemby, S. E., & Jöels, M. (2004). Chronic stress attenuates GABAergic inhibition and alters gene expression of parvocellular neurons in rat hypothalamus. *European Journal of Neuroscience*, 20(6), 1665–1673. <https://doi.org/10.1111/j.1460->

9568.2004.03568.x

Vertes, R. P. (2004). Differential Projections of the Infralimbic and Prelimbic Cortex in the Rat.

Synapse, 51(1), 32–58. <https://doi.org/10.1002/syn.10279>

Wallace, T., & Myers, B. (2021). Effects of Biological Sex and Stress Exposure on Ventromedial

Prefrontal Regulation of Mood-Related Behaviors. In *Frontiers in Behavioral Neuroscience*

(Vol. 15, p. 202). Frontiers Media S.A. <https://doi.org/10.3389/fnbeh.2021.737960>

Wallace, T., & Myers, B. (2023). Prefrontal representation of affective stimuli: importance of

stress, sex, and context. *Cerebral Cortex*. <https://doi.org/10.1093/CERCOR/BHAD110>

Wallace, T., Schaeuble, D., Pace, S. A., Schackmuth, M. K., Hentges, S. T., Chicco, A. J., &

Myers, B. (2021). Sexually divergent cortical control of affective-autonomic integration.

Psychoneuroendocrinology, 129, 2020.09.29.319210.

<https://doi.org/10.1016/j.psyneuen.2021.105238>

Wang, G., Drake, C. T., Rozenblit, M., Zhou, P., Alves, S. E., Herrick, S. P., Hayashi, S.,

Warrier, S., Iadecola, C., & Milner, T. A. (2006). Evidence that estrogen directly and

indirectly modulates C1 adrenergic bulbospinal neurons in the rostral ventrolateral medulla.

Brain Research, 1094(1), 163–178. <https://doi.org/10.1016/j.brainres.2006.03.089>

Wang, L. A., Nguyen, D. H., & Mifflin, S. W. (2019). Corticotropin-releasing hormone

projections from the paraventricular nucleus of the hypothalamus to the nucleus of the

solitary tract increase blood pressure. *Journal of Neurophysiology*, 121(2), 602–608.

<https://doi.org/10.1152/jn.00623.2018>

Warden, M. R., Selimbeyoglu, A., Mirzabekov, J. J., Lo, M., Thompson, K. R., Kim, S.-Y.,

Adhikari, A., Tye, K. M., Frank, L. M., & Deisseroth, K. (2012). A prefrontal cortex-

brainstem neuronal projection that controls response to behavioural challenge. *Nature*,

492(7429), 428–432. <https://doi.org/10.1038/nature11617>

Watanabe, Y., McKittrick, C. R., Blanchard, D. C., Blanchard, R. J., McEwen, B. S., & Sakai, R.

R. (1995). Effects of chronic social stress on tyrosine hydroxylase mRNA and protein levels. *Molecular Brain Research*, 32(1), 176–180. [https://doi.org/10.1016/0169-328X\(95\)00081-3](https://doi.org/10.1016/0169-328X(95)00081-3)

Wei, J., Yuen, E. Y., Liu, W., Li, X., Zhong, P., Karatsoreos, I. N., McEwen, B. S., & Yan, Z.

(2014). Estrogen protects against the detrimental effects of repeated stress on glutamatergic transmission and cognition. *Molecular Psychiatry*, 19(5), 588–598.

<https://doi.org/10.1038/mp.2013.83>

Wenker, I. C., Abe, C., Viar, K. E., Stornetta, D. S., Stornetta, R. L., & Guyenet, P. G. (2017).

Blood Pressure Regulation by the Rostral Ventrolateral Medulla in Conscious Rats: Effects of Hypoxia, Hypercapnia, Baroreceptor Denervation, and Anesthesia. *Journal of Neuroscience*, 37(17), 4565–4583. <https://doi.org/10.1523/JNEUROSCI.3922-16.2017>

Westlund, K. N., Bowker, R. M., Ziegler, M. G., & Coulter, J. D. (1983). Noradrenergic

projections to the spinal cord of the rat. *Brain Research*, 263(1), 15–31.

[https://doi.org/10.1016/0006-8993\(83\)91196-4](https://doi.org/10.1016/0006-8993(83)91196-4)

Wood, M., Adil, O., Wallace, T., Fourman, S., Wilson, S. P., Herman, J. P., & Myers, B. (2019).

Infralimbic prefrontal cortex structural and functional connectivity with the limbic forebrain: a combined viral genetic and optogenetic analysis. *Brain Structure and Function*, 224(1), 73–97. <https://doi.org/10.1007/s00429-018-1762-6>

Wood, S. K., & Valentino, R. J. (2017). The brain norepinephrine system, stress and

cardiovascular vulnerability. In *Neuroscience and Biobehavioral Reviews* (Vol. 74, pp. 393–400). Pergamon. <https://doi.org/10.1016/j.neubiorev.2016.04.018>

- Woods, N. I., Stefanini, F., Apodaca-Montano, D. L., Tan, I. M. C., Biane, J. S., & Kheirbek, M. A. (2020). The Dentate Gyrus Classifies Cortical Representations of Learned Stimuli. *Neuron*, *107*(1), 173-184.e6. <https://doi.org/10.1016/j.neuron.2020.04.002>
- Xu, Z. Q. D., Shi, T. J. S., & Hökfelt, T. (1998). Galanin/GMAP- and NPY-like immunoreactivities in locus coeruleus and noradrenergic nerve terminals in the hippocampal formation and cortex with notes on the galanin-R1 and -R2 receptors. *Journal of Comparative Neurology*, *392*(2), 227–251. [https://doi.org/10.1002/\(SICI\)1096-9861\(19980309\)392:2<227::AID-CNE6>3.0.CO;2-4](https://doi.org/10.1002/(SICI)1096-9861(19980309)392:2<227::AID-CNE6>3.0.CO;2-4)
- Xue, B., Zhang, Z., Beltz, T. G., Johnson, R. F., Guo, F., Hay, M., & Johnson, A. K. (2013). Estrogen receptor- β in the paraventricular nucleus and rostroventrolateral medulla plays an essential protective role in aldosterone/salt-induced hypertension in female rats. *Hypertension*, *61*(6), 1255–1262. <https://doi.org/10.1161/HYPERTENSIONAHA.111.00903>
- Yang, B., Sanches-Padilla, J., Kondapalli, J., Morison, S. L., Delpire, E., Awatramani, R., & Surmeier, D. J. (2021). Locus coeruleus anchors a trisynaptic circuit controlling fear-induced suppression of feeding. *Neuron*, *109*(5), 823-838.e6. <https://doi.org/10.1016/j.neuron.2020.12.023>
- Yasui, Y., Breder, C. D., Safer, C. B., & Cechetto, D. F. (1991). Autonomic responses and efferent pathways from the insular cortex in the rat. *Journal of Comparative Neurology*, *303*(3), 355–374. <https://doi.org/10.1002/cne.903030303>
- Yousuf, H., Smies, C. W., Hafenbreidel, M., Tuscher, J. J., Fortress, A. M., Frick, K. M., & Mueller, D. (2019). Infralimbic Estradiol Enhances Neuronal Excitability and Facilitates Extinction of Cocaine Seeking in Female Rats via a BDNF/TrkB Mechanism. *Frontiers in*

- Behavioral Neuroscience*, 13, 471255. <https://doi.org/10.3389/fnbeh.2019.00168>
- Zhang, R., Jankord, R., Flak, J. N., Solomon, M. B., D'Alessio, D. A., & Herman, J. P. (2010). Role of glucocorticoids in tuning hindbrain stress integration. *Journal of Neuroscience*, 30(44), 14907–14914. <https://doi.org/10.1523/JNEUROSCI.0522-10.2010>
- Zhao, Z., Wang, L., Gao, W., Hu, F., Zhang, J., Ren, Y., Lin, R., Feng, Q., Cheng, M., Ju, D., Chi, Q., Wang, D., Song, S., Luo, M., & Zhan, C. (2017). A Central Catecholaminergic Circuit Controls Blood Glucose Levels during Stress. *Neuron*, 95(1), 138-152.e5. <https://doi.org/10.1016/j.neuron.2017.05.031>
- Zhu, M. Y., Klimek, V., Dilley, G. E., Haycock, J. W., Stockmeier, C., Overholser, J. C., Meltzer, H. Y., & Ordway, G. A. (1999). Elevated levels of tyrosine hydroxylase in the locus coeruleus in major depression. *Biological Psychiatry*, 46(9), 1275–1286. [https://doi.org/10.1016/S0006-3223\(99\)00135-3](https://doi.org/10.1016/S0006-3223(99)00135-3)
- Ziegler, D. R., Cullinan, W. E., & Herman, J. P. (2005). Organization and regulation of paraventricular nucleus glutamate signaling systems: N-methyl-D-aspartate receptors. *Journal of Comparative Neurology*, 484(1), 43–56. <https://doi.org/10.1002/cne.20445>
- Ziegler, G., Dahnke, R., Yeragani, V. K., & Bär, K. J. (2009). The relation of ventromedial prefrontal cortex activity and heart rate fluctuations at rest. *European Journal of Neuroscience*, 30(11), 2205–2210. <https://doi.org/10.1111/j.1460-9568.2009.07008.x>

Appendix

Table S1 Distribution of estrous cycle phase during Experiment 3 described in Chapter 2.

Assay	Group	Estrous Phase (% within group)			
		Proestrus	Estrus	Metestrus	Diestrus
Real-Time Place Preference	YFP	20	30	40	10
	ChR2	12	24	30	34
Restraint - Acute Stress	YFP	0	10	30	60
	ChR2	12	8	40	40
c-Fos	YFP	0	60	30	10
	ChR2	28	24	24	24

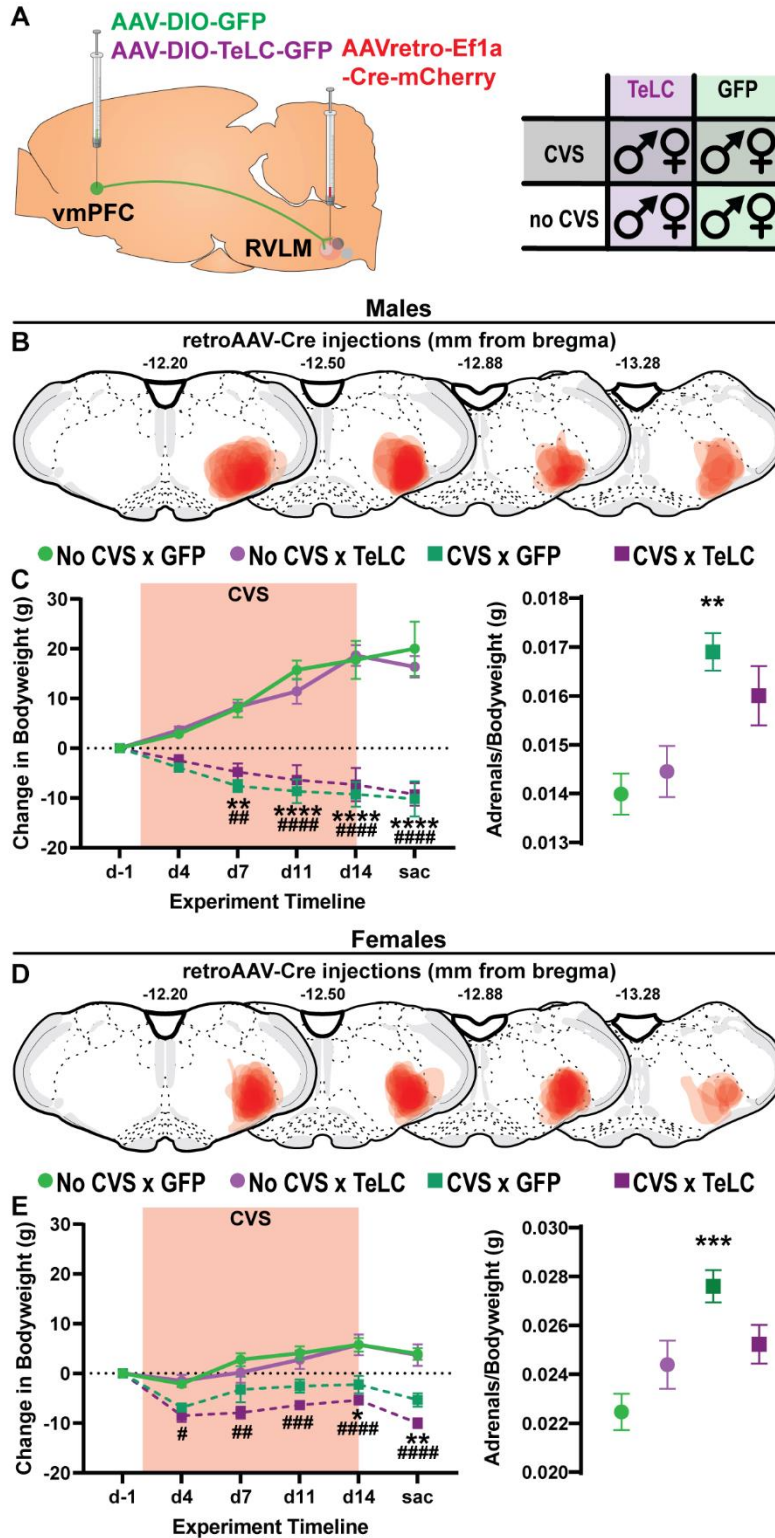


Figure S1 Intersectional TeLC approach targeted RVLM-projecting vmPFC neurons. Schema for vmPFC-RVLM circuit disruption used in 2x2x2 study (A). RVLM retroAAV-Cre injections were mapped onto Swanson Rat Brain Atlas (3rd edition) coronal sections in male rats (B). Male body weights were recorded periodically throughout the experiment, as well as adrenal weights

at the time of death (C). RVLM retroAAV-Cre injections were mapped onto Swanson Rat Brain Atlas (3rd edition) coronal sections in female rats (D). Male body weights were recorded periodically throughout the experiment, as well as adrenal weights at the time of death (E). AAV-DIO-GFP: Cre-dependent adeno-associated virus encoding GFP expression, AAV-DIO-TeLC-GFP: Cre-dependent adeno-associated virus encoding TeLC and GFP expression, AAVretro-Ef1a-Cre-mCherry: retrograde traveling adeno-associated virus encoding Cre under the promoter eukaryotic translation elongation factor 1 α , CVS: chronic variable stress, GFP: green fluorescent protein, no CVS: no chronic variable stress, sac: day rats were euthanized, SynB2: synaptobrevin-2, TeLC: tetanus toxin light-chain, vmPFC: ventromedial prefrontal cortex. No CVS x GFP vs CVS x GFP: * $p < 0.05$, ** $p < 0.01$, *** $p < 0.001$, **** $p < 0.0001$; No CVS x TeLC vs CVS x TeLC: # $p < 0.05$, ## $p < 0.01$, ### $p < 0.001$, #### $p < 0.0001$; No CVS x GFP vs no CVS x TeLC: ! $p < 0.05$, !! $p < 0.01$, !!! $p < 0.001$, !!!! $p < 0.0001$; CVS x GFP vs CVS x TeLC: ^ $p < 0.05$, ^^ $p < 0.01$, ^^ ^ $p < 0.001$, ^^ ^^ $p < 0.0001$.

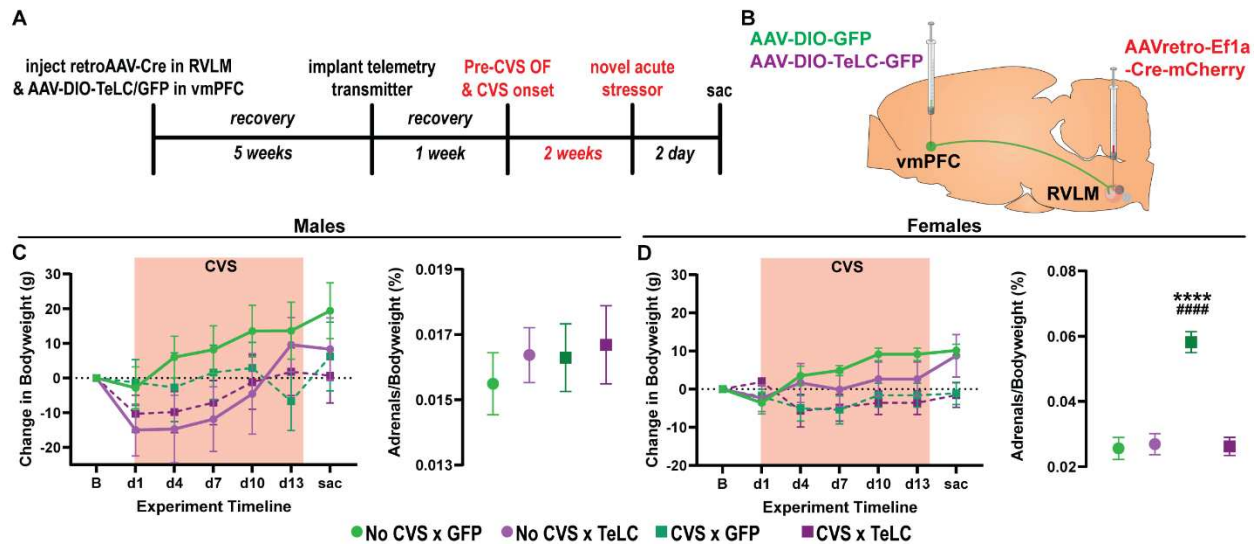


Figure S2 TeLC-mediated circuit disruption in RVLM-projecting vmPFC neurons. Experimental timeline for vmPFC-RVLM disruption experiments (A). Representative images of viral injections targeting the vmPFC and RVLM used to target RVLM-projecting vmPFC neurons (B). Schema for vmPFC-RVLM circuit disruption (C). retroAAV-Cre injections targeting the RVLM were mapped onto Swanson Rat Brain Atlas (3rd edition) coronal sections in male rats (D). Male body weights and adrenal weights were logged throughout the experiment at the time of death (E). RVLM retroAAV-Cre injections were mapped onto Swanson Rat Brain Atlas (3rd edition) coronal sections in female rats (F). Female body weights were logged during the experiment, as well as adrenal weights (G). AAV-DIO-GFP: Cre-dependent adeno-associated virus encoding GFP expression, AAV-DIO-TeLC-GFP: Cre-dependent adeno-associated virus encoding TeLC and GFP expression, AAVretro-Ef1a-Cre-mCherry: retrograde traveling adeno-associated virus encoding Cre under the promoter eukaryotic translation elongation factor 1 α , CVS: chronic variable stress, GFP: green fluorescent protein, no CVS: no chronic variable stress, sac: day rats were euthanized, SynB2: synaptobrevin-2, TeLC: tetanus toxin light-chain, vmPFC: ventromedial prefrontal cortex. No CVS x GFP vs CVS x GFP: **** $p < 0.0001$; No CVS x TeLC vs CVS x TeLC: #### $p < 0.0001$

Table S2 Somatic data from rats used in RVLM gene expression experiments. Described in Experiment 1 of Chapter 3. Effect of CVS within sex * p<0.05

Sex	Stress	Bodyweight - D1 (g)	Bodyweight - D13/14 (g)	Heart weight (g)	Heart weight/bodyweight
Male	no CVS	372.83±7.72	363.80±7.15	1.264±0.018	0.335±0.005
	CVS	381.44±9.07	378.10±9.33	1.321±0.028 *	0.355±0.007 *
Female	no CVS	216.5±11.39	222.63±9.02	0.767±0.066	0.278±0.142
	CVS	223.5±8.44	216.58±10.33	0.870±0.045 *	0.359±0.019

Table S3 Distribution of estrous cycle phase during RVLM gene expression experiments. Described in Experiment 1 of Chapter 3.

Assay	Group	Estrous Phase (% within group)			
		Proestrus	Estrus	Metestrus	Diestrous
Gene Expression - Nanostring	No CVS	0	37	26	37
	CVS	58	8	17	17

Table S4 Effects of chronic stress on male ventrolateral medulla gene expression profiles

Gene	P value	Mean of CVS	Mean of No CVS	Difference	SE of difference	t ratio	df	Fold Change
ARA1b	0.795875	344.6	329	15.57	58.87	0.2645	12	0.047418413
ARA2a	0.452188	583.4	482.6	100.8	129.7	0.777	12	0.208868628
ARB1	0.331424	99.76	85.16	14.61	14.43	1.012	12	0.171441992
ARB2	0.591052	301.7	274.9	26.78	48.52	0.552	12	0.097489996
COMT	0.080723	1121	845.2	275.5	144.5	1.907	12	0.326313299
CaMK2B	0.839756	4937	4751	186.2	901.3	0.2066	12	0.039149653
ChAT	0.415746	298.4	127.2	171.2	203.1	0.8429	12	1.34591195
DBH	0.139965	180.9	116.6	44.27	28.01	1.581	12	0.379931389
EEAT1 (SLC1A3)	0.212308	5710	4461	1249	947.8	1.317	12	0.279982067
EEAT2 (SLC1A2) (GLT-1)	0.622338	34186	31218	2968	5871	0.5055	12	0.095073355
EEAT3 (SLC1A1)	0.491599	1560	1432	127.9	180.2	0.7095	12	0.089385475
EEAT4 (SLC1A6)	0.464851	112.5	122.3	-9.787	12.96	0.7549	12	-0.080130826
FAAH	0.774706	434.7	423.3	11.4	38.93	0.2928	12	0.026931254
GABRA1	0.341869	3098	2219	878.4	887.5	0.9897	12	0.39612438
GABRA3	0.641891	559.8	606	-46.19	96.83	0.4771	12	-0.076237624
GABRA4	0.274047	1221	1040	180.7	157.6	1.146	12	0.174038462
GABRB1	0.451745	2452	2090	362.8	466.4	0.7778	12	0.173205742
GABRB2	0.399095	2289	1878	411.5	470.6	0.8743	12	0.21884984
GABRB3	0.671981	3326	3047	278.7	642.1	0.434	12	0.091565474
GABRG2	0.469069	5074	4718	356.3	476.8	0.7477	12	0.075455702
GABRG3	0.828677	161.9	155.2	6.763	30.58	0.2212	12	0.043170103
GABRP	0.950232	26.68	26.49	0.1914	3.004	0.06373	12	0.007172518
GAD 1	0.792138	2224	2314	-90.16	334.6	0.2695	12	-0.038893691
GAD 2	0.953114	5248	5198	49.59	826	0.06004	12	0.009619084
Gephyrin	0.821481	2000	1942	58.42	253.3	0.2306	12	0.029866117
GluA1 (GRIA1)	0.359453	572.9	470	102.9	108	0.9529	12	0.21893617
GluA2 (GRIA2)	0.793309	4229	4002	226.6	845.9	0.2679	12	0.056721639
GluN1 (GRIN1)	0.49045	1481	1252	228.8	321.6	0.7114	12	0.182907348
GluN2A (GRIN2A)	0.537909	747.3	597.4	150	236.5	0.6341	12	0.250920656
GluN2C (GRIN2B)	0.332574	434.6	296.2	138.4	137.1	1.01	12	0.467251857
GluR5 (GRIK1)	0.793897	2456	2567	-110.3	412.8	0.2671	12	-0.043241138
Glucocorticoid Receptor	0.476816	1493	1297	195.8	266.6	0.7344	12	0.151117965
Glutaminase	0.981234	18768	18848	-79.64	3316	0.02402	12	-0.004244482
Glutaminase 2	0.898997	1043	1062	-19.13	147.6	0.1296	12	-0.017890772
Glutamine Synthetase	0.895123	41286	40673	613.2	4554	0.1346	12	0.015071423
Glycine Receptor alpha 1	0.553212	1051	864.2	186.9	306.3	0.61	12	0.216153668
Glycine Receptor alpha 2	0.4788	585.6	600.6	-35.04	47.93	0.731	12	-0.058275058
Glycine Receptor alpha 3	0.314385	502.2	594.8	-92.59	88.18	1.05	12	-0.155682582
Glycine Receptor alpha 4	0.763889	28.01	29.75	-1.739	5.658	0.3073	12	-0.058487395
Glycine Receptor beta	0.959242	15801	15882	-80.75	1548	0.05218	12	-0.005100113
HSD11B1	0.853338	2134	2040	93.98	497.5	0.1889	12	0.046078431
HSD11B2	0.067655	35.16	26.49	8.669	4.316	2.008	12	0.327293318
KA1 (GRIK4)	0.404736	969.1	799.1	170	196.9	0.8636	12	0.212739332
KA2 (GRIK5)	0.246916	737.7	532.3	205.4	168.7	1.217	12	0.385872628
MAGL	0.384921	1395	1203	192.4	213.3	0.9018	12	0.159600998
Mineralcorticoid Receptor	0.843703	1364	1296	68.22	338.6	0.2015	12	0.052469136
NOS	0.189857	521.3	401.5	119.8	86.23	1.39	12	0.298381071
PKA catalytic subunit A (PRKACA)	0.419984	5044	4465	579.1	693.5	0.8351	12	0.129675252
PKA catalytic subunit B (PRKACB)	0.686159	9696	9201	495.1	1196	0.414	12	0.0537985
PKCa (PRKCA)	0.261948	1012	787.6	224.5	190.7	1.177	12	0.284916201
PKCb (PRKCB)	0.771214	1212	1143	68.97	231.9	0.2974	12	0.060367454
PKCy (PRKCG)	0.048973	138.9	99.84	39.06	17.83	2.19	12	0.391225962
PLCB1	0.519206	549.2	441.3	107.8	162.4	0.6641	12	0.244504872
PLCB2	0.719215	79.97	73.26	6.713	18.24	0.3681	12	0.091591592
PLCB4	0.882662	604.1	587.5	16.61	110.1	0.1508	12	0.028255319
PLCD3	0.099196	185	143.9	41.15	23.03	1.787	12	0.28561501
PLCG1	0.277525	596	494.3	101.8	89.45	1.138	12	0.205745499
PLCH2	0.269761	47.45	35.49	11.95	10.33	1.157	12	0.336996337
PNMT	0.748421	59.5	53.26	6.241	19.02	0.3282	12	0.117161097
PSD95 (DLG4)	0.353125	2146	1642	503.5	521.2	0.966	12	0.306942753
TH	0.045694	557.8	366.4	191.4	85.86	2.229	12	0.522379913
mGluR1	0.404585	469.6	401.3	68.31	79.07	0.8639	12	0.17019686
mGluR3	0.83079	1543	1466	76.84	351.9	0.2184	12	0.052523874
mGluR4	0.384158	611.7	512.8	98.84	109.4	0.9033	12	0.192862715
mGluR5	0.971715	702	696.5	5.501	152	0.0362	12	0.007896626
mGluR6	0.813436	25.76	24.81	0.9557	3.962	0.2412	12	0.038291012
mGluR7	0.676136	1397	1289	107.5	251.1	0.4281	12	0.083785881
mGluR8	0.939757	1031	1011	20.15	281.1	0.07717	12	0.019782394
VGAT (SLC32A1)	0.720769	292.6	273.9	18.77	51.29	0.366	12	0.068273092
vGluT2	0.864966	2971	3060	-88.41	508.8	0.1737	12	-0.029084967

Table S5 Effects of chronic stress on female ventrolateral medulla gene expression profiles

Gene	P value	Mean of CVS	Mean of No CVS	Difference	SE of difference	t ratio	df	Fold Change
ARA1b	0.248216	259.8	209.3	50.51	42.33	1.193	18	0.241280459
ARA2a	0.501606	365.4	305	60.36	88.02	0.6858	18	0.198032787
ARB1	0.043231	36.62	22.81	13.81	6.352	2.175	18	0.605436212
ARB2	0.436575	254	285.8	-31.76	39.91	0.7957	18	-0.11126662
COMT	0.035275	1077	584.8	492.6	216.4	2.276	18	0.841655267
CaMK2B	0.322848	4556	3934	621.5	611.4	1.017	18	0.158108795
ChAT	0.044898	109.2	19.02	90.19	41.84	2.156	18	4.741324921
DBH	0.111891	69.06	47.79	21.27	12.72	1.672	18	0.445072191
EEAT1 (SLC1A3)	0.038022	3570	2326	1244	555.4	2.239	18	0.534823732
EEAT2 (SLC1A2) (GLT-1)	0.042129	18432	12301	6132	2803	2.188	18	0.498414763
EEAT3 (SLC1A1)	0.049511	1038	609.8	428.2	203.3	2.106	18	0.702197442
EEAT4 (SLC1A6)	0.243352	98.93	79.46	19.47	16.14	1.206	18	0.245028945
Esr1	0.012123	41.4	31.92	9.477	3.398	2.789	18	0.296992481
Esr2	0.047043	69.46	45.37	24.09	11.3	2.132	18	0.5309676
FAAH	0.247947	267.4	226.9	40.44	33.87	1.194	18	0.178492728
GABRA1	0.015162	2095	630.8	1464	545.5	2.684	18	2.321179455
GABRA3	0.021557	506.1	400.5	105.7	42	2.516	18	0.263670412
GABRA4	0.013178	725.1	1029	-303.4	110.3	2.75	18	-0.295335277
GABRB1	0.013564	3027	1648	1378	503.7	2.736	18	0.836771845
GABRB2	0.018678	2281	1177	1104	427	2.585	18	0.93797791
GABRB3	0.03223	1823	898	924.9	398.5	2.321	18	1.030066815
GABRG2	0.014052	3943	3262	680.3	250.1	2.72	18	0.208767627
GABRG3	0.013733	211.9	99.47	112.4	41.17	2.73	18	1.13029054
GABRP	0.793059	7.942	8.199	-0.2571	0.9655	0.2663	18	-0.031345286
GAD 1	0.827031	927.3	953.9	-26.62	120.1	0.2217	18	-0.027885523
GAD 2	0.119608	3875	3067	807.1	493.9	1.634	18	0.263449625
Gephyrin	0.007882	1983	1376	607	203.1	2.988	18	0.441133721
GluA1 (GRIA1)	0.043819	577.2	259.9	317.3	146.4	2.168	18	1.220854175
GluA2 (GRIA2)	0.031746	3089	1347	1742	748	2.328	18	1.293244246
GluN1 (GRIN1)	0.032903	1077	440.7	636	275.3	2.311	18	1.443839346
GluN2A (GRIN2A)	0.014933	1201	227.7	973.6	361.8	2.691	18	4.27448397
GluN2C (GRIN2B)	0.009932	801.4	111.4	690	239.4	2.882	18	6.193895871
GluR5 (GRIK1)	0.076988	2547	3771	-1224	652.3	1.876	18	-0.324582339
Glucocorticoid Receptor	0.024738	1207	510.3	696.8	284.4	2.45	18	1.365275328
Glutaminase	0.04802	8579	12490	-3912	1844	2.122	18	-0.313130504
Glutaminase 2	0.024	891.2	325.9	565.3	229.4	2.485	18	1.73458116
Glutamine Synthetase	0.025826	39424	20049	19375	7976	2.429	18	0.966382363
Glycine Receptor alpha 1	0.014985	526.6	173.1	353.5	131.4	2.689	18	2.042172155
Glycine Receptor alpha 2	0.50976	436.7	472.6	-35.89	53.36	0.6726	18	-0.075962759
Glycine Receptor alpha 3	0.829253	377.5	369.8	7.683	35.11	0.2188	18	0.020822066
Glycine Receptor alpha 4	0.171349	15.82	11.81	4.009	2.814	1.425	18	0.33954276
Glycine Receptor beta	0.124284	10326	8907	1419	880.1	1.612	18	0.1593129
HSD11B1	0.00494	2325	1024	1301	406.2	3.202	18	1.270507813
HSD11B2	0.292962	16.83	12.94	3.889	3.59	1.083	18	0.300618238
KA1 (GRIK4)	0.01339	1048	338.3	709.6	258.8	2.742	18	2.097842152
KA2 (GRIK5)	0.018754	1025	352.8	671.7	260.1	2.583	18	1.905328798
MAGL	0.359677	1333	1430	-96.82	103	0.94	18	-0.067832168
Mineralocorticoid Receptor	0.036607	1097	423.6	673.5	298.3	2.258	18	1.589707271
NOS	0.051249	447.5	201.3	246.2	117.9	2.088	18	1.223050174
PKA catalytic subunit A (PRKACA)	0.041831	4130	2455	1675	764.5	2.191	18	0.682281059
PKA catalytic subunit B (PRKACB)	0.061866	5994	4904	1090	547.5	1.991	18	0.22267537
PKCa (PRKCA)	0.033716	1377	600.9	775.7	337.4	2.299	18	1.291562656
PKCb (PRKCB)	0.383825	1168	960.9	207.2	232.1	0.8926	18	0.21552711
PKCy (PRKCG)	0.106209	74.93	47.98	26.95	15.85	1.701	18	0.561692372
PLCB1	0.011096	1242	149.8	1092	386	2.83	18	7.29105474
PLCB2	0.346366	82.25	69.09	13.16	13.61	0.967	18	0.19047619
PLCB4	0.102454	967.1	519.2	447.9	260.3	1.721	18	0.862673344
PLCD3	0.987907	127.6	127.9	-0.2675	17.41	0.01537	18	-0.002345582
PLCG1	0.038632	732	420.7	311.4	139.6	2.231	18	0.739957214
PLCH2	0.026118	64.82	28.45	36.37	15.01	2.424	18	1.278383128
PNMT	0.167512	65.89	30.38	35.51	24.69	1.438	18	1.168861093
PSD95 (DLG4)	0.013088	2950	859.3	2091	759.2	2.754	18	2.433026882
Pgr	0.044791	344.6	206.1	138.6	64.25	2.157	18	0.672003882
TH	0.02917	319.2	147.9	171.3	72.29	2.37	18	1.15821501
mGluR1	0.032705	357.1	200.1	157	67.84	2.314	18	0.784607696
mGluR3	0.011458	1335	384.4	951	337.8	2.815	18	2.472944849
mGluR4	0.007568	671	432.6	238.4	79.29	3.007	18	0.551086454
mGluR5	0.040649	748.7	483.3	265.5	120.4	2.206	18	0.54914132
mGluR6	0.246262	13.34	8.995	4.344	3.625	1.199	18	0.483046137
mGluR7	0.010585	1420	611.6	808.6	283.5	2.852	18	1.32177894
mGluR8	0.851735	648.7	608.5	40.28	212.5	0.1896	18	0.066064092
vGAT (SLC32A1)	0.201175	659.8	558.1	101.7	76.68	1.327	18	0.182225408
vGlut2	0.807531	2480	2548	-67.77	274.1	0.2472	18	-0.026687598

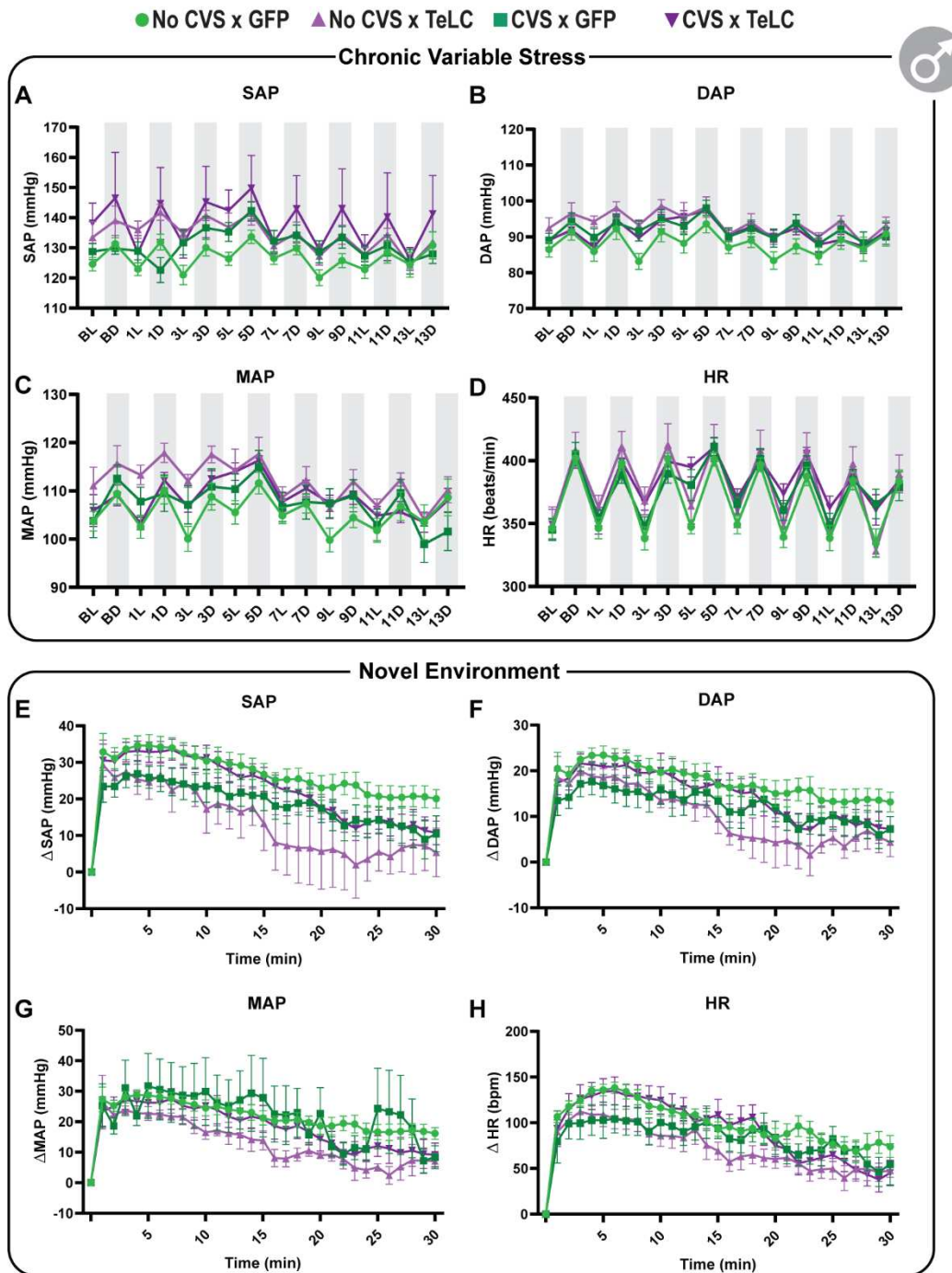


Figure S3 Male circadian hemodynamic recordings.

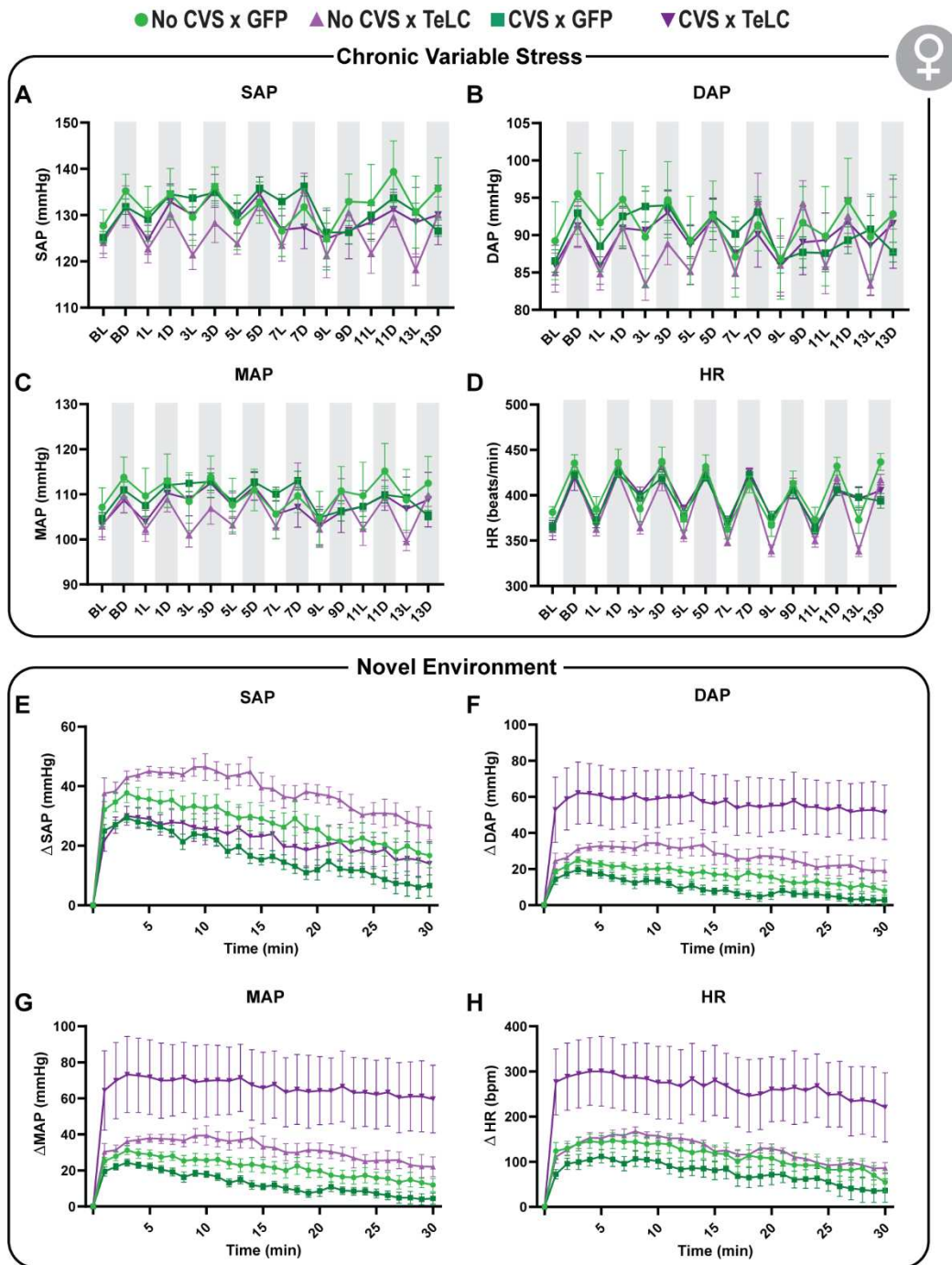


Figure S4 Female circadian hemodynamic recordings.

Table S6 Distribution of estrous cycle phase during circuit disruption endocrine experiments. Described in Experiment 2 of Chapter 3.

Assay	Group	Estrous Phase (% within group)			
		Proestrus	Estrus	Metestrus	Diestrous
Restraint - Novel Stresor	No CVS x GFP	54	8	15	23
	No CVS x TeLC	17	8	33	42
	CVS x GFP	25	25	17	33
	CVS x TeLC	21	14	36	29
Open Field - CVS rats only	CVS x GFP	54	12	23	12
	CVS x TeLC	57	7	29	7
Tissue Harvest	No CVS x GFP	54	8	38	0
	No CVS x TeLC	50	17	8	25
	CVS x GFP	50	17	25	8
	CVS x TeLC	65	14	21	0

Table S7 Distribution of estrous cycle phase during circuit disruption telemetry experiments. Described in Experiment 3 of Chapter 3.

Assay	Group	Estrous Phase (% within group)			
		Proestrus	Estrus	Metestrus	Diestrous
Novel Environment	No CVS x GFP	13	25	25	37
	No CVS x TeLC	23	33	11	33
	CVS x GFP	0	30	40	30
	CVS x TeLC	10	50	20	20
Open Field - prior to CVS	CVS x GFP	20	50	30	0
	CVS x TeLC	20	20	40	20
Tissue Harvest	No CVS x GFP	20	30	0	40
	No CVS x TeLC	30	30	10	30
	CVS x GFP	25	37.5	0	25
	CVS x TeLC	23	33	11	33

Table S8 Gene target sequences for Nanostring probes

Gene	HUGO Gene	GenBank Accession #	mRNA position	Target Sequence	NSID
Actb	Actb	NM_031144.2	20-119	CCGCGAGTACAAC CTTCTTGCAAGTCCT CCGTCGCCGGTCCA CACCCGCCACCAAGT TCGCCATGGATGAC GATATCGTGGCGCT CGTCGTCGACAACG G	NM_031144.2:19
ARA1b	Adra1b	NM_016991.2	950-1049	TGCGCCAATGATG ACAAAGAATGTGGG GTCACCGAAGAACC CTTCTACGCCCTCTT TTCTCCCTGGGCT CCTTCTACATCCCGC TCGCGGTCATCCTG	NM_016991.2:949
ARA2a	Adra2a	NM_012739.2	1156-1255	TGTTGGTCCCCTTC TTTTTACCTACACG CTCATAGCGGTCCG CTGCCGGTGCCCT ACCAAGCTCTTCAACT TCTTCTTCTGGTTCTG GCTACTGCAACA	NM_012739.2:1155
ARB1	Adrb1	NM_012701.1	321-420	GGGACTGCTGGTGG TGCCTTTCGGGGCC ACCATTGTGGTGTG GGGCCGCTGGGAGT ACGGCTCCTTCTTCT GTGAGCTCTGGACT TCGGTAGACGTGCT A	NM_012701.1:320
ARB2	Adrb2	NM_012492.2	731-830	CACAAGCAAGCCATC GACTGTTATGCCAAG GAGACTTGCTGTGA CTTCTTACGAACCA GGCCTATGCTATCG CTTCTCTATCGTAT CTTTCTACGTGC	NM_012492.2:730
CaMK2B	Camk2b	NM_001042356.1	121-220	GTACCAGTATACGA GGATATTGGCAAGG GGGCTTTCTCTGTG GTCCGACGCTGTGT CAAGCTCTGCACCG GCCATGAGTATGCA GCTAAGATCATTAA	NM_001042356.1:120

ChAT	Chat	NM_001170593.1	102-201	TTCAGTCAGTCGGG GCGGCTGCTGGGAC CTGACAAGTCGTC GTCTGAGGCTCTACT ACAGAACCTAGGGC GCGGCCCAACCTC TGACACTGCTGCCA C	NM_001170593.1:101
COMT	Comt	NM_012531.2	1071-1170	CCAGACTGTCATACA CTGGCACATTTAAA GGTAGTGAGCCAC TATGCAAAATCATT CAATAACCTGAAAA GCACCTATGGATGA AAGGCTGAATTG	NM_012531.2:1070
DBH	Dbh	NM_013158.2	1029-1128	GAATATACAAGGCC GGCGGACTCCTCT GGCATCCGTCTACA CTACACAGCTAGTCT CCGACCAATGAGG CAGGCATCATGGAG CTTGACTGGTGTA C	NM_013158.2:1028
EEAT1 (SLC1A3)	Slc1a3	NM_001289943.1	820-919	CTTGATCGCAGGGA AGATTGTTGAGATG GAAGATATGGGTGT GATTGGGGGGCAGC TTGCCATGTATACAG TGACAGTCATCGTC GGCCTCCTCATTAT	NM_001289943.1:819
EEAT2 (SLC1A2) (GLT-1)	Slc1a2	NM_001035233.1	1199-1298	GTGCTGGAACCTTG CCTGTACCTTCCGT TGCTTGGAGATAAT CTAGGGATTGACAA GCGTGTGACCATG TGTGCTCCAGTC GGAGCAACCATTAA	NM_001035233.1:1198
EEAT3 (SLC1A1)	Slc1a1	NM_013032.3	1576-1675	CAGATACGAAGAAGT CTTACGTCAATGGG GGCTTCTCGGTAGA CAAATCTGACCCAT CTCGTTCACTCAGAC CTCGAGTTCTAGAT GCCTGGCCTTAG	NM_013032.3:1575
EEAT4 (SLC1A6)	Slc1a6	NM_032065.1	686-785	TGGTCAGAAATATGT TTCCACCAACCTTG TGGAGGCCTGCTTC AAACAGTTTAAACA CAGTACAGCACAG AGTGGTAACAAGGA CGATTGTAAGGAC	NM_032065.1:685

FAAH	Faah	NM_024132.3	1207-1306	TGACGGTGGCCGCA GTTTTCTCCAAACT TCAAAGGTGACTTTG TGGATCCCTGCTTG GGAGACCTGATCTTA ATTCTGAGGCTGCC CAGCTGGTTAAA	NM_024132.3:1206
GABRA1	Gabra1	NM_183326.2	1158-1257	ATGGACTGGTTATT GCAGTGTGCTATGC CTTCGTGTTCTCGG CTCTGATTGAGTTG CCACAGTAAACTATT TCACCAAGAGAGGG TATGCGTGGGATG	NM_183326.2:1157
GABRA3	Gabra3	NM_017069.3	191-290	CTTGTACTGTGAATC TCACAGGTCTCTCCA AGTTGCTGTCTAAGA AGATGATAACCCAC AAATGTGGCACTTCT ATGTGACCAGAGTT GGACTTCTTCT	NM_017069.3:190
GABRA4	Gabra4	NM_080587.3	716-815	GAGAAGTCAGTGA GGTACCAAGGAGT CCTCAGCTTAGTTC AGTATGATCTAATTG GCCAGACTGTATCCA GTGAGACTATCAAAT CTATTACAGGTG	NM_080587.3:715
GABRB1	Gabrb1	NM_012956.1	751-850	TCACAACAGGGGCA TATCCACGACTATCA CTAAGTTTTCGTCTA AAGAGAAACATCGGT TACTTCATTTTGCAG ACCTACATGCCCTCC ACACTGATTAC	NM_012956.1:750
GABRB2	Gabrb2	NM_012957.2	801-900	CTATGATGCTTCTGC TGCACGGTTGCAT TAGGAATTACAACG TCCTGACGATGACCA CAATCAATACCCATC TCCGGGAGACTCTC CCTAAAATCCC	NM_012957.2:800
GABRB3	Gabrb3	NM_017065.1	1161-1260	ACGGGAATATCCTAC TAGCACCGATGGAT GTTCAATGAAATG AATGAGTTGCAGG CAGCGTTGGTGACA CCAGGAATTCAGCAA TATCCTTTGACAA	NM_017065.1:1160

GABRG2	Gabrg2	NM_183327.1	671-770	GTTCTGTTGAAGTG GGAGACACAAGGTC ATGGAGGCTGTATC AGTTTTCTTTGTTG GATTGAGGAATACCA CTGAAGTAGTGAAG ACAACTTCTGGTGA	NM_183327.1:670
GABRG3	Gabrg3	NM_024370.3	1047-1146	GGTGTCTATGTCAC TGCCATGGACCTCTT TGTGACTGTGTGCTT CTTGTGTTGCTTTGC CGCACTGATGGAGT ATGCTACTCTCAACT ACTATTGAGC	NM_024370.3:1046
GABRP	Gabrp	NM_031029.1	647-746	GACTCGAAAACCTG CGCCTTGCTCAGTA CACCATCCAACAGTA TTTCACCCTGGTCAC CGTATCCCAGCAGG AGACAGGAAACTATA CGCGGTTGGTTTT	NM_031029.1:646
GAD 1	Gad1	NM_017007.1	261-360	AACATATGATACTTG GTGTGGCGTAGCCC ATGGATGCACCAGA AAACTGGCCTGAA GATCTGTGTTTCTT GCAAAGGACCAATA GCCTGGAAGAGAAG	NM_017007.1:260
GAD 2	Gad2	NM_012563.1	586-685	TTAAACAGGGCATC CCCGATATTTAATC AGCTGTCTACCGGA TTGGATATGTTGGA TTAGCAGCAGATTG GTTGACATCAACAGC AAACACGAACAT	NM_012563.1:585
Gephyrin	Gphn	NM_022865.3	1637-1736	TCCAGTGGTTGCCG TTATGTCAACAGGGA ATGAGCTACTAAATC CTGAAGATGACCTCT TACCAGGAAAGATT GGGACAGCAATCGA TCAACACTTCTA	NM_022865.3:1636
GluA1 (GRIA1)	Gria1	NM_031608.1	856-955	AAAAGAATGGCATCG GGTACCACTACATCC TCGCCAATCTGGGC TTCATGGACATTGAC TTAAATAAGTTCAAG GAGAGCGGAGCCAA TGTGACAGGTTT	NM_031608.1:855

GluA2 (GRIA2)	Gria2	NM_017261.2	1533-1632	GAATAAACTACACAA TTAACATCATGGAGC TCAAACAATGGAC CCCGAAGATTGGG TACTGGAGTGAAGT GGATAAAATGTTGT CACCCAACTGA	NM_017261.2:1532
Glucocorticoid Receptor	Nr3c1	NM_012576.2	4996-5095	AGCTTTCCTTGAAGC GTATAAGAGCCATG CTCCTTTAGTATGTG GGGAAGAAGAGAGC TGTCATAGTTTTGAG TACAGTGAGAAGAT GCGGTACTGTCT	NM_012576.2:4995
GluN1 (GRIN1)	Grin1	NM_017010.1	2616-2715	TCATGGAAGATCTG GATAAGACATGGGTT CGGTATCAGGAATG CGACTCCCGCAGCA ATGCTCCTGCAACCC TCACCTTTGAGAACA TGGCAGGGGTCTT	NM_017010.1:2615
GluN2A (GRIN2A)	Grin2a	NM_012573.2	3366-3465	AAGTATCCAAGGAC TGTAGCGATGTTGA CCGCACCTACATGAA AACCAAAGCAAGTTC TCCCAGGGATAAGA TCTATACCATTGATG GTGAGAAGGAGC	NM_012573.2:3365
GluN2C (GRIN2B)	Grin2b	NM_012574.1	3171-3270	TTCACGCATTCAGAC TGCAAGTCTTACAAT AACCACCCCTGTGA GGAAAACCTGTCA GTGACTACATTAGCG AGGTAGAGAGAACA TTTGGTAACCTGC	NM_012574.1:3170
GluR5 (GRIK1)	Grik1	NM_017241.2	616-715	ACCTATTTATATCA ACCTTACCCGACT ATGCGGCTATCAGC AGGGCGTCTGGA TTTGGTCTCTATTA CAACTGAAAACAGT GACGGTGGTGA	NM_017241.2:615
Glutaminase	Gls	NM_012569.2	983-1082	ATCGCTATGTTGGG AAGGAGCCAAGTGG ATTAAGATTCAACAA GCTCTTTTGAATGA AGATGATAACCACA TAATCCGATGGTAAA TGCTGGAGCAAT	NM_012569.2:982

Glutaminase 2	Gls2	NM_138904.1	1971-2070	TATAGCTTAAGTGAC ATCCTCCACCAGAAA GTAGCCAGGGTTTT ACCCAGGTCCCCATT TCAACTTCCTGGAG AGCCTCTAGCTACAT GCATATGTAT	NM_138904.1:1970
Glutamine Synthetase	Glul	NM_017073.3	1657-1756	TTCTCCGGTGAAAC CAGCTTCTATTGAA GTCTGGTGAGGAGT TGGAGGTTGGTCTC TTGGCTTCCTAGCT TAGGGAGGGGAGT TCACCCTCCCTTC	NM_017073.3:1656
Glycine Receptor alpha 1	Glr1	NM_013133.1	1121-1220	ATCTGGATGGCTGTT TGCCTGCTTTCGT GTTCTCGGCCCTGC TGGAAATGCCGCT GTCAACTTTGTGTCC CGGCAACACAAGGA ACTCCTTCGATTTA	NM_013133.1:1120
Glycine Receptor alpha 2	Glr2	NM_012568.2	1078-1177	TGAAGAACTTCCAA TGGATGTCAGACC TGTACAATGCAGCTG GAGAGTTTTGGGTA CACCATGAATGACCT GATATTTGAGTGGTT AAGTGATGGTCC	NM_012568.2:1077
Glycine Receptor alpha 3	Glr3	NM_053724.3	725-824	AAGATTTGCGATACT GCACTAAACACTACA ATACAGGAAAAGTTTA CATGCATAGAAGTAC GATTTTCATCTTGAGC GGCAAATGGGCTAC TACTTGATCCA	NM_053724.3:724
Glycine Receptor alpha 4	Glr4	NM_001191914.1	1033-1132	GTCTCTCGTCAGCAT AAGGAATTTATGAGA CTTCGTAGAAAGCA GAGAGCTCGACACA TGGAAGAAGACATCA TAAGAGAGGGCCGC TTCTATTTTCGTG	NM_001191914.1:1032
Glycine Receptor beta	Glrβ	NM_053296.1	551-650	CTTTGGACTTAACTC TGTTTCCCATGGACA CACAAAGCTGCAAG ATGCAACTTGAGAG CTTTGGTTACACCAC TGATGATTTGAGATT CATCTGGCAGTC	NM_053296.1:550

HSD11B1	Hsd11b1	NM_017080.2	1091-1190	AGGTATACTATGACA AATCATCTTGGACTC CACTTCTGCTTGGGA ATCCAGGAAGGAGG ATCATGGAATTTCTT TCATTACGGTCATAT AACAGGGACCT	NM_017080.2:1090
HSD11B2	Hsd11b2	NM_017081.2	1709-1808	CAGAGTAAATCCCTC TTGACTGGCTCAAGA TTTAGGTTCCCAACC ACTGGCTCCCAGCC ACATGGAAGCTGTAT GCTGTATTTGTCTGG TTGTTGCATT	NM_017081.2:1708
KA1 (GRIK4)	Grik4	NM_012572.1	1626-1725	TCATGACGCTGGGA ATTAGTATTCTTTAC AGAGTTCATATGGGA CGCAGACCGGCTA TTTCTCCTTCTGGA CCCCTTTTCTCCAGG AGTCTGGCTCTT	NM_012572.1:1625
KA2 (GRIK5)	Grik5	NM_031508.2	1061-1160	CATCTGGACGGTAT CGTAGAGGACTCCT CCAACATCTTGGGCT TTTCCATGTTCAACA CCTCCCATCCCTTCT ACCCGGAGTTTGTG CGCAGCCTCAACA	NM_031508.2:1060
MAGL	Mgll	NM_138502.2	536-635	CTGGCATGATCCTAA TTTCACTCTGATCC TTGCCAATCCGGAAT CTGCATCGACTTGA AGGTCCTTGCTGCC AAACTGCTCAATTTT GTCCTGCCAAA	NM_138502.2:535
mGluR1	Grm1	NM_001114330.1	1898-1997	GATGATTACAAAATC CAGATGAACAAAAGC GGAATGGTACGATC TGTGTGCAGTGAGC CTTGCTTAAAGGGTC AGATTAAAGGCATAC GAAAGGAGAAG	NM_001114330.1:1897
mGluR3	Grm3	NM_001105712.1	2576-2675	TTCTCCCTATATTT TATGTGACATCAAGT GACTACAGAGTGCA GACGACAACAATGT GCATCTCCGTTAGC CTGAGCGGTTTCGT GGTCTTGGGCTGTT	NM_001105712.1:2575

mGluR4	Grm4	NM_022666.1	2162-2261	TCGCATGGACCCCG TGGATGGCACCAG CTGCTTAAGTACATC AGGAACGTCAACTTC TCAGGCATTGCGGG GAACCCGTGAACCTT CAATGAGAACGGA	NM_022666.1:2161
mGluR5	Grm5	NM_017012.1	2136-2235	CATCTGCCTGGGAT ACTTATGTACCTTTT GCCTCATTGCAAGC CCAAGCAGATTTACT GCTATCTTCAGAGAA TTGGCATTGGACTCT CTCCAGCCATG	NM_017012.1:2135
mGluR6	Grm6	NM_022920.1	1131-1230	ATCTTGCCAAAAGG GCTTCAATCGACGG ATTTGACCAACTT CATGACTCGTTCCTT GGAGAACAACCGCA GAAACATCTGGTTTG CCGAGTTCTGGG	NM_022920.1:1130
mGluR7	Grm7	NM_031040.1	1436-1535	GATGCTTACTTCACA TCCCGGACACTTGAA AACAAACAGGAGAAAT GTATGGTTTGCCGA ATACTGGGAAGAAAA CTTCAACTGCAAGTT GACAATTAGTG	NM_031040.1:1435
mGluR8	Grm8	NM_022202.1	1961-2060	GTTACTCCATCACCT TTTTGATGATTGCCG CACCTGACACGATCA TCTGCTCCTCCGAC GGATCTTCTGGGA CTTGGTATGTGTTTC AGCTATGCAGC	NM_022202.1:1960
Mineralcorticoid Receptor	Nr3c2	NM_013131.1	1976-2075	GAGCTATTACCCTGA AGCCAGCATCCAT CATCTGCTATCGTTG GTGTGAATTCGGGT GGACAGTCCTTTCAC TACCGATTGGTGC TCAAGGTACAATA	NM_013131.1:1975
NOS	Nos1	NM_052799.1	57-156	CTGCAGGAGTCATTT TAGCTTAGTCTTCTG AAGGACACAGATAC CATGGAAGAGAACA CGTTTGGGGTTTCTCAG CAGATCCAACCCAAT GTAATTTCTGTTC	NM_052799.1:56

PKA catalytic subunit A (PRKACA)	Prkaca	NM_001100922.1	866-965	CCTATCCAGATCTAT GAGAAAATCGTCTCT GGAAAGTGCGGTT CCCATCCCACTCAG CTCTGACTTGAAGGA CCTGCTTCGGAACC TTCTGCAGGTGG	NM_001100922.1:865
PKA catalytic subunit B (PRKACB)	Prkacb	NM_001077645.1	556-655	CTCAAGCCGGAAAA CCTCTTAATTGACCA CCAGGGTTACATCCA GGTCACAGATTTTG GGTTCGCAAGAGA GTCAAGGGCAGGAC TTGGACATTGTGTG	NM_001077645.1:555
PKCa (PRKCA)	Prkca	NM_001105713.1	733-832	CACAGAGAAGAGGG GGCGGATTACCTG AAGGCAGAGGTAC AGATGAAAAGTGCA CGTCACCGTACGAG ATGCAAAAAATCTAA TCCCTATGGATCCA	NM_001105713.1:732
PKCb (PRKCB)	Prkcb	NM_001172305.1	291-390	CCGACTTCATTGGG GCTTAGGTTTGCAG GGATTCCAGAGTCA GGTCTGCTGCTTTGT TGTACACAAGCGCT GCCATGAATTCGTCA CGTTCTCCTGCCC	NM_001172305.1:290
PKCy (PRKCG)	Prkcg	NM_012628.1	2031-2130	GAACCCACCATCCG GGCTCATGGCTTTTT CCGTTGGATCGATT GGGAGAGGTTGGAG AGACTGGAATTGC GCCTCCTTTTAGACC ACGTCCGTGTGGCC	NM_012628.1:2030
PLCB1	Plcb1	NM_001077641.1	2580-2679	TTGTCTACATAGAAG TCAAAGACTATGTCC CAGACACGTATGCA GATGTAATTGAAGCA TTATCAAACCAATC CGATATGTCAATCTG ATGGAACAGAG	NM_001077641.1:2579
PLCB2	Plcb2	NM_053478.1	768-867	TCTTCACTTCTTATC ATGCTAAAGCCAAAC CCTACATGACCAAG GAGCACCTGACCAA ATTTCATCAATCAGAA GCAACGAGACCCTC GACTCAATTCCTT	NM_053478.1:767

PLCB4	Plcb4	NM_024353.1	4661-4760	TCATCTAACATTAC CACACGACAAGACTA GTAAACAGGAATCAT AGATGTTTTGCATGA TGCACAAGCACC AAT TATGACTAACCCATT GAGACACAGT	NM_024353.1:4660
PLCD3	Plcd3	NM_001105845.2	725-824	ACGTGGACATGAAT GACATGTACGCCTAC CGCCTTTCAAGGA GTGTGACCATTCTAA CAACGAGCGTCTGG AAGGGCTGAGATC GAGGCTTTCTCCG	NM_001105845.2:724
PLCG1	Plcg1	NM_013187.1	3541-3640	CAGTAACCCAGAGTT TGCCTTTCTGCGCTT TGTGGTGTATGAGG AAGACATGTTTAGTG ACCAGAACTTCTTGG CTCAGGCTACTTCC CAGTAAAAGGC	NM_013187.1:3540
PLCH2	Plch2	XM_008764396.1	1318-1417	CAACAAATATGCCTT CATCAAGAATGAGTA CCCAAGTATCCCTGT CCATTGAGAACCACT GTAGTGTGTTCCAGC AGAAAAAGATGGCC CAGTATCTCACT	XM_008764396.1:1317
PNMT	Pnmt	NM_031526.1	581-680	TGTGAGCCCGGATC TCCCAAGCTCCGG CAGGCTTTGTATCAT ATCACGAGCTGCT GAGGCCCGGGGTA ATCTCCTTTCATCG GGGCCCTGGAGGAG	NM_031526.1:580
Ppjh	Ppjh	XM_001073803.4	31-130	TGGCGGTGGCAAAT TCAAGTCCCGTCAAT CCAGTGGTCTTCTTT GATGTCAGTATTGG CGGCCAGGAAGTTG GTCGCATGAAGATC GAGCTCTTGCAGA	XM_001073803.4:30
PSD95 (DLG4)	Dlg4	NM_019621.1	1151-1250	TTGACCTCCGCAATG CCAGTCACGAACAG GCTGCCATTGCCCT GAAGAATGCGGGTC AGACGGTCACGATC ATCGCTCAGTATAAA CCAGAAGATATAG	NM_019621.1:1150

Rplp1	Rplp1	NM_001007604.1	403-502	AAGAAGGAAGAATCT GAAGAATCCGAGGA TGACATGGGCTTTG GTCTTTTGGACTAAA CTGCTTTTGTAAACA TGTCCAATAAAGAGC TGAACCTGTAAA	NM_001007604.1:402
Sdha	Sdha	NM_130428.1	1461-1560	CCTCCGATTAAGGCA AATGCTGGAGAAGA GTCCGTTATGAATCT TGACAAGTTGAGATT TGCTGATGGAAGTG TAAGAACATCAGAGC TGCGCCTCAGCA	NM_130428.1:1460
TH	Th	NM_012740.2	1641-1740	ATCAAACCTACCAGC CTGTGACTTTGTGT CCGAGAGCTTCAAT GACGCCAAGGACAA GCTCAGGAATATG CCTCTCGTATCCAGC GCCATTCTCTGT	NM_012740.2:1640
vGAT (SLC32A1)	Slc32a1	NM_031782.1	456-555	AACGTGACAAACGC CATTGAGGGCATGTT CGTGCTGGGTCTAC CCTACGCCATCCTCC ACGGCGGCTACCTG GGGTTGTTCTCATC ATCTTCGCCGGG	NM_031782.1:455
vGlut2	Slc17a6	NM_053427.1	943-1042	CTTACCTCTACCCTC AATATGCTGATCCCA TCTGCAGCCAGAGT GCATTATGGATGCG TCATCTTTGTTAGAA TATTGCAAGGACTTG TGGAGGGCGTCA	NM_053427.1:942